Institut für Geowissenschaften
Mathematisch-Naturwissenschaftliche Fakultät
Universität Potsdam

Characterization of atmospheric processes related to hydro-meteorological extreme events over the south-central Andes

DISSERTATION

von

Maryam Ramezani Ziarani

zur Erlangung des akademischen Grades

DOCTOR RERUM NATURALIUM
»Dr. rer. nat.«

in der Wissenschaftsdisziplin Fernerkundung

eingereicht an der
Mathematisch-Naturwissenschaftlichen Fakultät
der Universität Potsdam

Disputation: Potsdam, May 2020

Betreuer: Prof. Dr. Bodo Bookhagen

Tag der Disputation: 18. Mai 2020

Published online in the
Institutional Repository of the University of Potsdam:
https://doi.org/10.25932/publishup-47175
https://nbn-resolving.org/urn:nbn:de:kobv:517-opus4-471755

Abstract

The significant environmental and socioeconomic consequences of hydrometeorological extreme events, such as extreme rainfall, are constituted as a most important motivation for analyzing these events in the south-central Andes of NW Argentina. The steep topographic and climatic gradients and their interactions frequently lead to the formation of deep convective storms and consequently trigger extreme rainfall generation.

In this dissertation, I focus on identifying the dominant climatic variables and atmospheric conditions and their spatiotemporal variability leading to deep convection and extreme rainfall in the south-central Andes.

This dissertation first examines the significant contribution of temperature on atmospheric humidity (dew-point temperature, Td) and on convection (convective available potential energy, CAPE) for deep convective storms and hence, extreme rainfall along the topographic and climatic gradients. It was found that both climatic variables play an important role in extreme rainfall generation. However, their contributions differ depending on topographic and climatic sub-regions, as well as rainfall percentiles.

Second, this dissertation explores if (near real-time) the measurements conducted by the Global Navigation Satellite System (GNSS) on integrated water vapor (IWV) provide reliable data for explaining atmospheric humidity. I argue that GNSS-IWV, in conjunction with other atmospheric stability parameters such as CAPE, is able to decipher the extreme rainfall in the eastern central Andes. In my work, I rely on a multivariable regression analysis described by a theoretical relationship and fitting function analysis.

Third, this dissertation identifies the local impact of convection on extreme rainfall in the eastern Andes. Relying on a Principal Component Analysis (PCA) it was found that during the existence of moist and warm air, extreme rainfall is observed more often during local night hours. The analysis includes the mechanisms for this observation.

Exploring the atmospheric conditions and climatic variables leading to extreme rainfall is one of the main findings of this dissertation. The conditions and variables are a prerequisite for understanding the dynamics of extreme rainfall and predicting these events in the eastern Andes.

Zusammenfassung

Die entscheidenden ökologischen und sozioökonomischen Folgen hydrometeorologischer Extremereignisse, wie z.B. extremer Niederschläge, stellen eine wichtige Motivation für die Analyse dieser Ereignisse in den südlich-zentralen Anden von NW Argentinien dar. Die steilen topographischen und klimatischen Gradienten und deren Wechselwirkungen führen häufig zu einer starken konvektiven Regenfallbildung und sind häufig auch die Auslöser von Starkniederschlägen.

In dieser Dissertation konzentriere ich mich auf die Identifizierung der dominanten klimatischen Variablen und atmosphärischen Rahmenbedingungen und ihrer räumlich-zeitliche Variabilität, die zu starker Konvektion und extremen Niederschlägen in den südlich-zentralen Anden führt.

Diese Dissertation untersucht zunächst den wichtigen Beitrag der Temperatur zur Luftfeuchtigkeit (Taupunkttemperatur, Td) und zur Konvektion (konvektive verfügbare potenzielle Energie, CAPE) für starke, konvektive Stürme und damit extreme Niederschläge entlang der topographischen und klimatischen Gradienten. Es wurde festgestellt, dass beide klimatischen Variablen eine wichtige Rolle bei der Erzeugung extremer Niederschläge spielen. Ihr Beitrag hängt jedoch von den topographischen und klimatischen Teilregionen sowie den Niederschlagsperzentilen ab.

Zweitens, auf der Grundlage einer multivariablen Regressionsanalyse, die durch eine theoretische Beziehungs- und Anpassungsfunktionsanalyse beschrieben wird, untersucht diese Arbeit, ob integrierter Wasserdampf (IWV) auf der Grundlage von GNSS (Global Navigation Satellite System) Messungen zuverlässige Daten sind, um die Luftfeuchtigkeit zu erklären. Das GNSS-IWV in Verbindung mit anderen atmosphärischen Stabilitätsparametern wie z.B. CAPE ist in der Lage, die extremen Niederschläge in den östlichen zentralen Anden zu entschlüsseln.

Drittens, diese Dissertation identifiziert die lokalen Auswirkungen der Konvektion auf extreme Niederschläge in den östlichen Anden. Auf der Grundlage einer Hauptkomponentenanalyse (PCA) wurde festgestellt, dass die extremen Niederschläge häufiger während der lokalen Nachtstunden beobachtet werden, wenn feuchte und warme Luft vorhanden ist.

Die Erforschung der atmosphärischen Rahmenbedingungen und klimatischen Variablen, die zu extremen Niederschlägen führen, ist eines der wichtigste Ergebnisse dieser Arbeit. Sie ist Voraussetzung für das Verständnis der Dynamik von extremen Niederschlägen und wichtig für die Vorhersage dieser Ereignisse in den östlichen Anden.

Publications and Author Contributions

This thesis is comprised of three independent studies published or in review in peer-reviewed journals. Individual studies are found in Chapters 2 to 4.

Chapter 2 - Using Convective Available Potential Energy (CAPE) and Dew-Point Temperature to Characterize Rainfall-Extreme Events in the South- Central Andes

Maryam Ramezani Ziarani, Bodo Bookhagen, Torsten Schmidt, Jens Wickert, Alejandro de la Torre and Rodrigo Hierro

Conceptualization, M.R.Z., B.B., T.S., J.W., A.D.T. and R.H.; methodology, M.R.Z., B.B., T.S., J.W., A.D.T. and R.H.; software, M.R.Z., B.B.; validation, M.R.Z., B.B.; formal analysis, M.R.Z., B.B.; investigation, M.R.Z., B.B.; T.S.; resources, M.R.Z., B.B.; writing—original draft preparation, M.R.Z.; writing—review and editing, M.R.Z., B.B., T.S., J.W., A.D.T.; visualization, M.R.Z., B.B.; supervision, B.B., T.S., J.W., A.D.T.; project administration, B.B.; funding acquisition, B.B., T.S., J.W.

A version of the chapter has been published in the peer-reviewed journal Atmosphere:
*Maryam Ramezani Ziarani, Bodo Bookhagen, Torsten Schmidt, Jens Wickert, Alejandro de la Torre and Rodrigo Hierro. Using Convective Available Potential Energy (CAPE) and Dew-Point Temperature to Characterize Rainfall-Extreme Events in the South- Central Andes. Atmosphere, 2019, 10(7), 379.*https://doi.org/10.3390/atmos10070379.

Chapter 3 - Using GNSS-derived integrated water vapour and CAPE to decipher rainfall in the eastern central Andes

Maryam Ramezani Ziarani, Bodo Bookhagen, Torsten Schmidt, Jens Wickert, Alejandro de la Torre, Zhiguo Deng and Andrea Calori

Conceptualization, M.R.Z., B.B., T.S., J.W., A.D.T., Z.D. and A.C; methodology, M.R.Z., B.B., T.S., J.W., A.D.T., Z.D. and A.C; software, M.R.Z., B.B.; validation, M.R.Z., B.B.; formal analysis, M.R.Z., B.B.; investigation, M.R.Z., B.B.; resources, M.R.Z., B.B.; writing—original draft preparation, M.R.Z.; writing—review and editing, M.R.Z., B.B., T.S., J.W., A.D.T.; visualization, M.R.Z.; supervision, B.B., T.S., J.W., A.D.T.; project administration, B.B.; funding acquisition, B.B., T.S., J.W.

This article is in review at the Remote Sensing peer-reviewed journal.

Chapter 4 - On the behavior of rainfall maxima at the eastern Andes

Hierro, R., Burgos Fonseca, Y., Ramezani Ziarani, M., Llamedo, P., Schmidt, T., de la Torre, A., Alexander, P.

I contributed in Conceptualization, methodology, software, investigation and review and editing.

A version of the chapter has been published in the peer-reviewed journal Atmospheric Research.
*Hierro, R., Burgos Fonseca, Y., Ramezani Ziarani, M., Llamedo, P., Schmidt, T., de la Torre, A., Alexander, P. On the behavior of rainfall maxima at the eastern Andes. Atmospheric Research, 2020, 234, 104792.*https://doi.org/10.1016/j.atmosres.2019.104792.

Acknowledgments

At first I would like to thank my supervisor, Bodo Bookhagen for his ongoing guidance and excellent support. I was very lucky to had you as my supervisor. A million thanks to you!!

I would like to thank my advisors, Torsten Schmidt, Jens Wickert and Alejandro De la Torre for their excellent support. Thank you for everything!

I would like to express my thanks to my family, my lovely mom and dad, my lovely siblings and lovely nephew for their continuous support and encouragement.

I would like to thank my fellow PhD students, my officemates, our previous project's coordinator, Henry Wichura and our recent coordinator, Verónica Torres Acosta as well as our project's leader, Manfred Strecker.

And, an immense thank to my love, my fiancé . Hamid, thank you for being there through good times and bad. You mean a lot to me!

Contents

List of Figures

List of Tables

Chapter 1

Introduction and Motivation

Motivation

The south–central Andes of NW Argentina are exposed to frequent hydrometeorological extreme events due to the complex couplings between atmosphere and topography (e.g., Bookhagen and Strecker, 2008; Castino et al., 2017; Ramezani Ziarani et al., 2019; Vera et al., 2006a; Marengo et al., 2012) (Figure 1.1A,B). This complex interaction leads to processes that are difficult to decipher but are of importance when attempting to understand extreme rainfall dynamics in the eastern and south–central Andes.

The majority of past studies identify the spatial and temporal context of extreme rainfall events, but they often do not take into account the atmospheric boundary conditions leading to deep convection and extreme rainfall. This work identifies the dominant climatic variables and atmospheric conditions that trigger extreme rainfall generation and develops an empirical framework for conditions leading to rainfall extremes.

For a more thorough motivation, I will first describe previous studies of extreme events and describe previous frameworks for understanding orographic rainfall.

Previous Studies of Parameterization of Mean and Extreme Rainfall

Several past studies analyzed the spatiotemporal distribution of rainfall in South America and in the greater central-eastern Andes located in the NW Argentine Andes (Boers et al., 2014a,b, 2015, 2016; Khan et al., 2007; Castino et al., 2017; Pingel et al., 2016; Carvalho et al., 2002; Lenters and Cook, 1999; Espinoza et al., 2015; Thibeault et al., 2010; Minvielle and Garreaud, 2011; Hierro et al., 2015; Moya-Álvarez et al., 2018). Some studies analyzed the Andean rainfall variability (e.g., Garreaud and Aceituno, 2001; Castino et al., 2017; Bookhagen et al., 2011; Barros and Lang, 2003). The study of the rainfall variability in NW Argentine Andes by Castino et al. (2017) suggested that different regions along the topographic gradient react differently to changing climate conditions. Furthermore, Boers et al. (2015) performed a complex network analysis of extreme rainfall events in South America. They explained the intraseasonal rainfall variability in South America by a dipole between southeastern South America (SESA) and southeastern Brazil (SEBRA) by analyzing the dynamical characteristic of extreme rainfall over both regions (Boers

et al., 2015). An additional study, Boers et al. (2016), investigated the geographical and spatiotemporal distribution of rainfall during the South American monsoon season. An additional study, De la Torre et al. (2015), analyzed the formation of deep convection leading to extreme rainfall as a result of the effect of topography on the vertical velocity of the air over the Andes. Furthermore, Carvalho et al. (2002) analyzed the regional distribution of extreme rainfall in southeastern South America. Based on their findings, the distribution of extreme rainfall highly depends on South Atlantic Convergence Zone (SACZ) activity (Carvalho et al., 2002). A different study investigated the spatial distribution of rainfall in connection with large-scale atmospheric circulation over the southern tropical Andes (Espinoza et al., 2015). They found that the variation in the seasonal rainfall cycle is linked to low-level wind direction over the Andean foothills. Some studies projected the rainfall variation over the South American Altiplano due to climate change (e.g., Thibeault et al., 2010; Minvielle and Garreaud, 2011). Based on a regression analysis, they found, reduced rainfall in the Altiplano by the end of this century due to climate change and temperature variation (Minvielle and Garreaud, 2011).

Previous Studies of Parameterization of Mean Orographic Rainfall

Some other previous studies analyzed mean orographic rainfall in the regions where complex terrain is similar to South America (e.g., Smith, 1979, 2003; Smith and Barstad, 2004; Smith, 2006; Smith and Evans, 2007). Smith (1979) analyzed orographic rainfall based on the upslope model, also used by Minder et al. (2011). Their model investigates the precipitation rate under idealized conditions defined by idealized mean-annual temperature profiles and when the saturated air with given specific humidity (q_v, the mixing ratio), density (ρ), and wind velocity ($\bar{U}$) reaches and parallels the topography $h(x, y)$. Under these conditions the precipitation rate is:

$$S(x, y) = \rho q_v \bar{U} \cdot \nabla h(x, y) \tag{1.1}$$

This model relies on two main parameters defined as moisture flux ($\rho q_v \bar{U}$) and the topographic slope (∇h) (Smith, 1979, 2006).

It is rare to have idealized conditions concerning atmospheric temperature and density, as assumed in the upslope model. Smith and Barstad (2004) improved the model and created an analytically tractable linear model of orographic rainfall in complex terrain in the Olympic Mountains in Washington State. They considered airflow dynamics, cloud time scales, advection of condensed water, and leeside evaporation. However, the main constraints of their model are: it is not suitable for unstable conditions, and it does not account for the vertical variations of atmospheric parameters (Smith and Barstad, 2004; Barstad and Schüller, 2011). Also, their model focuses on mean rainfall but does not investigate the event or extreme rainfall.

Bookhagen and Burbank (2010) analyzed the influence of topography and relief on rainfall. They concluded that a simple relief metric can be used as a first-order parameter for characterizing the location of orographic rainfall induced by monsoonal climates. They found that locations of high relief are good indicators for the occurrence of mean annual maximum rainfall (Bookhagen and Burbank, 2006). Similarly, Bookhagen and Strecker (2008) identified the threshold elevation that leads to the orographic rainfall peak along the eastern Andes. All of these studies that analyze the orographic rainfall focus on mean rainfall using static climatic variables and do not allow for atmospheric variability.

Most of the past studies described above do not take into account the atmospheric boundary conditions leading to deep convection and extreme rainfall (e.g., Castino et al., 2017; Rohrmann et al., 2014; Boers et al., 2015, 2016; Bookhagen and Strecker, 2008; Castino et al., 2016; De la Torre et al., 2015). The lack of a proper understanding of the dominant climatic variables and atmospheric conditions that trigger extreme rainfall generation along the climatic and topographic gradients in the south–central Andes is the motivation for the present study of extreme rainfall in order to reduce the impact of severe flooding in downstream areas and to reduce the destruction of infrastructure necessary for economic success and social well-being.

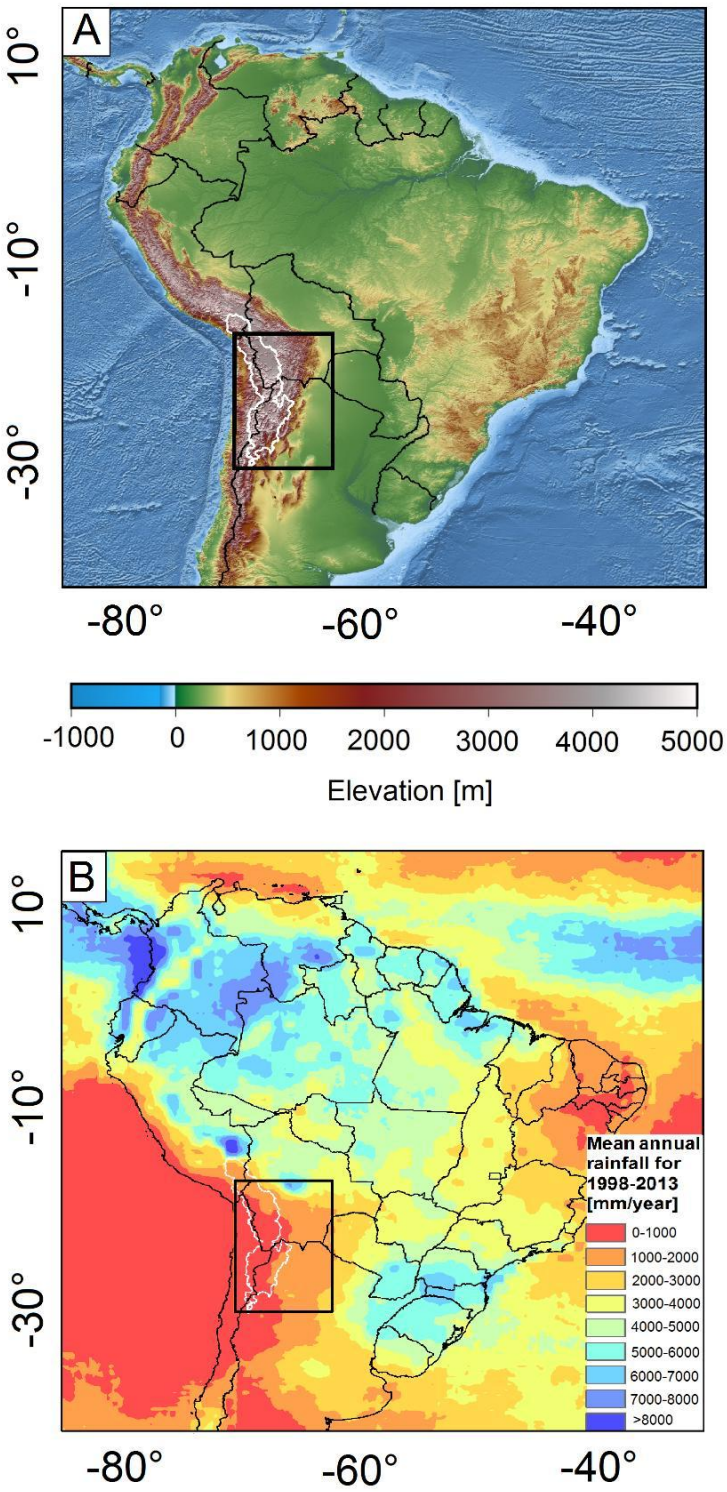

Figure 1.1 – Topographic and Climatic overview of South America. (A) Topography taken from: https://www.gebco.net/data_and_products/gridded_bathymetry_data/version_20141103 data. The study region in NW Argentina is indicated by a black box and the outline of the internally-drained Central Andes is in white. (B) Mean annual rainfall derived from TRMM data (Kummerow et al., 1998), product 3B42 (Huffman et al., 2007), https://disc.gsfc.nasa.gov/datasets/TRMM_3B42_Daily_7/summary (Version 7) (1999-2013) shows the wet band along the eastern Andes.

Climatic Setting of South America

The South American Monsoon System (SAMS) is characterized as the most important climatic feature of South America (Vera et al., 2006a). During the austral summer months (DJF) the large scale circulation is characterized by:

(1) an anticyclonic circulation over Bolivia at upper levels, which is known as the Bolivian High (BH). It results from both the condensational heating of the Amazon basin and the heat released by strong convection and rainfall over the Bolivian Altiplano (Chen et al., 1999; Gutman and Schwerdtfeger, 1965; Lenters and Cook, 1997) (Figure 1.2);

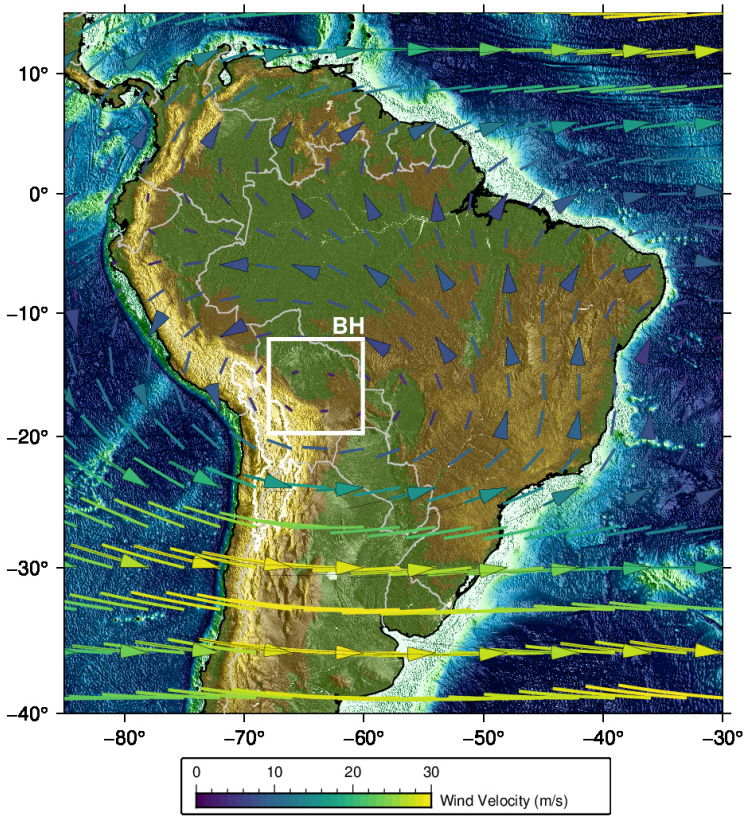

Figure 1.2 – Average 200-hPa wind speed for DJF (1999–2013) based on ERA-interim reanalysis data shows the Bolivian High (BH), white box activity eastward of the south-central Andes ∼70° W and 17° S. This is often associated with deep convection. The arrows indicate wind direction and are proportional to wind speed. White polygon outlines the Central Andean Plateau. The strong upper-level westerlies represented in the east of south-central Andes trigger the formation of the Mesoscale Convection Systems (MCSs) in connection with the South American Low-Level jet (SALLJ) activity.

(2) the South Atlantic Convergence Zone (SACZ); and (3) the South American Low-Level Jet east of the Andes (SALLJ) as the most important low-level features (Marengo et al., 2012) (Figure 1.4).

At seasonal timescales and during the austral summer (DJF), the southward movement of the intertropical convergence zone (ITCZ) and the thermal difference between land and ocean lead to the transportation of moist air from the Amazon and tropical North Atlantic to subtropical South America (Zhou and Lau, 1998; Boers et al., 2015). The ITCZ occurs at the transition between the northeast and southeast trade wind systems and forms a zone of surface wind convergence (Figure 1.3). The latitudinal location of the ITCZ in the Atlantic extends from the equatorial region during austral summer to about 10°–15°N in late austral winter (August) (Grodsky and Carton, 2003) (Figure 1.3).

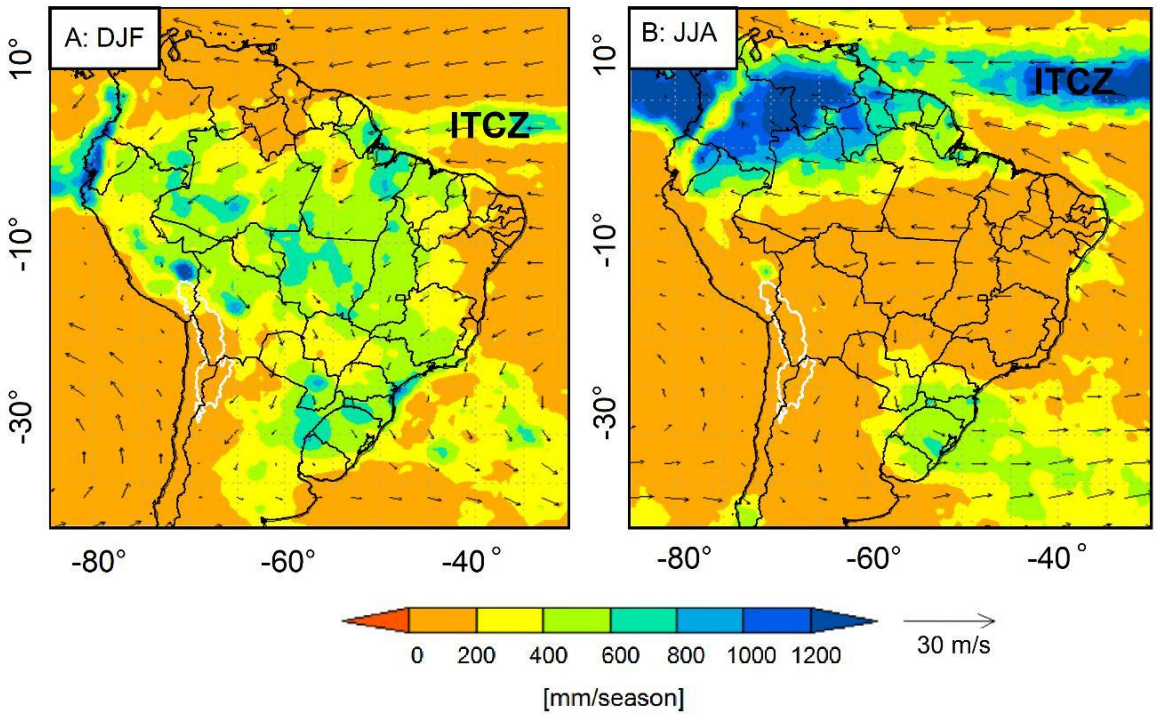

Figure 1.3 – Mean seasonal rainfall derived from TRMM data (Kummerow et al., 1998), product 3B42 (Huffman et al., 2007) https://disc.gsfc.nasa.gov/datasets/TRMM_3B42_Daily_7/summary (Version 7) (1999-2013) for DJF (A) and for JJA (B). The arrows indicate wind direction at 850-hPa and are proportional to wind speed (based on ERA-interim reanalysis data). The ITCZ is represented as a band of high rainfall at the transition between the northeast and southeast trade winds at different latitudinal locations for DJF (A) and for JJA (B).

The direction of the moist air being transported to subtropical South America forms the SACZ and the SALLJ dipole pattern (Vera et al., 2006a; Marengo et al., 2012). The westerly flow associates with the formation of SACZ (Carvalho et al., 2002, 2004).

The SACZ is characterized as a band of strong convective activity that expands from the northwest (Amazonia) into the southeast (south Atlantic) (e.g., Barreiro et al., 2002; Kodama, 1992; Carvalho et al., 2004, 2002).

The southward flow is defined as SALLJ, a low-level wind that transports the moist air from the tropical North Atlantic and the Amazon to subtropical South America along the eastern Andes (Marengo et al., 2004). The SALLJ associates with extreme rainfall in southeastern South America (SESA) (Marengo et al., 2004; Boers et al., 2015; Marengo et al., 2012). The 850 hPa austral summer months (DJF) wind anomaly represents a large anomaly during the DJF season east of the central Andes (Figure 1.4).

The two phases of the dipole are defined by: (1) strengthening of SACZ and hence suppression of convection to the south (2) suppression of SACZ and hence development of convection in the sub-tropical and intensification of the SALLJ (Marengo et al., 2012).

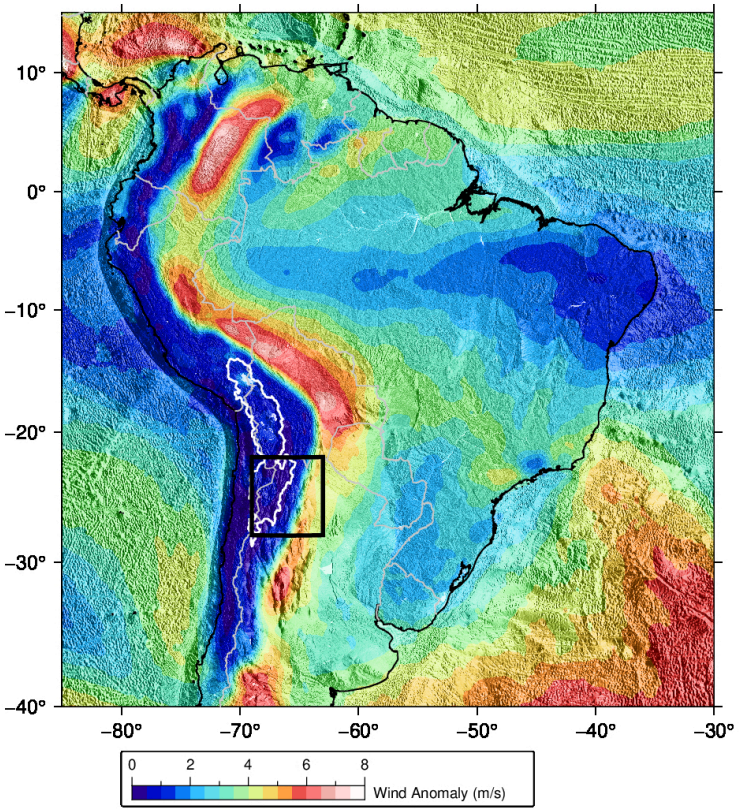

Figure 1.4 – The 850-hPa austral summer months (DJF) wind anomaly with respect to the rest of the year (1999–2013) based on ERA-interim reanalysis data. There is a large anomaly during the DJF season east of the central Andes (bright red colors). Note similar effects in the study area outlined by a black box. The white line outlines the central Andean plateau. Also, note the moderate to high anomalies from SESA to the Central Andes.

The Bonner (1968) identified a criteria for detecting the low-level jet events over the North American Great Plains. Based on Bonner (1968) criteria the low-level jet is observed when the low level wind speed (850 hPa) exceeds 12 m/s, the 850–700 hPa wind shear exceeds 6 m/s and once the meridional component of wind is negative and larger than zonal component. The Montini et al. (2019) introduced a new criteria for detecting the SALLJ events considering the seasonal variations of wind over South America. Based

on Montini et al. (2019) criteria the SALLJ event is observed when wind speed at 850 hPa and the vertical profile of wind speed between 850 and 700 hPa are greater than their 75th seasonal percentile thresholds. The SALLJ activity over Santa Cruz de la Sierra -a location along jet activity- relying the criteria above and considering magnitude of wind speed and vertical profile of wind is detected and shown in (Figure 1.5A,B) and (Figure 1.6).

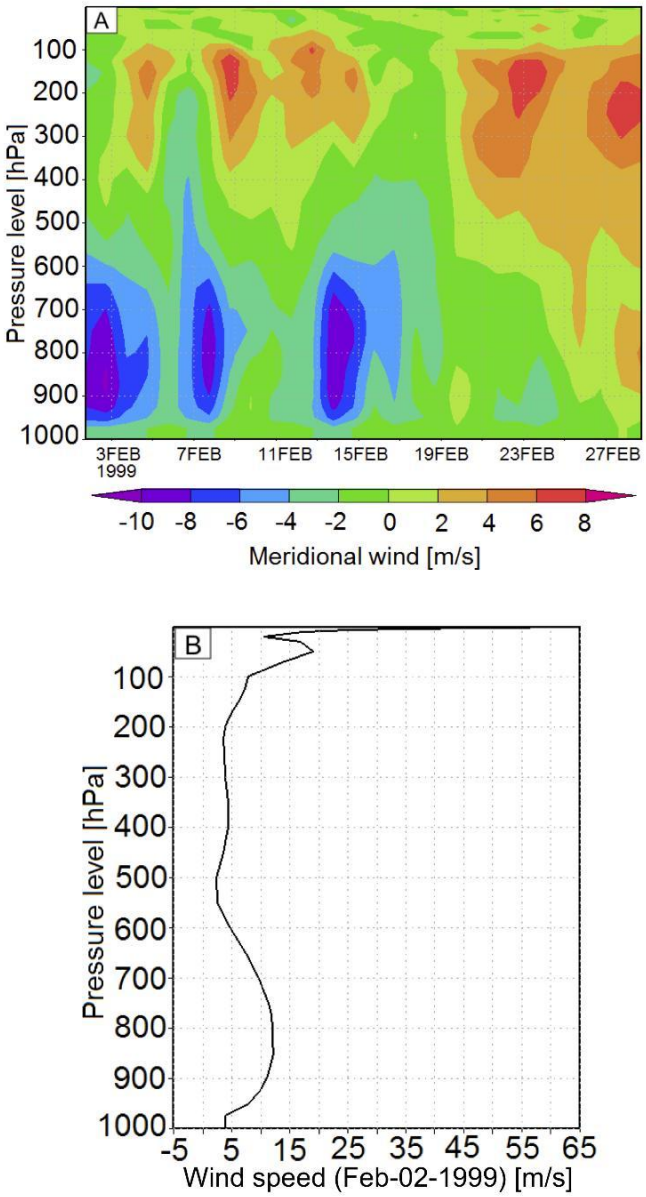

Figure 1.5 – The vertical profile of the meridional component of wind for February 1999 based on ERA-interim reanalysis data (A). The vertical profile of wind for 2nd of Feb 1999 (B). An episode of LLJ is detected on 2nd of Feb 1999 in Santa Cruz de la Sierra. The meridional component on 2nd of Feb 1999 is negative and indicates the northerly wind direction. The wind speed (850-hPa) and the 850–700-hPa wind shear show the South American Low-Level jet (SALLJ) activity over Santa Cruz de la Sierra.

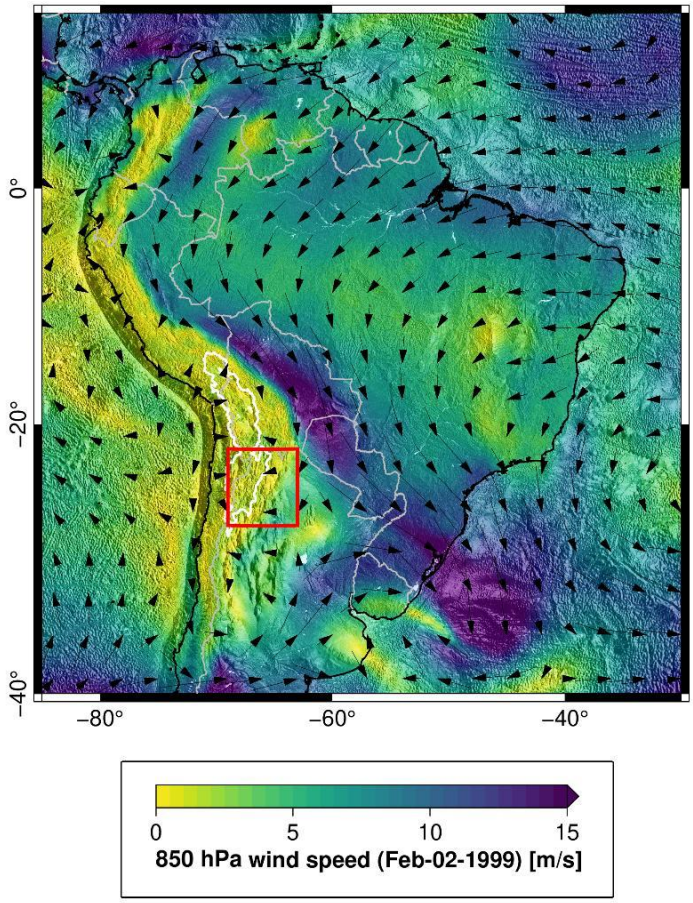

Figure 1.6 – The 850-hPa wind speed for 2nd of Feb 1999 based on ERA-interim reanalysis data. The active episode of South American Low-Level jet (SALLJ) is represented east of the Andes. The study area is indicated by the red box and wind direction is indicated by black arrows (size is proportional to velocity). The white line outlines the central Andean plateau.

From Continental to Regional Effects: Topographic Barriers and Mesoscale Convection Systems (MCSs)

The interplay of topography and the wind systems at low and upper levels mentioned above is often responsible for the formation of the mesoscale convective systems (MCSs) (Rohrmann et al., 2014; Rasmussen and Houze, 2011; Salio et al., 2007; Durkee et al., 2009). These frequently lead to heavy rainfall along the eastern Andes. As mentioned above, the moist air is transported to subtropical South America along the eastern Andes by the South American Low-Level Jet (SALLJ) (Marengo et al., 2004). This moist and warm air is affected by the subsidence of dry air transported by westerly upper-level wind systems to the south-central Andes. As a result, it is interrupted to rise, and hence, the MCSs are formed. The later phase is characterized by temperature rises through solar heating that triggers the condition for forming

deep convective storms along the south-central Andes (Romatschke and Houze, 2010; Rasmussen and Houze, 2016; Pingel et al., 2016; Rohrmann et al., 2014; Rasmussen and Houze, 2011).

Geographic and Climatic Setting of NW Argentina

The Andes are located along the west coast of South America and extend from about 10° N in tropics to 53° S in subtropics (Garreaud, 2009). The Central Andean Plateau (Altiplano-Puna Plateau), the second-highest Plateau on the Earth, lies in the west with a mean elevation of approximately 3,700 m (Allmendinger et al., 1997). The northern central Andean Plateau is referred to as Altiplano, in contrast, the southern Andean Plateau, which is called the Puna Plateau (or Puna de Atacama Plateau) (Figure 1.1A). In the east of the south-central Andes, there is the low-elevation foreland area with elevations of 800m (Figure 1.1A).

The south-central Andes in NW Argentina is exposed to a high rainfall asymmetry (Figure 1.1A,B). The east-west direction is identified by steep rainfall gradients (Bookhagen and Strecker, 2008, 2012) caused by high topographic gradients. A rainfall asymmetry also exists in the north-south direction resulting from the climatic regime variation from the tropical central Andes to the subtropical south-central Andes (Rohrmann et al., 2014; Boers et al., 2015).

The Andes extend from the tropics to the subtropics (Garreaud, 2009), therefore the south-central Andes in NW Argentina are sensitive to the tropical and subtropical upper-level large scale circulation. During austral summer (DJF), the upper-level westerlies get stronger in its southernmost position in the subtropics (Figure 1.7A,B). This upper level wind is controlled by the Bolivian High (BH) (Chen et al., 1999; Gutman and Schwerdtfeger, 1965; Lenters and Cook, 1997) (Figure 1.2). This upper level wind leads to the more frequent formation of deep convective storms in connection with the South American Low-Level jet (SALLJ) activity over the subtropical region compared to tropical regions along the eastern Andes. This suggests the existence of different climatic regimes along the topographic and climatic gradients over the south-central Andes (Castino et al., 2017).

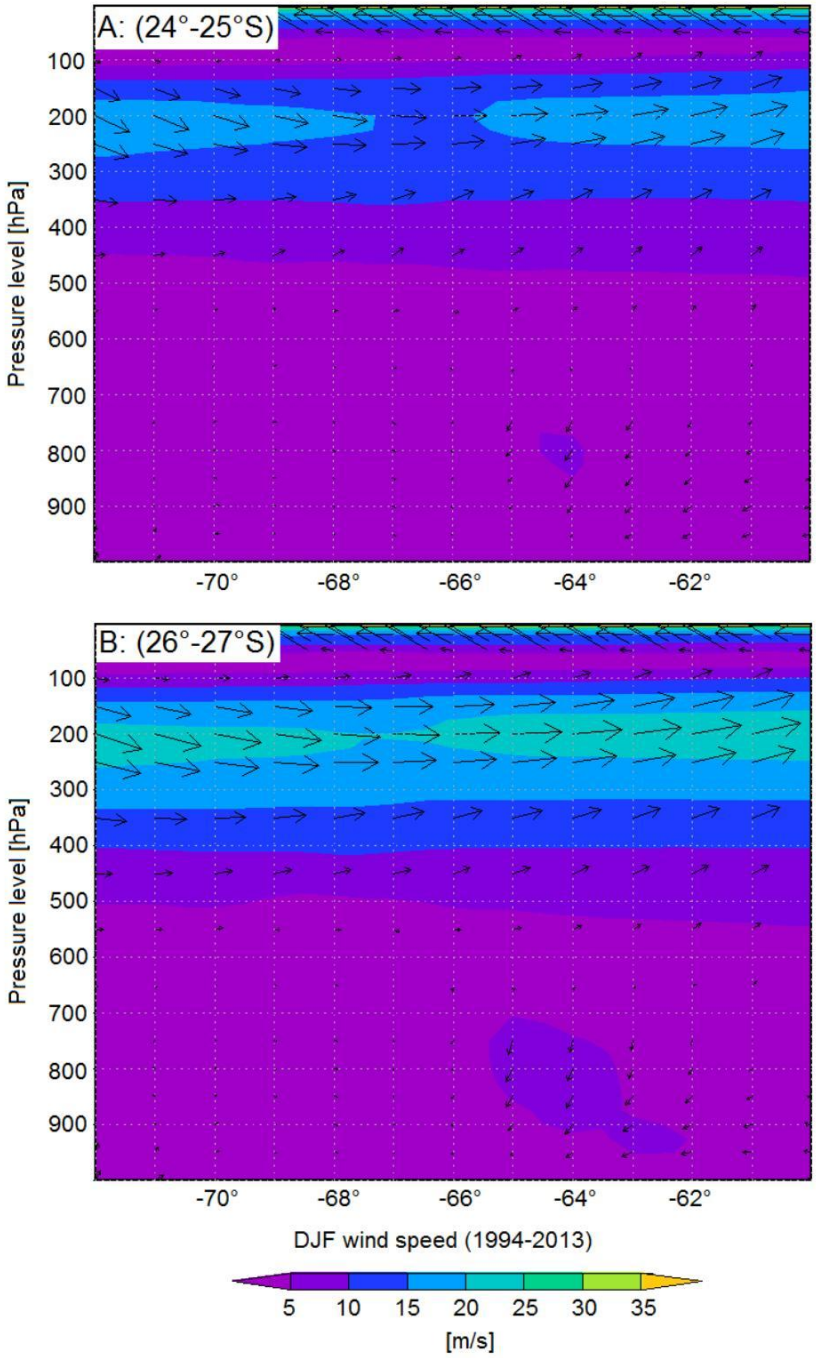

Figure 1.7 – Pressure-longitude cross section of the wind speed (1994-2013) based on ERA-interim reanalysis data at tropical (A) and subtropical (B) south-central Andes during austral summer (DJF). The stronger westerlies at the upper levels associated with the subtropical jet are represented in the subtropics. This leads to a higher formation of deep convective storms over the subtropical region.

Research Questions

This thesis mainly focuses on identifying the atmospheric driving processes of extreme rainfall in the eastern Andes of NW Argentina. This area is frequently affected by hydrometeorological extreme events that cause infrastructural damage and economic losses. This study relies on multi-dataset analysis including: ECMWF (European Centre for Medium-Range Weather Forecasts)-Re-Analysis (ERA-interim) data (Dee et al., 2011), https://apps.ecmwf.int/datasets/data/interim-full-daily/levtype=sfc/, TRMM (Tropical Rainfall Measuring Mission) rainfall data (Kummerow et al., 1998), product 3B42 (Huffman et al., 2007), https://disc.gsfc.nasa.gov/datasets/TRMM_3B42_Daily_7/summary (Version 7) and GNSS (Global Navigation Satellite System), https://www.ign.gob.ar data which helps to perform a reliable analysis of the spatiotemporal variability of extreme rainfall in the eastern Andes. The main aim of this study is to identify the dominant atmospheric conditions and climatic variables that trigger extreme rainfall along the steep topographic and climatic gradients over the eastern Andes.

This goal is addressed by answering the following research questions that will contribute to a better understanding of the role of dominant climatic variables on extreme rainfall generation over the southern Central Andes:

- Can the spatiotemporal pattern of extreme rainfall events be described by a combination of dewpoint temperature and CAPE (convective available potential energy)? These have been identified as crucial climatic variables responsible for triggering deep convective storm systems, and are, hence, of importance for forming extreme rainfall events along the steep topographic and climatic gradients in the south-central Andes (Chapter 2).

- Can high temporal resolution integrated water vapor (IWV) based on Global Navigation Satellite System (GNSS) data be used as a reliable humidity indicator together with other dominant climate variables such as CAPE to understand convective processes in the eastern Andes? Can GNSS-IWV station data be used as a predictor for extreme rainfall in the eastern central Andes, and what are the associated timescales? (Chapter 3).

- At a regional perspective of the Central Andes, what is the effect of local convection, and what formation times are associated with these events? (Chapter 4).

Chapter 2

Using Convective Available Potential Energy (CAPE) and Dew-Point Temperature to Characterize Rainfall-Extreme Events in the South- Central Andes[†]

Maryam Ramezani Ziarani[1,2], Bodo Bookhagen[1], Torsten Schmidt[2], Jens Wickert [2,3], Alejandro de la Torre[4], Rodrigo Hierro[4]

[1] *University of Potsdam, Institute of Geosciences, Karl-Liebknecht-Str. 24-25, 14476 Potsdam, Germany*

[2] *German Research Centre for Geosciences GFZ, 14473 Potsdam, Germany*

[3] *Institute of Geodesy and Geoinformation Science, Faculty VI, Technische Universität Berlin, 10623 Berlin, Germany*

[4] *CONICET, Facultad de Ingeniería, Universidad Austral, LIDTUA (CIC), 1629 Pilar, Buenos Aires, Argentina*

Abstract

The interactions between atmosphere and steep topography in the eastern south–central Andes result in complex relations with inhomogenous rainfall distributions. The atmospheric conditions leading to deep convection and extreme rainfall and their spatial patterns—both at the valley and mountain-belt scales—are not well understood. In this study, we aim to identify the dominant atmospheric conditions and their spatial variability by analyzing the convective available potential energy (CAPE) and dew-point temperature (T_d). We explain the crucial effect of temperature on extreme rainfall generation along the steep climatic and topographic gradients in the NW Argentine Andes stretching from the low-elevation eastern foreland to the high-elevation central Andean Plateau in the west. Our analysis relies on version 2.0 of the ECMWF's (European Centre for Medium-Range Weather Forecasts) Re-Analysis (ERA-interim) data and TRMM (Tropical Rainfall Measuring Mission) data. We make the following key observations: first, we observe distinctive gradients along and across strike of the Andes in dew-point temperature and CAPE that both control rainfall distributions. Second, we identify a nonlinear correlation between rainfall and a combination of dew-point temperature and CAPE through a multivariable regression analysis. The correlation changes in space along the climatic and topographic gradients and helps to explain controlling factors

[†] *published as Maryam Ramezani Ziarani, Bodo Bookhagen, Torsten Schmidt , Jens Wickert, Alejandro de la Torre and Rodrigo Hierro. "Using Convective Available Potential Energy (CAPE) and Dew-Point Temperature to Characterize Rainfall-Extreme Events in the South- Central Andes." Atmosphere 2019, 10, 379.* https://doi.org/10.3390/atmos10070379

for extreme-rainfall generation. Third, we observe more contribution (or higher importance) of T_d in the tropical low-elevation foreland and intermediate-elevation areas as compared to the high-elevation central Andean Plateau for 90th percentile rainfall. In contrast, we observe a higher contribution of CAPE in the intermediate-elevation area between low and high elevation, especially in the transition zone between the tropical and subtropical areas for the 90th percentile rainfall. Fourth, we find that the parameters of the multivariable regression using CAPE and T_d can explain rainfall with higher statistical significance for the 90th percentile compared to lower rainfall percentiles. Based on our results, the spatial pattern of rainfall-extreme events during the past ∼16 years can be described by a combination of dew-point temperature and CAPE in the south–central Andes.

Keyword: eastern south–central Andes; extreme rainfall; deep convection; convective available potential energy; dew-point temperature.

Introduction

The south–central Andes are characterized by steep gradients in topography, climate, and ecology supporting a diverse environment with economic significance. This region is repeatedly affected by hydrometeorological extreme events that impact infrastructures through mass movements and cause flooding downstream in agricultural, societal important, and populated areas, (e.g., Olen and Bookhagen, 2018; Castino et al., 2017; Boers et al., 2014a).

The understanding and investigation of extreme rainfall in the south–central Andes of NW Argentina has been hampered by complex interaction between the atmosphere and steep topography that can be summarized by the following four specific challenges: (1) High relief and steep terrain with elevations ranging from ∼800 m in the foreland to >6000 m at mountain peaks cause complex rainfall patterns with strong, local impact (Bookhagen and Strecker, 2012; Castino et al., 2017). Past studies describe the strong orographic rainfall effect of the south–central Andes (Bookhagen and Strecker, 2008). The analysis of orographic rainfall and intense storms in the south–central Andes has been challenging because of sparse instrumental data (Castino et al., 2017, 2016; De la Torre et al., 2015) and high terrain variability that complicates deriving precipitation amounts from weather models (Norris et al., 2017); (2) highly seasonal wind patterns control the moisture influx and rainfall intensity in this region (Garreaud, 2009; Vuille and Keimig, 2004). Specifically, the strong warm and dry upper-level westerlies that occur east of the Andes during the austral summer trigger deep convection in connection with low-level wind flow and associated shear that cause extreme rainfall in this region (Garreaud, 2009; Vuille and Keimig, 2004; Rasmussen and Houze, 2016; Pingel et al., 2016; Rohrmann et al., 2014); (3) the region lies at the climatic transition zone between the tropical and subtropical atmospheric circulation regimes. Transfer of moisture and thermal energy occurs along and across the transition zone between these two climatic regimes (Rasmussen et al., 2016; Rohrmann et al., 2014; Romatschke and Houze, 2010; Boers et al., 2014a). The tropics are regions characterized by more humidity and lower frequencies of storm formation; however, the sub-tropical regions have a higher frequencies of deep convective storms and higher seasonal rainfall. Both moisture transport from the tropics and deep convective activity in the sub tropics, result in high convection and rainfall in this region (Rohrmann et al., 2014); and (4) formation of mesoscale convective systems (MCSs): the complex interplay of topography, moisture transport, and the wind and thermal fields mentioned above lead to the formation of deep convection (Rohrmann et al., 2014) that results in extreme rainfall. Water vapour originates in the tropical North Atlantic and the Amazon, is transported through the

trade winds westwards and travels southward to subtropical South America along the eastern Andes through the South American Low-Level Jet (SALLJ), a low-level wind system (Marengo et al., 2004). This moist and warm air is prevented from rising due to the subsidence of dry air coming through westerly wind systems to the south–central Andes. Because of the wind shear between upper level winds and the SALLJ, MCSs are formed. Once temperature rises, for example through solar heating, the associated thermal energy provides the condition for forming deep convective storms along the south–central Andes (Romatschke and Houze, 2010; Rasmussen and Houze, 2016; Pingel et al., 2016; Rohrmann et al., 2014). The combination of these atmospheric processes described above show that the south–central Andes are a region characterized by highly seasonal and extreme rainfall events.

As mentioned above, the temperature rise triggers the condition for formation of deep convective storms along the south–central Andes. Past studies indicate the crucial role of the atmospheric temperature on rainfall intensity. For example, references Berg and Haerter (2013); Berg et al. (2009, 2013) investigated the strong impact of temperature on convective rainfall. In all of these studies, the changes in the intensity of rainfall with temperature were explained by the Clausius–Clapeyron (CC) relation. The CC relation explains the rate of about 6.8% $^{\circ}C^{-1}$ increase of rainfall with increasing temperature (Panthou et al., 2014; Lepore et al., 2015). The convective storms which are triggered by temperature rise increase the atmospheric water content and hence increase (extreme) rainfall amount. It has been suggested that dew-point temperature can be used as a meteorological variable to indicate the humidity rate and hence extreme rainfall amounts and also can be compared with the CC relation (Lepore et al., 2015). Lepore et al. (2015) investigated the relationship between extreme rainfall and dew-point temperature in the east of the Rocky Mountains in the United States where orographic storms are similar to southeastern South America (Rasmussen and Houze, 2011). Haider et al. (2018) also investigated the relation between dew-point temperature and precipitation extremes. They identified dew-point temperature as a reliable variable for understanding the extreme rainfall under a warming climate over the tropics. They suggested that a close scaling to the CC relationship is observed when surface air temperature is substituted by dew-point temperature.

The deep convection and rainfall extremes are not only triggered by available water content but by temperature effects on the atmospheric stability. The parameter describing atmospheric stability is the convective available potential energy (CAPE) (Lepore et al., 2015). CAPE indicates the amount of energy available for convection (North and Erukhimova, 2009). If CAPE is efficiently transferred to parcel kinetic energy the amount of energy of a rising air parcel and therefore the rainfall intensity are commensurate to $\sqrt{CAPE}$, which is defined by meteorological parcel theory (Bluestein, 1993; North and Erukhimova, 2009; Lepore et al., 2015) (assuming idealized conditions). Gettelman et al. (2002) investigated a positive correlation between CAPE and surface temperature over the tropics. They show that an increase in surface temperature leads to higher CAPE. Other studies show the crucial role of convection associated with extreme rainfall over the tropical systems (Monkam, 2002). Furthermore, Mesgana and Thian (2017) defined CAPE as a proxy for extreme rainfall over the United States and Southern Canada. Thus, CAPE can be used as an atmospheric stability parameter to parameterize extreme rainfall.

Several previous studies analyzed the spatiotemporal distribution of annual and extreme rainfall in the greater NW Argentine Andes, but often do not take into account the atmospheric boundary conditions leading to deep

convection and extreme rainfall (e.g., Castino et al., 2017; Rohrmann et al., 2014; Boers et al., 2015, 2016; Bookhagen and Strecker, 2008; Castino et al., 2016; De la Torre et al., 2015).

The aim of our study is to identify the dominant atmospheric conditions and climatic variables leading to deep convection and rainfall extreme events in the south–central Andes by focusing on convective available potential energy (CAPE) and dew-point temperature (T_d).

Continental and Regional Climatic Setting

Climatic Setting of South America

The Andes are located along the west coast of South America and extend from about 10° N to 53° S (Garreaud, 2009). Moisture transport in South America is controlled by the SALLJ and the activity of the South Atlantic Convergence Zone (SACZ). Both of these atmospheric circulation systems constitute the most important components of the South American Monsoon System (SAMS), (e.g., Vera et al., 2006a; Marengo et al., 2012). The SAMS and its associated strong convective activity contribute to intense rainfall over tropical and sub-tropical regions in South America during the austral summer months (DJF), (e.g., Carvalho et al., 2012; Vera et al., 2006a; Marengo et al., 2012; Zhou and Lau, 1998).

During the austral summer season, moist air flows from the Amazon and tropical North Atlantic to subtropical South America due to the southward shift of the intertropical convergence zone (ITCZ) and the thermal difference between land and ocean (Zhou and Lau, 1998; Boers et al., 2015). The ITCZ is a zone of wind convergence near the equatorial region (more detailed descriptions of the ITCZ can be found in, for example, (Grodsky and Carton, 2003)). The direction of this moist air flowing to the subtropical South America is associated with the South American rainfall dipole, which is often considered the most important component of SAMS (Vera et al., 2006a; Marengo et al., 2012).

The eastward anomalies of this flow generate heavy rainfall along the SACZ (Carvalho et al., 2002, 2004). The SACZ is defined as the region with a strong convective activity band stretching from the northwest (Amazonia) into the southeast (south Atlantic), (e.g., Barreiro et al., 2002; Kodama, 1992; Carvalho et al., 2004, 2002). The southward anomalies (SALLJ) at the eastern flank of the Andes trigger heavy rainfall in south–eastern South America (SESA) (Marengo et al., 2004; Boers et al., 2015). The deep convection is triggered by temperature rise and thermal energy during the daytime through solar heating (Romatschke and Houze, 2010). The diurnal timing investigated by Romatschke and Houze (2010) documents the strongest activity of SALLJ during the night, which was triggered by the deep convection during the afternoon and evening (local times). This is explained by a strong wind shear between upper level winds and the SALLJ that leads to intense instability and rising of the low level flow in the eastern south–central Andes (Romatschke and Houze, 2010).

As it is represented in Climatological wind speed (1999–2013) at 850 hPa (Figure 2.1), during austral summer (DJF) the strong northeast trade winds near the equatorial region turn to the southwest after reaching the Andes and producing a high wind speed east of the central Andes (Marengo et al., 2004).

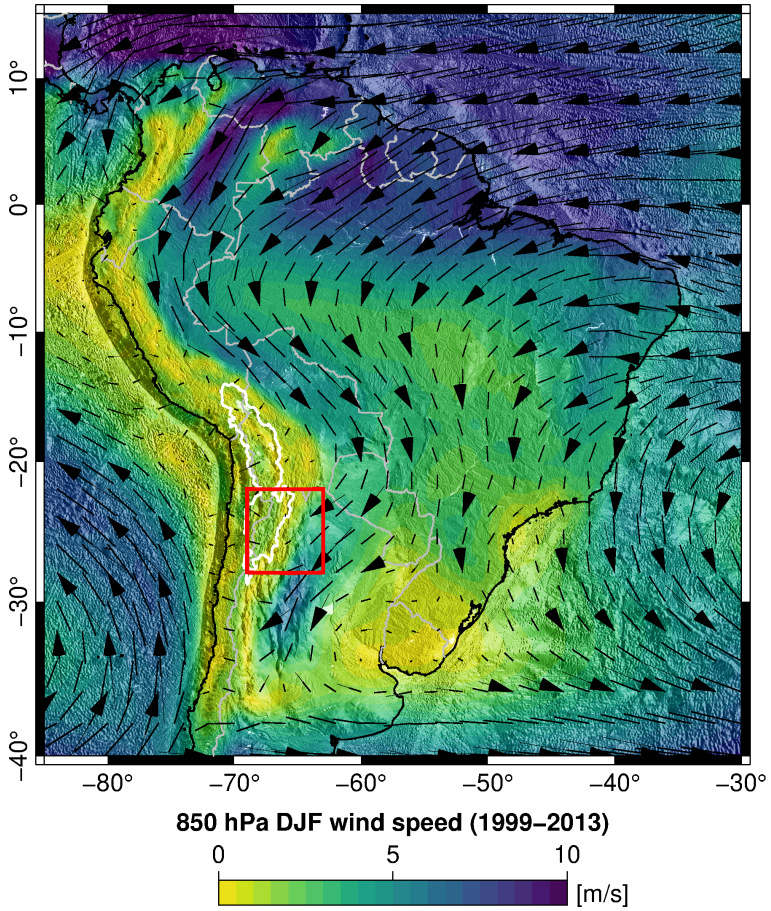

Figure 2.1 – The 850-hPa austral summer months (DJF) mean wind speed (1999–2013) based on ERA-interim reanalysis data. The high wind speed is shown east of the central Andes. Note that wind speed is stronger during SALLJ active episodes than the represented seasonal mean in this figure. The study area is indicated by the red box and wind direction is indicated by black arrows (size is proportional to velocity). White line outlines the central Andean Plateau.

The divergent circulation during the austral summer (Figure 2.2) represents the low-level convergence activity over both, the northern and southern central Andes as a result of extreme convection during afternoon and evening, which is followed by the early and mid-daytime thermal energy (Romatschke and Houze, 2010). Divergent circulation is defined as (Wallace and Hobbs, 2006):

$$\left(\frac{\partial u}{\partial x}+\frac{\partial v}{\partial y}+\frac{\partial w}{\partial p}\right)=0 \tag{2.1}$$

$$\frac{\partial w}{\partial p}=-\nabla\cdot V, \tag{2.2}$$

where (Equation (2.1)) is the continuity equation in pressure coordinates. $\nabla \cdot V$ in (Equation (2.2)) is the horizontal component of divergence, w is the vertical velocity and p is pressure level. The horizontal divergence is defined as $(\nabla \cdot V > 0)$ while $(\nabla \cdot V < 0)$ shows the horizontal convergence.

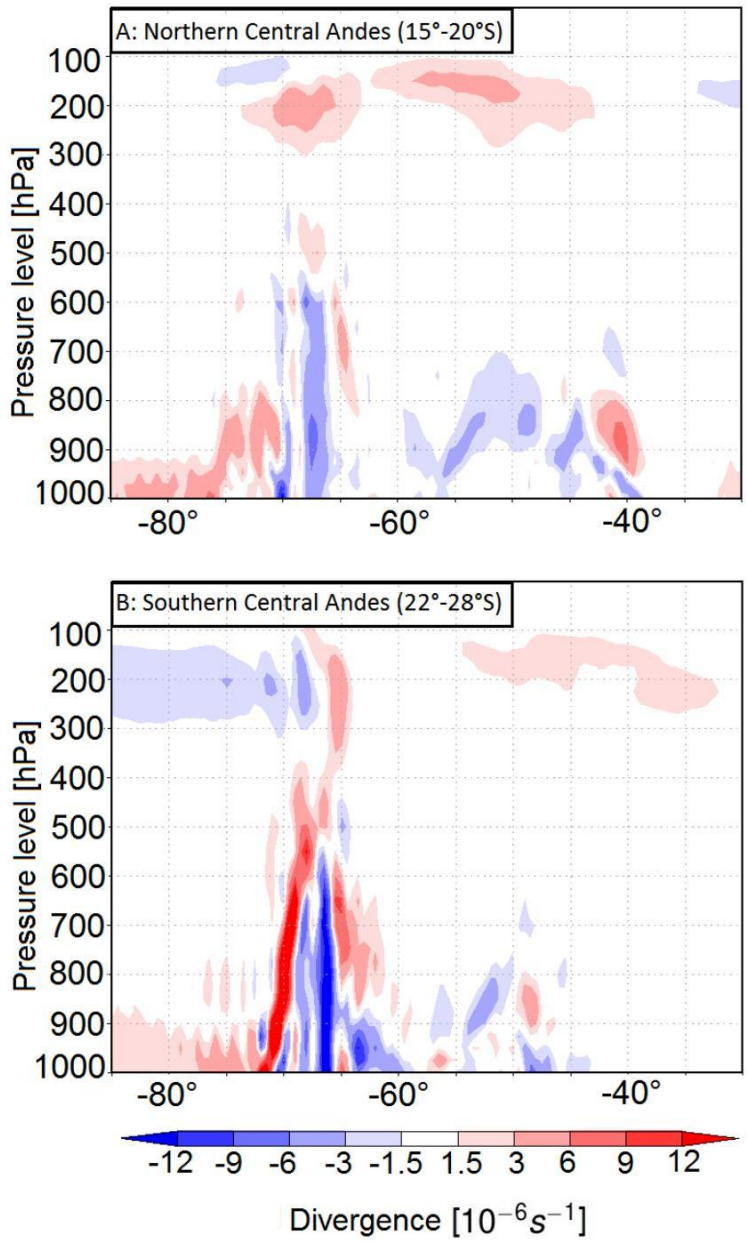

Figure 2.2 – Average divergences for DJF (1999–2013) for the latitude band 15°–20° S (A) and for the latitude band 22°–28° S (B) based on ERA-interim reanalysis data. See Equation (2.2) for the divergent calculation. Negative divergence is located east of the Andes at 67° W and indicates the low-level convergence activity along the mountain front of the south–central Andes. The upper level divergence at 200 hPa is associated with the Bolivian High (Figure 2.3, white box) and is a result of strong convection during austral summer. Note the stronger negative and positive divergence values in the sub-tropical south–central Andes (B).

The wind at upper levels in the study area is often controlled by the Bolivian High (BH) (Figures 2.2 and 2.3), an upper-level anticyclone associated with diabatic warming caused by the release of latent heat in the middle troposphere by large-scale convective activity in the Amazon Basin (Chen et al., 1999; Gutman and Schwerdtfeger, 1965; Lenters and Cook, 1997). Anticyclonic upper level flow is formed parallel to the high with strong subsidence to the west of the high that modulates convection in connection with low level flow in the region (Lenters and Cook, 1997).This circulation system sits eastward of the central Andean Plateau above the low-elevation foreland area and significantly influences convective rainfall patterns in connection with SALLJ and SACZ (Castino et al., 2017; Gandu and Silva Dias, 1998; Virji, 1981; Kousky and Kayano, 1994; Kousky and Alonso Gan, 1981; Vuille, 1999; Lenters and Cook, 1999; Vuille and Keimig, 2004).

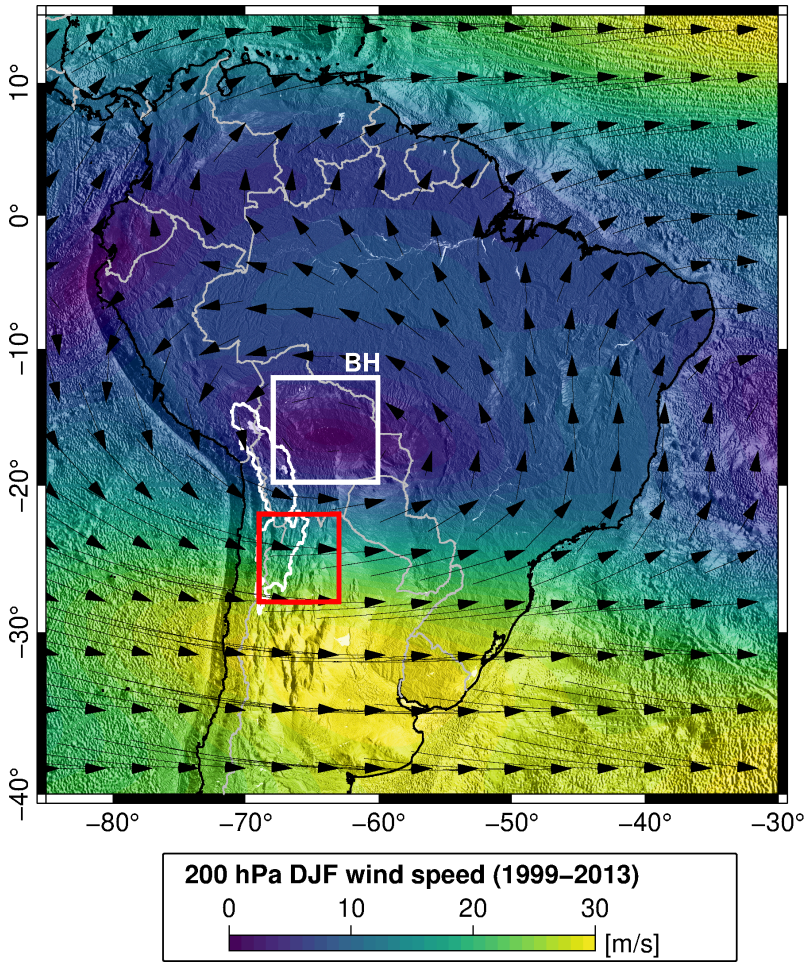

Figure 2.3 – Average 200-hPa wind speed for DJF (1999–2013) based on ERA-interim reanalysis data shows the Bolivian High (BH), white box activity eastward of the south–central Andes ∼70° W and 17° S as well as the strong upper level westerlies in the study area (red box). These are often associated with deep convection. Black arrows and line indicate wind direction and are proportional to wind speed. White polygon outlines the central Andean Plateau.

Regional Geographic and Climatic Setting of NW Argentina

The south–central Andes in NW Argentina are characterized by a strong rainfall asymmetry (Figure 2.4B). In the east-west direction exists one of the steepest rainfall gradients on Earth (Bookhagen and Strecker, 2008), resulting from the high topography and latitudinal position. In the west, the central Andean Plateau (Altiplano-Puna Plateau), the second highest Plateau on the Earth, extends from about 15° S to 27° S with a mean elevation about 3700 m (Allmendinger et al., 1997). The northern central Andean Plateau is called Altiplano, whereas the southern Andean Plateau is referred to as the Puna Plateau (or Puna de Atacama Plateau) (Figure 2.4A, A1). The central Andean Plateau is internally drained and the geomorphic areas of the Altiplano and Puna delineate different hydrologic catchment regimes. The low-elevation foreland area with elevations of 800m is located in the east of the south–central Andes (Figure 2.4A, A3). In the north-south direction, the rainfall intensity varies as the climatic regime shifts from the tropical central Andes to the subtropical south–central Andes (Rohrmann et al., 2014; Boers et al., 2015).

2.2.1 Study Region: NW Argentina

In order to analyze the climatic conditions leading to extreme rainfall in the study area, we divide the region (63°–69° W, 22°–28° S) into nine boxes with equal areas (1.5° ×1.5°) along the steepest climatic and topographic gradient (Figure 2.4A). The boxes go from high elevation to low elevation (numbers) and from the tropical central Andes to the subtropical south–central Andes (letters): A1, B1 and C1 are located in the high-elevation Puna Plateau (the southern central Andean Plateau); A2, B2 and C2 characterize an intermediate-elevation area exhibiting intramontane basins and high relief, and A3, B3 and C3 indicate the low-elevation foreland area. The north-south gradient stretches from the tropics (A1, A2 and A3), a transition zone between tropic and subtropic (B1, B2 and B3) and the subtropics (C1, C2 and C3). In the study area both the dew-point temperature and CAPE east-west (from A3 to A1, B3 to B1 and C3 to C1) gradients (Figure 2.4C,D) coincide with the rainfall gradient (Figure 2.4B) from low elevation foreland regions to the high-elevation central Andean Plateau.

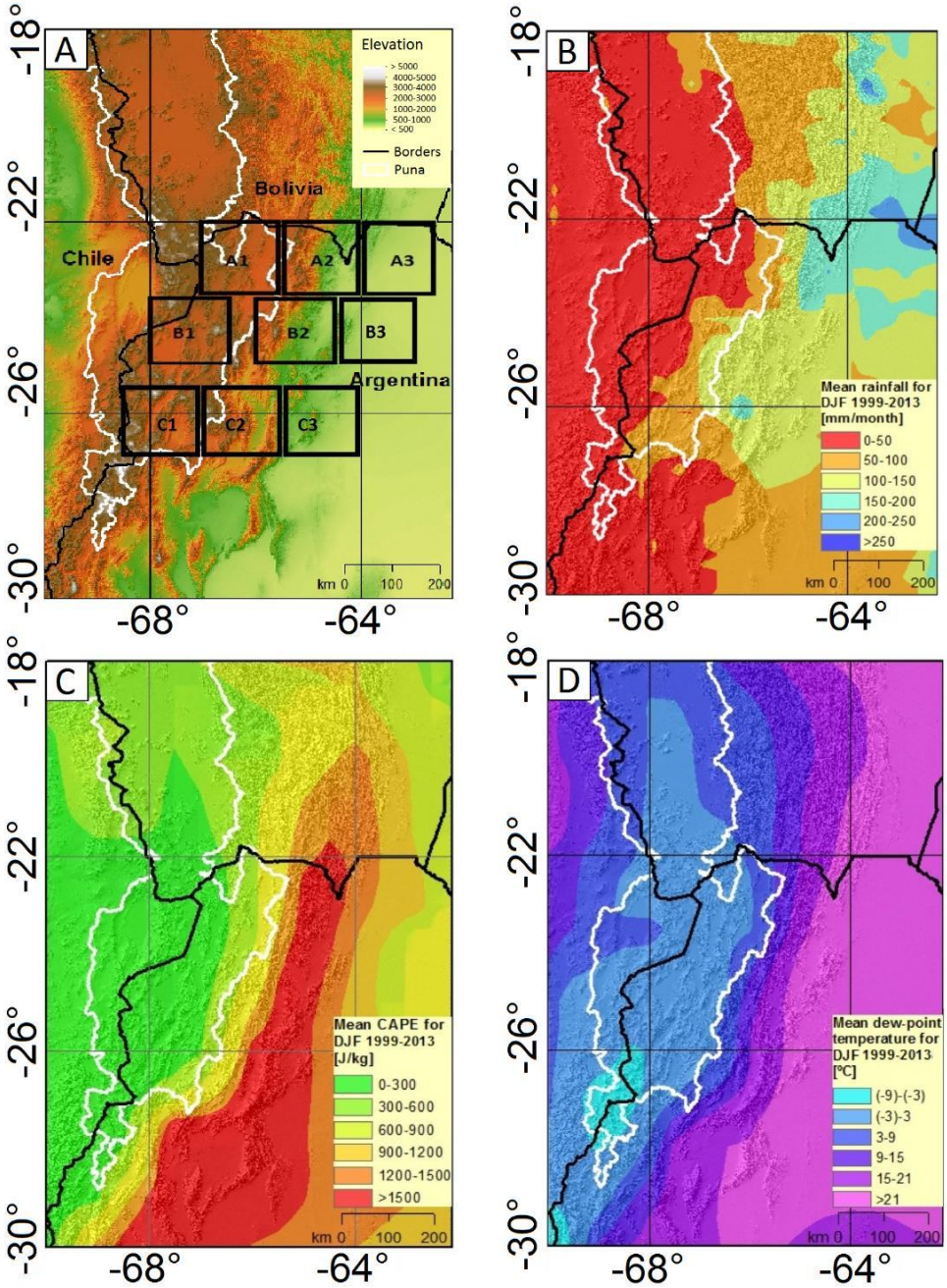

Figure 2.4 – (A) Topographic and climatic overviews of the study region in NW Argentina. White line outlines the central Andean Plateau, black lines are international borders. Boxes A1, B1, and C1 are in the high-elevation Puna Plateau (southern central Andean Plateau), boxes A2, B2, C2 are located in the intermediate elevation zone characterized by intramontane basins and high relief, and boxes A3, B3, C3 lie in the low-elevation foreland area. (B) Seasonal mean rainfall (DJF) derived from TRMM 3B42 (1999-2013) shows the E–W rainfall gradient with wet, low elevation foreland regions and the dry, high-elevation central Andean Plateau. (C) Seasonal mean CAPE based on ERA-interim reanalysis data shows the E–W atmospheric stability gradient. (D) Seasonal mean dew-point temperature based on ERA-interim reanalysis data shows the E-W atmospheric moisture availability gradient.

Data and Methods

Data

We used the version 2.0 of the ECMWF's (European Centre for Medium-Range Weather Forecasts) Re-Analysis (ERA-interim) data (Dee et al., 2011), https://apps.ecmwf.int/datasets/data/interim-full-daily/levtype=sfc/ to analyze temperature, dew-point temperature and CAPE. Dew-point temperature indicates the absolute specific humidity of the atmosphere (Westra et al., 2014). High values of dew-point temperature describes near saturated air and high-moisture availability in the air. CAPE is an area between the level of free convection (LFC) and the level of neutral buoyancy (LNB). The level of free convection is the pressure level with the positive buoyancy, where temperature of the surrounding air reduces faster than the moist adiabatic lapse rate of a saturated parcel. The level of neutral buoyancy is the pressure level where the temperature of the air parcel is equal to the surrounding air (Blanchard, 1998). T_{vp} and T_{ve} are the virtual temperature of the air parcel and surrounding environment, respectively. R_d is the gas constant and P is pressure (Ye et al., 1998):

$$CAPE = \int_{LFC}^{LNB} R_d(T_{vp} - T_{ve}) d\ln(P). \tag{2.3}$$

In addition to CAPE, convective inhibition (CIN) is also characterized as an important parameter which quantifies the energy provided by the triggering mechanisms for deep convection to be developed (Hierro et al., 2013; Rasmussen and Houze, 2016). CIN is defined as the amount of energy that the rising air parcel needs to overcome in order to reach to the level of free convection from its stable layer (Colby, 1984). The early and mid-daytime thermal energy causes the well-mixed boundary layer which leads to high CAPE and low CIN that favors the deep convection and extreme rainfall (Rasmussen and Houze, 2016). Since our study aims at understanding the effect of temperature rise through solar heating on deep convection, we put our focus on atmospheric stability parameter CAPE which is considered to be high as a result of daytime solar heating.

ERA-interim reanalysis data used in this study have a spatial resolution of $0.75^\circ \times 0.75^\circ$ and a temporal resolution of 6 h. We calculated the mean daily values from six hourly data.

TRMM (Tropical Rainfall Measuring Mission) data (Kummerow et al., 1998), product 3B42 (Huffman et al., 2007), https://disc.gsfc.nasa.gov/datasets/TRMM_3B42_Daily_7/summary (Version 7) with a spatial resolution of $0.25^\circ \times 0.25^\circ$ and daily temporal resolution have been used to identify rainfall values. TRMM rainfall data are interpolated on the ERA-interim grid (0.75°). We have interpolated data using the bilinear interpolation method. TRMM data has been shown to be a reliable dataset for capturing mean and extreme rainfall in South America (Carvalho et al., 2012; Boers et al., 2015). Our analysis was performed from 1998 to 2013. We defined an extreme event as rainfall above the 90th percentile of the rainfall time series. For example, for a daily 16 year time series, we used: 16 years of data $\times$ 365 days per year $\times$ 10% = 584 events at each study box, because we have calculated the mean value of all grid points for each study box. We have explored other methodologies (fitting gamma or stretched exponential distributions), but these were generally affected by statistic significance, because of the steep rainfall gradient in that region. See Figure 2.5 for the events above the 90th percentiles and Figure 2.4A for the boxes.

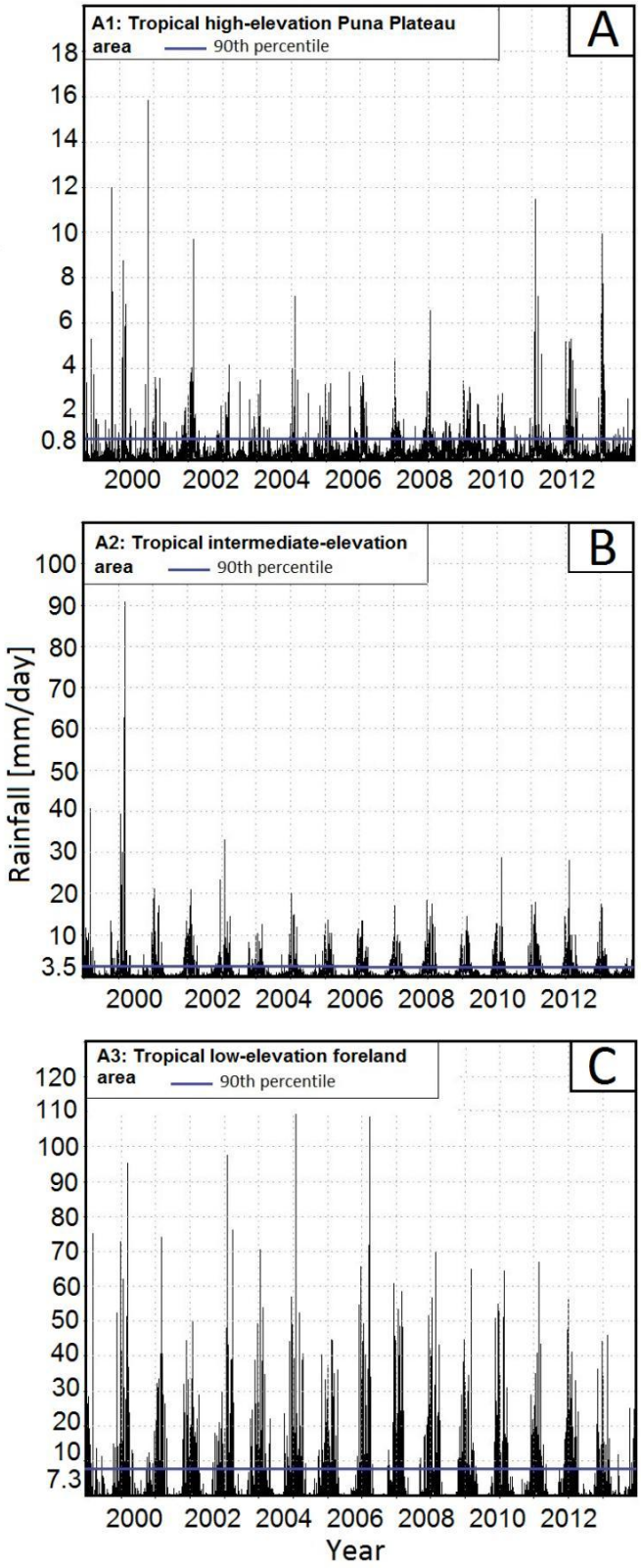

Figure 2.5 – TRMM 3B42 rainfall time series data (1998–2013) over the boxes A1 (A), A2 (B) and A3 (C). The 90th percentile is shown by blue vertical line and varies from 0.8 mm/day on the high-elevation Puna Plateau, to 3.5 mm/day in the intermediate elevation and to 7.3 mm/day in the low-elevation foreland area. Note the different Y-axis scales.

Identifying the Effect of Temperature on Deep Convective Storms and Extreme Rainfall Formation

We analyze the dominant climatic variables leading to extreme rainfall events by focusing on dew-point temperature and convective available potential energy to show the effect of temperature on atmospheric humidity (T_d) and on convection (CAPE) for deep convective storms (Lepore et al., 2015). We argue that these will help us to understand extreme rainfall events that are often triggered by deep convective storms along the steep climatic and topographic gradient in the eastern south–central Andes (22–28°S) (Rohrmann et al., 2014). Our study consists of the following steps:

First, we analyze the temporal correlation between temperature, dew-point temperature, and CAPE in conjunction with rainfall during the austral summer months. We also show the spatiotemporal correlation between both climatic variables and rainfall along the steep topographic gradient.

Second, we regress daily rainfall events that are above the 90th percentile onto daily values of CAPE and dew-point temperature in each box during event days using 16 years of data. This analysis indicates an exponential relationship between rainfall and dew-point temperature and suggests a power-law relation between rainfall and CAPE. Our regression coefficients undergo a comparison with the value ranges of CAPE and dew-point temperature in each box along the topographic and climatic gradient.

Previous research by North and Erukhimova (2009) and based on the CC relationship and idealized parcel theory suggested a relation between rainfall and both climatic variables of the type:

$$\ln rainfall = c + \alpha * T_d + \beta * \ln CAPE. \tag{2.4}$$

Their model also reveals exponential sensitivity of rainfall to dew-point temperature and a power-law relationship between rainfall and CAPE (Lepore et al., 2015).

Real data show that the slope coefficients α and β deviate from their theoretical values of α = 0.068 (CC relationship coefficient) and β = 0.5 (parcel-theory coefficient) due to different meteorological boundary conditions (North and Erukhimova, 2009; Lepore et al., 2015).

Third, we fit the regression model (Equation (2.4)) (North and Erukhimova, 2009; Lepore et al., 2015) which shows a log-linear relationship between rainfall and both variables based on meteorological data described by convective available potential energy (CAPE) and dew-point temperature (T_d) in our study region. We have used a linear model fitting function that uses the Wilkinson notation.

We divided the rainfall distributions into the 50th, 75th, and 90th percentiles and separately analyzed their relationship to the driving variables. For extreme (90th) and moderate (75th) rainfall percentiles, we regress daily values of these rainfall percentiles onto daily values of CAPE and dew-point-temperature during these days. For lower rainfall intensities, we regress daily rainfall that is above 50th percentile onto daily values of CAPE and dew-point-temperature during these days.

Results

The south–central Andes were characterized by extreme rainfall. We showed that the contribution of 90th percentile rainfall to total DJF rainfall was 70% and higher in this region (Figure 2.6) (Boers et al., 2015, 2014b). This highlights the significant contribution of deep convective storms to rainfall over this region. Our results showed the moderate to high temporal correlation between surface temperature and dew-point temperature and moderate correlation between surface temperature and CAPE east of the south–central Andes during the austral summer and during the daytime (Figure 2.7). Therefore, during the daytime, high solar heating and high temperatures trigger deep convection and extreme rainfall over the south–central Andes (Figure 2.6).

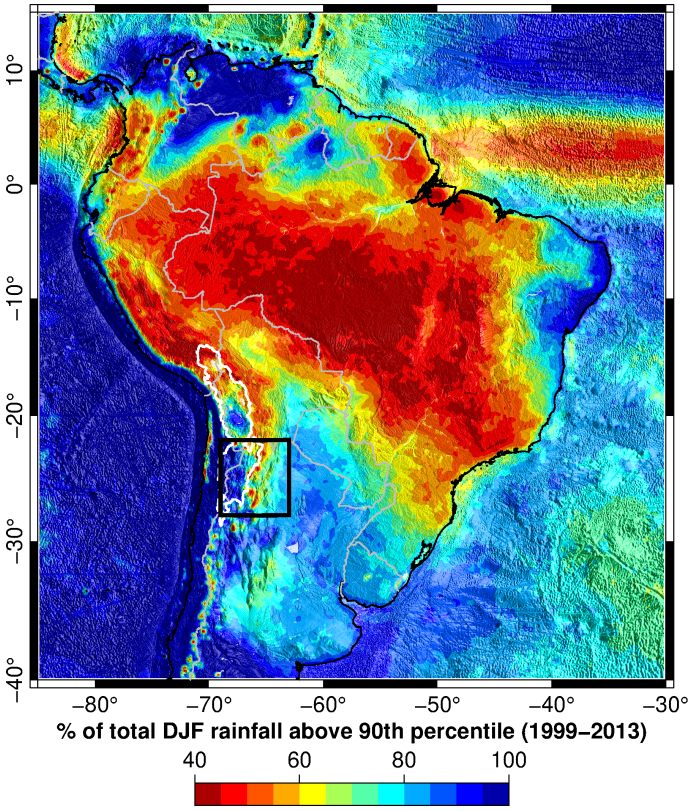

Figure 2.6 – Percentage of 90th percentile rainfall contribution to total DJF rainfall (1999–2013) derived from TRMM3B42 data. Note the high contribution in the south–central Andes in our study region (black box).The central Andean Plateau is marked in white and gray lines indicate international borders.

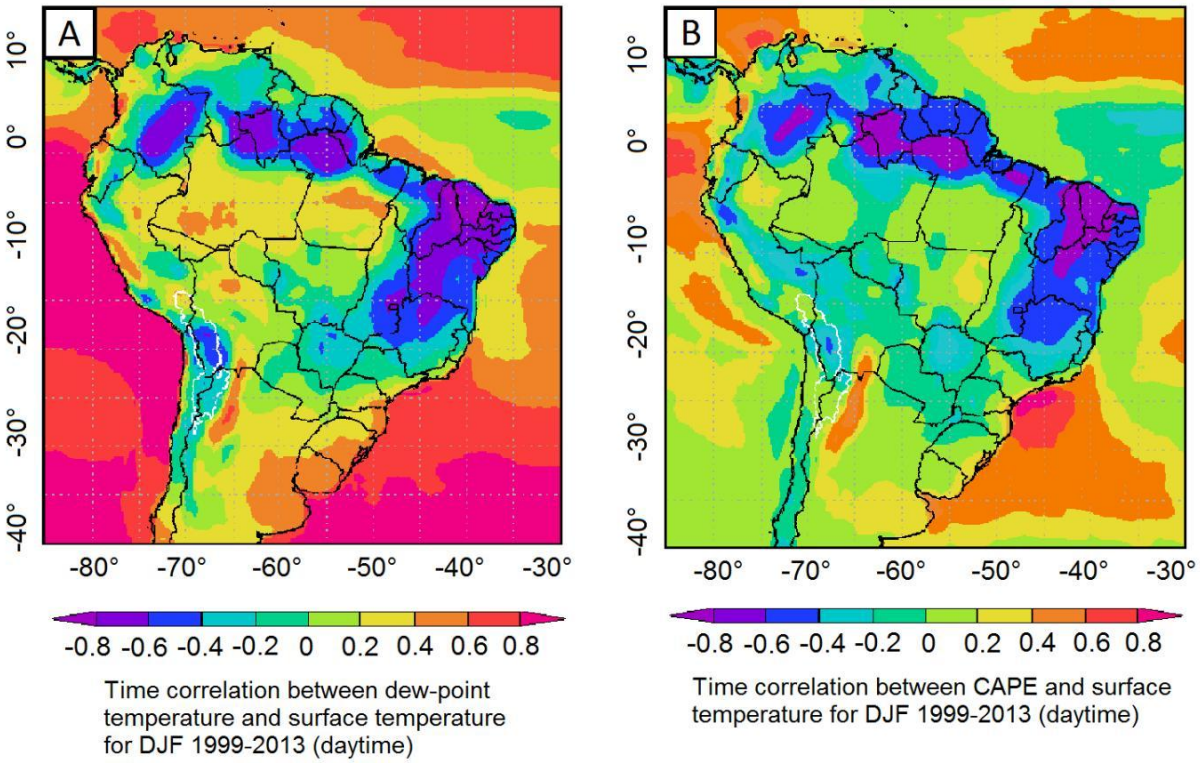

Figure 2.7 – Lag-free temporal correlation between dew-point temperature and surface temperature (A) and between convective available potential energy (CAPE) and surface temperature (B) during the austral summer and during the daytime (6 a.m.–6 p.m. local time) (1999–2013) based on ERA-interim reanalysis data. A high correlation coefficient suggests that both climatic variables and surface temperature are correlated eastward of the south–central Andes.

Our analysis of the spatial pattern of austral summer mean rainfall in conjunction with CAPE and dew-point temperature in each box in (Figure 2.4A–D) shows that both the dew-point temperature and CAPE east-west gradients (from A3 to A1, B3 to B1 and C3 to C1) (Figure 2.4C,D) coincide with the rainfall gradient from the wet, low elevation foreland regions to the dry, high-elevation central Andean Plateau (Figure 2.4B). Both, the spatial pattern shown by the area averaged boxes A3 and A2 compared to A1 (Figure 2.8A–C) and the temporal behavior, which is indicated by DJF seasonal mean from 1999 to 2013 (Figure 2.8A–C) of these meteorological variables, change along the steep topographic gradient in our study boxes in conjunction with rainfall.

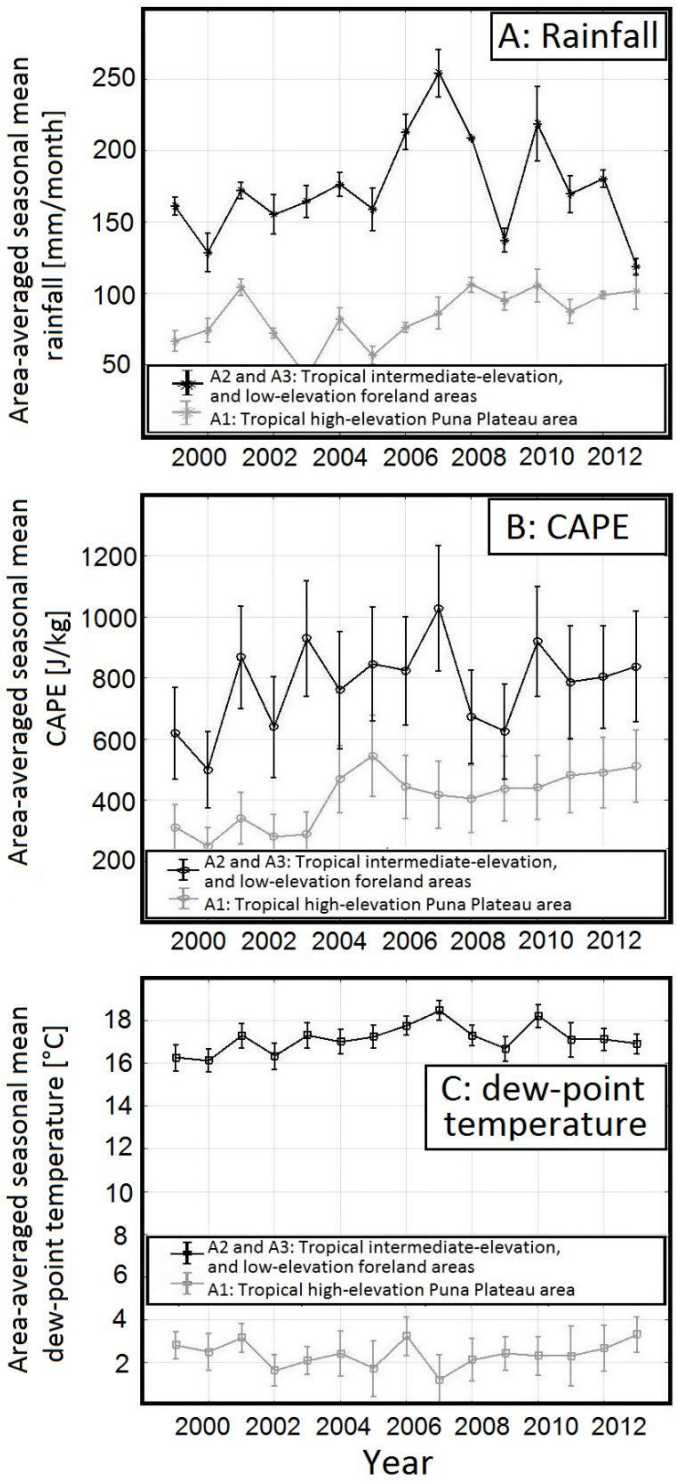

Figure 2.8 – The spatial (area averaged A3 and A2 (black) compared to area averaged A1 (gray)) and temporal (DJF seasonal mean 1999 to 2013) pattern of dew-point temperature and CAPE along our study boxes in conjunction with rainfall. (A) Area-averaged DJF seasonal mean rainfall, (B) area-averaged DJF seasonal mean CAPE, and (C) area-averaged DJF seasonal mean dew-point temperature are represented in these figures.

Next, we analyze the relationship between CAPE, dew-point temperature, and 90th percentile rainfall along the steep topographic gradient. We observe a nonlinear relationship between 90th percentile rainfall and associated CAPE and dew-point temperature (Figure 2.9A–C) Boxes A3, A2, and A1.

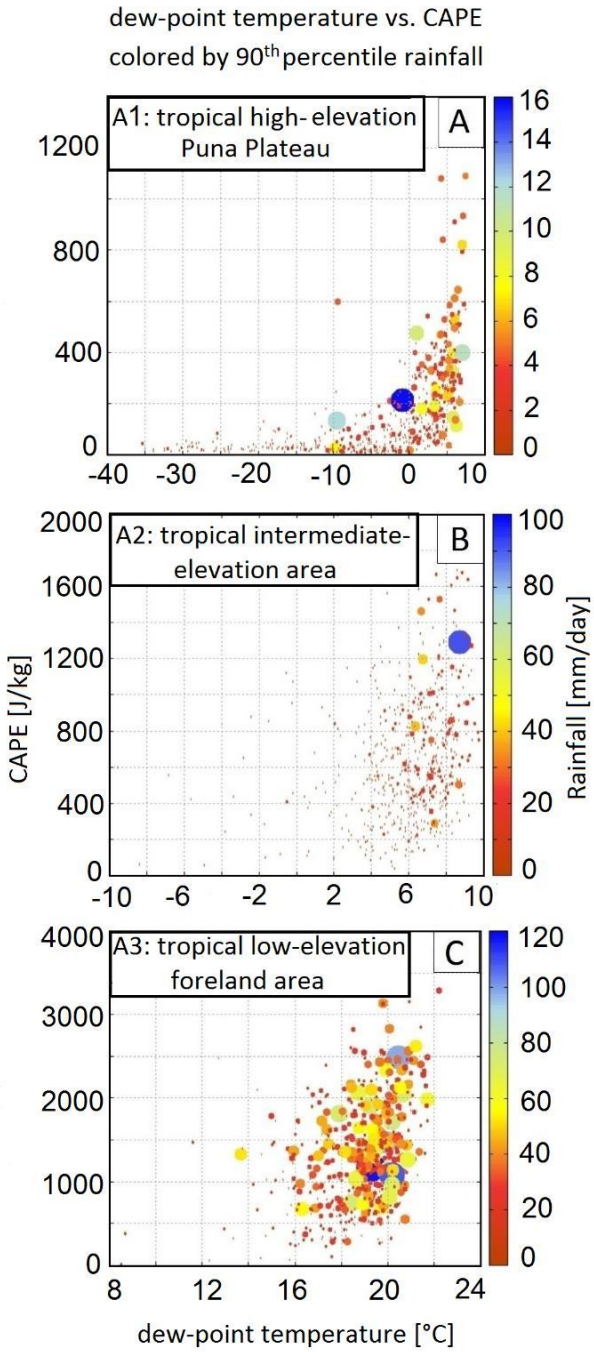

Figure 2.9 – Scatterplot showing dew-point temperature vs. CAPE colored by the 90th percentile rainfall amounts for boxes A1 (A), A2 (B) and A3 (C). Point sizes are also scaled by rainfall amount.

We have separately regressed the daily rainfall events that are above the 90th percentile onto daily values of dew-point temperature (Figure 2.10) and CAPE (Figure 2.11) to quantify conditions leading to extreme rainfall. We show the effect of temperature with respect to atmospheric humidity (T_d) and also with respect to convection (CAPE) for deep-convective storms (Lepore et al., 2015). This is particularly pronounced in the eastern south–central Andes along the latitude 22–28° S with a high distribution of MCS during austral summer months (Durkee and Mote, 2010). The regression coefficient (a) for the dew-point temperature and the regression coefficient (b) for CAPE reveal values around the CC relation and parcel theory, respectively. The regression coefficient (a) for the dew-point temperature is higher in the tropical and the transition zone between the tropical and subtropical areas and over intermediate-elevation (Box A2) and low-elevation foreland (Box A3) regions as compared to high-elevation Puna Plateau and subtropical regions (Figure 2.10). The regression coefficient (b) for the CAPE is higher in the transition zone between the tropical and subtropical and over the intermediate-elevation area as compared to all others regions (Figure 2.11).

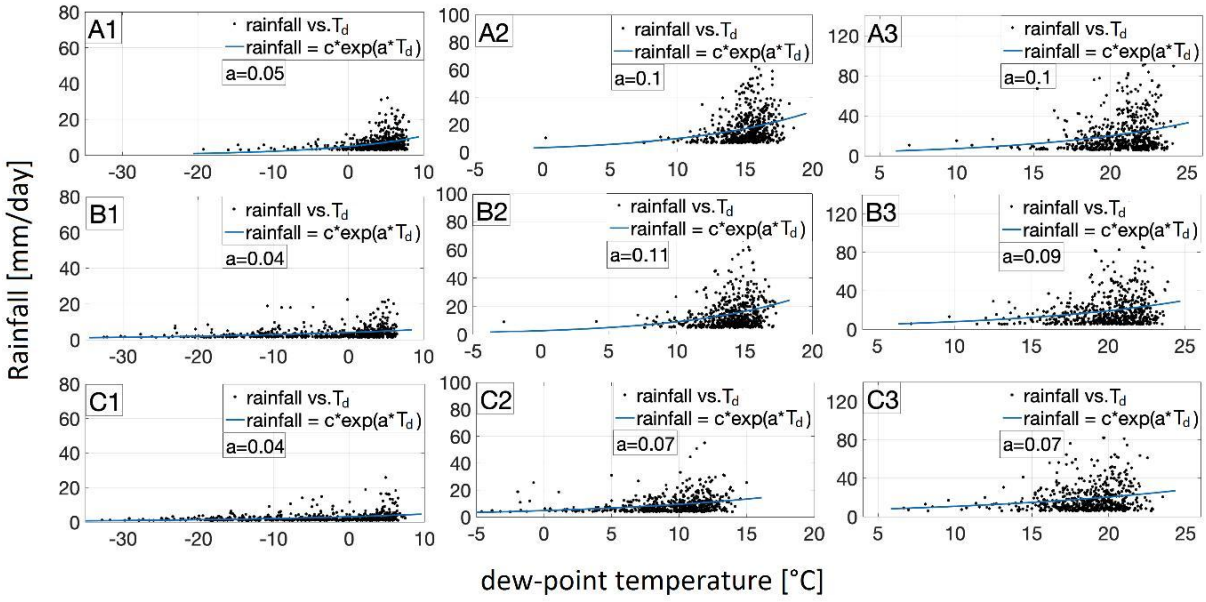

Figure 2.10 – Scatterplot showing the dew-point temperature vs. rainfall amounts for events above 90th percentile. (a) in regression equation ($rainfall = c * \exp(a * T_d)$) shows the regression coefficient for the independent variable dew-point temperature for all boxes along the climatic and topographic gradients. See Figure 2.4A for all boxes (A1–C3). Regression coefficient (a) reveals a value around CC relation (0.068 $^{\circ}C^{-1}$) in all boxes.

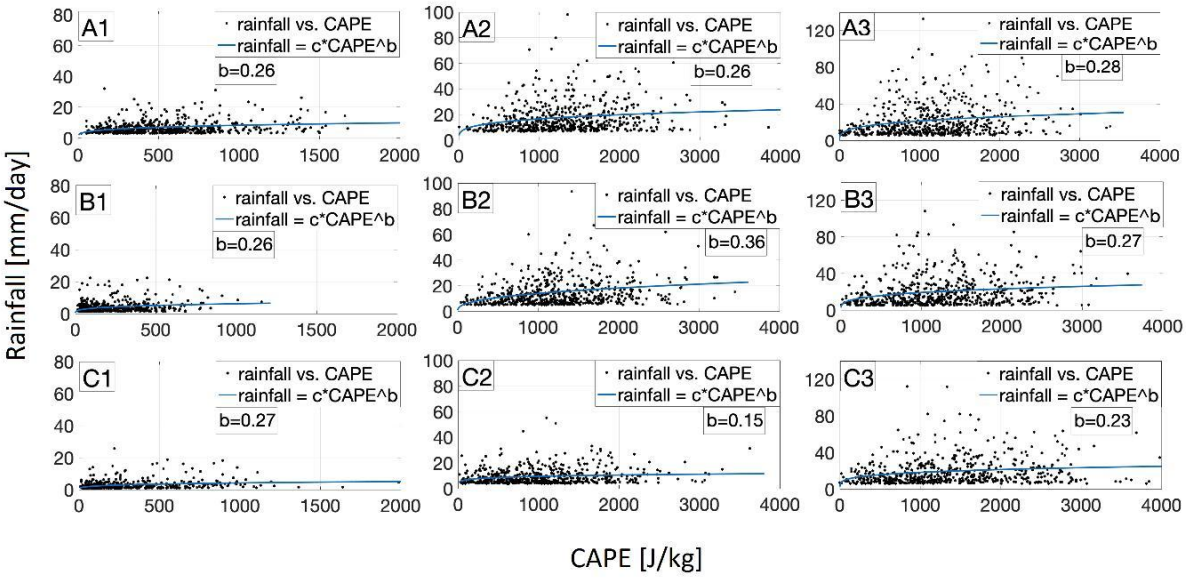

Figure 2.11 – Scatterplot showing the CAPE vs. rainfall amounts for events above 90th percentile. (b) in regression equation ($rainfall = c * CAPE^b$) shows the regression coefficient for the independent variable CAPE for all boxes along the climatic and topographic gradients. See Figure 2.4A for all boxes (A1–C3). Regression coefficient (b) reveals a value around parcel theory (0.5) in all boxes.

The log-linear model defined in Equation (2.4) also indicates exponential sensitivity of rainfall to dew-point temperature and a power-law relationship between rainfall and CAPE (Lepore et al., 2015). We used the linear multivariable regression model (Equation (2.4)) (Lepore et al., 2015) to show the joint effect of both climatic variables in our study region. The regression analysis reveals statistically significant relationships (p-value $<<$ 0.001) between the dew-point temperature and CAPE and 90th percentile rainfall over all nine areas. The regression coefficient (α) for the dew-point temperature in (Equation (2.4)) is higher and it is close to CC relationship (0.068 $^{\circ}C^{-1}$) for the extreme (90th percentile) rainfall in the tropical region and over intermediate-elevation (Box A2) and low-elevation foreland areas (Box A3) (Figure 2.12A). We show that the high contribution of dew-point temperature to extreme rainfall over these regions coincide with the higher dew-point temperature values (>10 $^{\circ}$C) for most of the events of the 90th percentiles rainfall over these boxes (Figure 2.13). We show that the dew-point temperature scaling of rainfall, based on our regression coefficients, are much higher than that derived from CC relation for the low rainfall percentile (50th percentile). This argues that the dew-point temperature scaling of rainfall for the lower rainfall percentiles cannot reliably explain rainfall amounts, likely because of the low rainfall intensities and other atmospheric driving processes.

The regression coefficient for CAPE (β in Equation (2.4) indicates that CAPE is the more important climatic variable for extreme (90th percentile) rainfall in the transition zone between the tropical and subtropical region and over the intermediate-elevation area (Figure 2.12B, B2). Based on the regression coefficient for CAPE (Figure 2.12B) in all three topographic regions for 90th percentile rainfall and regarding the value ranges of CAPE in each box, we indicate that there is a high contribution of CAPE also over the Altiplano–Puna region (Figure 2.14) as the regression coefficient does not reveal much lower value as those over low-elevation foreland and intermediate-elevation

areas. That is the case despite the low value ranges of CAPE for most of the events of 90th percentiles rainfall over Altiplano region.

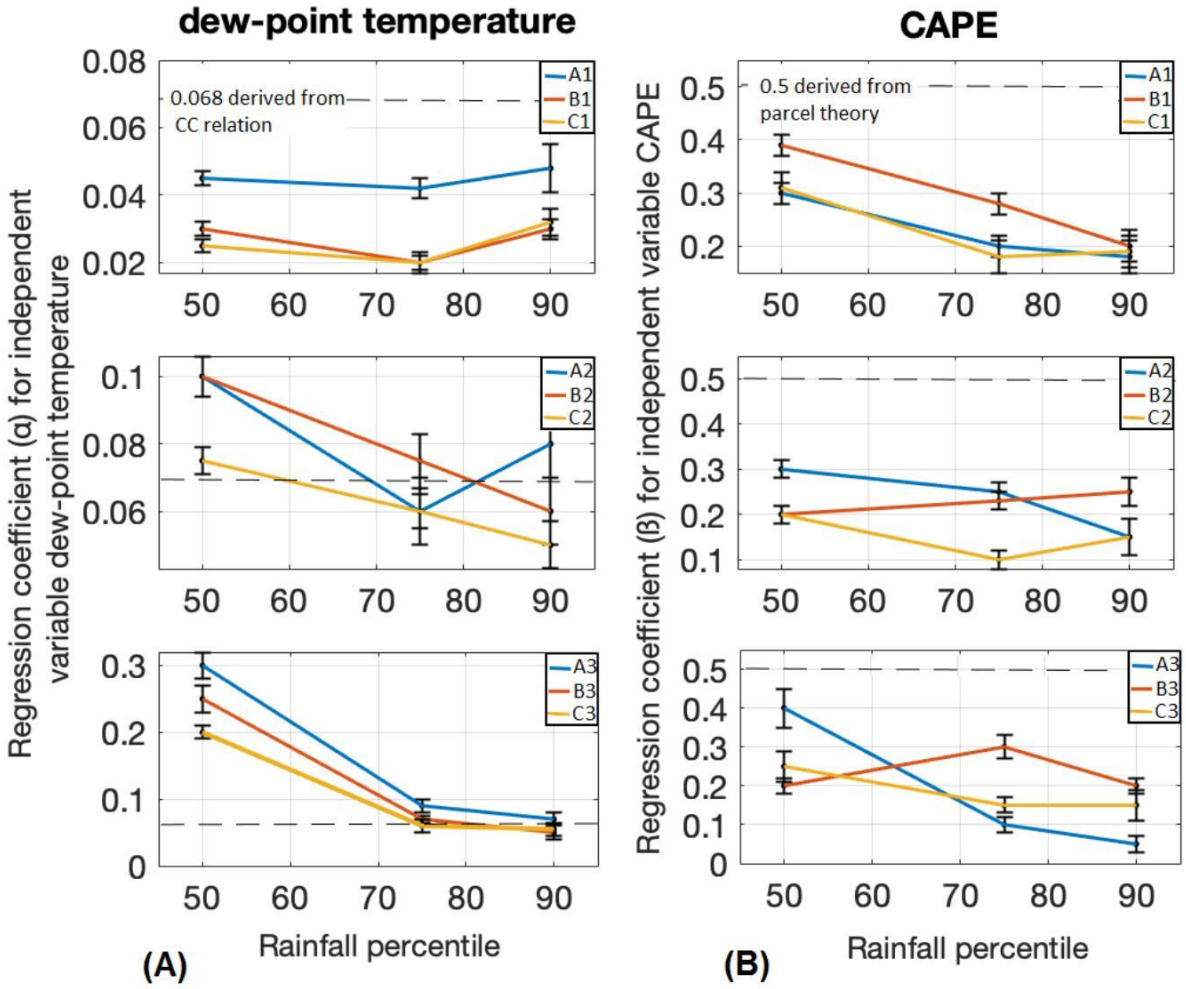

Figure 2.12 – ((A) dew-point temperature) Changes in the regression coefficient for the independent variable dew-point temperature for all boxes (Figure 2.4). Dashed line shows the coefficient based on CC relation with about 6.8% $^{\circ}C^{-1}$ increase of rainfall with temperature. (B) (CAPE) Changes in the regression coefficient for the independent variable CAPE for all boxes. Dashed line shows the coefficient based on parcel theory. Note that we have used a linear model fitting function to fit the regression model (Equation (2.4)) in our study region.

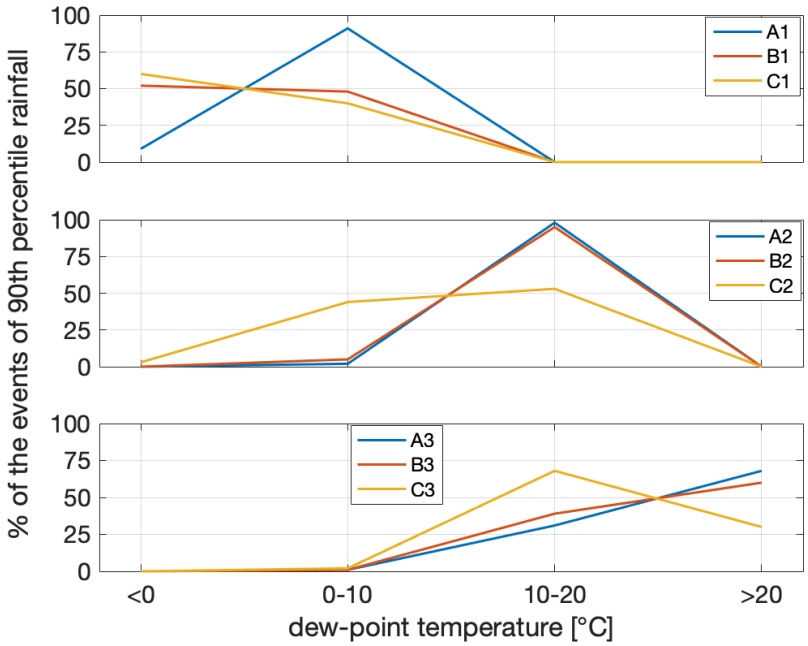

Figure 2.13 – Line plot showing the percentage of the events of 90th percentile rainfall for different value ranges of dew-point temperature. We show higher values of dew-point temperature for most of the events of 90th percentile rainfall over low-elevation foreland and intermediate-elevation areas as compared to Altiplano region.

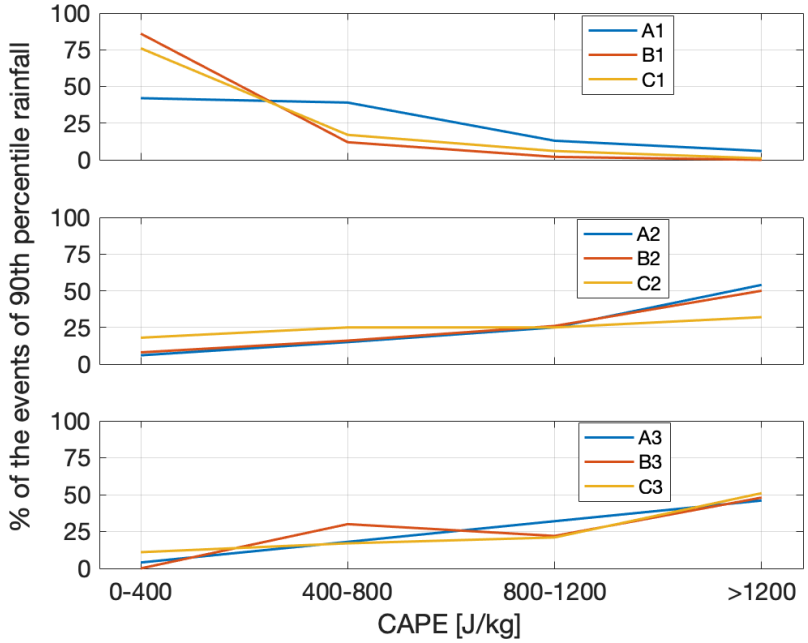

Figure 2.14 – Line plot showing the percentage of the events of 90th percentile rainfall for different value ranges of CAPE. We show higher values of CAPE for most of the events of 90th percentile rainfall over low-elevation foreland and intermediate-elevation areas as compared to Altiplano region.

Based on root mean squared error (RMSE) values, uncertainties decrease with increasing percentiles. This argues that rainfall can not be explained reasonably at the low percentile (50th) using CAPE and T_d (Figure 2.15).

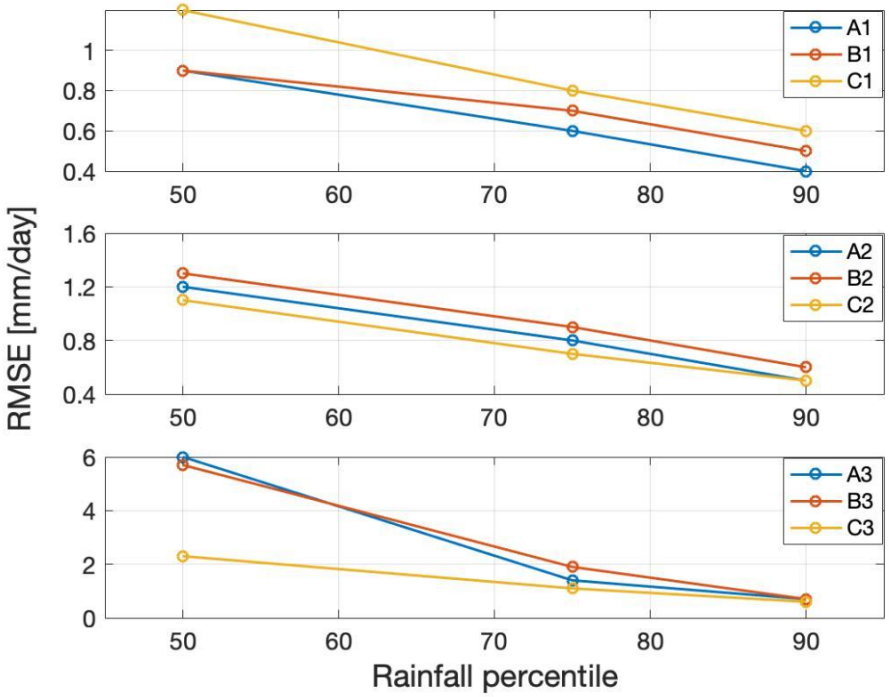

Figure 2.15 – Line plots showing the model RMSE value for 50th, 75th and 90th percentiles rainfall over all boxes. The model RMSE decreases with increasing rainfall percentile. That is, at higher rainfall percentiles, the model provides better constrained values and is likely a more realistic atmospheric-process explanation than at lower rainfall percentiles.

Discussion

Our observations show a strong dependence of extreme rainfall on CAPE and dew-point temperature (Figure 2.4). We have used a functional relationship (Equation (2.4)) to quantify their relative impacts.

Based on our regression coefficient (α in Equation (2.4)) dew-point temperature is the most important climatic variables for the extreme (90th percentile) rainfall in the tropical regions (Figure 2.12A) (A1, A2, and A3). This can be attributed to the fact that warmer tropical air can hold larger amounts of water vapor and hence can lead to higher occurrences and amounts of rainfall. Dew-point temperature is also a more important factor in the intermediate-elevation area and low-elevation foreland area (A2, B2, C2 and A3, B3, C3) compared to the high-elevation Puna Plateau (A1, B1 and C1) (Figure 2.12B). This is, because warmer air over these regions contains higher moisture availability and can lead to high convection and extreme rainfall (Figure 2.13). The highest contribution of dew-point temperature in the tropical intermediate-elevation area can be explained by the small differences between dew-point temperature and air temperature and consequently higher moisture availability (Figure 2.16).

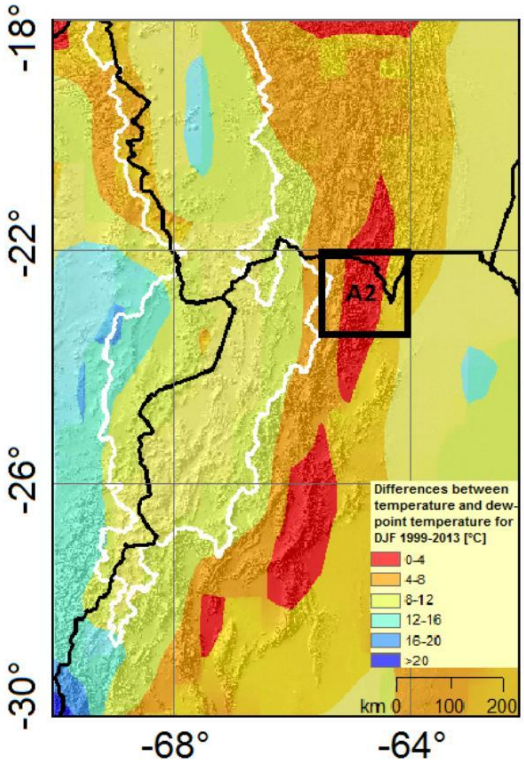

Figure 2.16 – The small differences between dew-point temperature and air temperature during austral summer (1999–2013) over the tropical and the intermediate-elevation area explains the high contribution of dew point temperature in extreme rainfall in this region (Figure 2.4A, Box A2). White line outlines the central Andean Plateau, black lines are international borders.

The larger differences between coefficient α for dew-point temperature in (Equation (2.4)) and their expected CC relationship ($0.068\,C^{-1}$) in the high-elevation Puna Plateau compared to intermediate-elevation area and low-elevation foreland area for the extreme rainfall argues that the mechanism of converting atmospheric moisture to rainfall is less efficient in the high-elevation Puna Plateau. Several studies have shown and documented the super-CC scaling of extreme rainfall by variations in intensify of convection processes with temperature (Berg and Haerter, 2013; Berg et al., 2013; Lepore et al., 2015). By comparing the regression coefficients of the 90th percentile (extreme rainfall) and the two lower percentiles at 75 and 50, the extreme 90th and moderate 75th rainfall percentiles in our analysis reveal a scale close to CC or in some cases super-CC ($2\times$CC) which is supported by other studies as mentioned above. We emphasize that the temperature scaling of rainfall for the lower rainfall percentiles cannot be explained reliably because of the low rainfall intensities and this is supported by other studies (Lenderink et al., 2017). Taken together, this suggests that the mechanism of transforming dew-point temperature to rainfall is more efficient when the rain intensity is higher (Lepore et al., 2015). It is important to mention that the low value of dew-point temperature does not always reflect the lower chance of rainfall occurrence. Even a dry layer can become unstable if lifted (potential instability) for example over high elevations in mountains (Rasmussen and Houze, 2011).

The regression and coefficient β for the CAPE (Equation (2.4)) indicates a high importance of CAPE for extreme rainfall in the study area (Figure 2.12B). This is of particular importance in the transition zone between the tropical and subtropical region and over intermediate elevations, because the transition zone is characterized by strong rising of warm and moist air and the formation of deep convective storms. The coefficient β for CAPE in (Equation (2.4)) in the high-elevation Puna Plateau for extreme rainfall is not much lower than those over two other lower topographic regions, which have larger absolute values of CAPE (Figure 2.14). Therefore, even the lower values of CAPE play an important role for extreme rainfall over high-elevation Puna Plateau. Based on previous studies (Rasmussen and Houze, 2011), it is likely that CAPE is important for convection initiation but it does not always contribute to its development. This can be seen south of 28°S and over the intermediate-elevation area where the high CAPE does not necessarily contribute to higher rainfall.

Past studies (Lepore et al., 2015) investigated the relationship between extreme rainfall and CAPE and dew-point temperature in the Eastern United States. Their results show a power-law relationship between rainfall and CAPE with a regression coefficient of ≈0.2–0.4 changing with geographic regions. For the dew-point temperature the regression coefficient changes significantly depending on the rainfall percentile. Our study suggests similar results, but different coefficients α and β, which change depending on the rainfall percentile as well as the topographic and climatic sub-regions.

Some other studies used different modeling approaches on investigation of rainfall along the topographic gradient. Smith and Barstad (2004); Bookhagen and Burbank (2010, 2006); Bookhagen and Strecker (2008) parameterized the mean orographic rainfall in south America and other regions where complex terrain is similar. These models rely on static climatic variables and allow reproducing an average rainfall patterns. But they do not allow for atmospheric variability along a larger geographic region. In our approach, we considered not only the topographic gradient, but also allow for atmospheric variability by including the dominant atmospheric conditions and climatic variables leading to deep convection and extreme rainfall events.

Conclusions

We analyzed extreme rainfall events by documenting the effect of temperature on atmospheric humidity (dew point temperature, T_d) and convective available potential energy (CAPE) on deep-convective storms in the south–central Andes in NW Argentina. We used a multivariable regression analysis to describe the correlation between rainfall percentiles and the two driving atmospheric variables: T_d and CAPE. We have separately analyzed low-elevation frontal areas (Andean foreland), intermediate-elevation areas (intermontane basins), and high-elevation areas (central Andean Plateau). We obtained the following key results:

First, based on our spatial analysis, the rainfall distribution in the south–central Andes correspond to spatial differences in CAPE and T_d (Figure 2.4B–D). The east-west gradients in both, dew-point temperature and CAPE (from A3 to A1, B3 to B1 and C3 to C1 in (Figure 2.4C,D), correlate with the rainfall gradient (Figure 2.4B). Our temporal analysis indicates that the temporal differences in CAPE and T_d correspond the rainfall distribution in the south–central Andes (Figure 2.8A–C).

Second, we find a correlation between extreme rainfall and a combination of dew-point temperature and CAPE through a multivariable regression analysis (Equation (2.4)). Our results based on p values $<<$ 0.001 show a sta-

tistically significant relationship between a non-linear combination of dew-point temperature and CAPE and 90th percentile rainfall. This suggests that spatial and temporal occurrences of rainfall at the 90th percentile (i.e., extreme rainfall) can be partially explained by combining dew-point temperature and CAPE.

Third, we observe that the atmospheric mechanism of transforming moisture to extreme rainfall is more efficient in the tropical low- and intermediate-elevation areas and the mechanism of transforming CAPE to extreme rainfall is more efficient in the transition zone between the tropical and subtropical and in the intermediate-elevation areas (Figure 2.12).

Fourth, we observe that the uncertainties (RMSE) of the model fit decrease with increasing rainfall percentiles (Figure 2.15). This suggests that the described modeling approach is more reliable for higher rainfall percentiles as these are primarily driven by CAPE and dew-point temperature variations.

Our study deciphers the important role of dew-point temperature and CAPE on extreme rainfall events in the south–central Andes. We show that hydrometeorological extreme events are triggered by different boundary conditions from north to south along the steep topographic gradient of the eastern Andes and that multiple conditions must be met before extreme rainfall events can be triggered.

Funding

This research was funded by the Deutsche Forschungsgemeinschaft (DFG) and the Brandenburg Ministry of Sciences, Research and Cultural Affairs, Germany, within the framework of the international research training group IGK2018 SuRfAce processes, TEctonics and Georesources: The Andean foreland basin of Argentina (StRATEGy).

Acknowledgments

We thank the Deutsche Forschungsgemeinschaft (DFG) and the Brandenburg Ministry of Sciences, Research and Cultural Affairs, Germany, within the framework of the international research training group IGK2018 SuRfAce processes, TEctonics and Georesources: The Andean foreland basin of Argentina (StRATEGy) for the financial support. We acknowledge the support of the Open Access Publishing Fund of University of Potsdam.

The authors declare no conflict of interest.

Chapter 3

Using GNSS-derived integrated water vapour and CAPE to decipher rainfall in the eastern central Andes[†]

Maryam RamezaniZiarani[1,2], Bodo Bookhagen[1], Torsten Schmidt[2], Jens Wickert [2,3], Alejandro de la Torre[4], Zhiguo Deng[2], Andrea Calori[5]

[1]*University of Potsdam, Institute of Geosciences, Karl-Liebknecht-Str. 24-25, 14476 Potsdam, Germany*

[2]*German Research Centre for Geosciences GFZ, 14473 Potsdam, Germany*

[3]*Institute of Geodesy and Geoinformation Science, Faculty VI, Technische Universität Berlin, 10623 Berlin, Germany*

[4]*CONICET, Facultad de Ingeniería, Universidad Austral, LIDTUA (CIC), 1629 Pilar, Buenos Aires, Argentina*

[5]*Facultad de Ingeniería, Universidad Nacional de Cuyo, Parque General San Martín, Ciudad Universitaria, CPM5502JMA Mendoza, Argentina*

Abstract

Atmospheric water vapour content is a key variable that controls the development of deep convective storms and rainfall extremes over the central Andes. Direct measurements of water vapor are challenging, but recent developments in microwave processing allow the use of phase delays from the L-band radar to measure water vapour content throughout the atmosphere: The Global Navigation Satellite System (GNSS) based integrated water vapour (IWV) monitoring shows promising data to measure vertically integrated water vapour at high temporal resolutions. In addition to IWV, the convective available potential energy (CAPE) is also identified as key climatic variable for the formation of deep convective storms and rainfall in the central Andes. Our analysis relies on GNSS data from the Argentine Continuous Satellite Monitoring Network, Red Argentina de Monitoreo Satelital Continuo (RAMSAC) network from 1999 to 2013. CAPE is derived from version 2.0 of the ECMWF's (European Centre for Medium-Range Weather Forecasts) Re-Analysis (ERA-interim) data and rainfall from TRMM (Tropical Rainfall Measuring Mission) data. In this study, we first analyse the rainfall characteristics of two GNSS-IWV stations by comparing their complementary cumulative distribution function (CCDF). Second, we derive the relation between rainfall and both, CAPE and GNSS-IWV, separately. We show that the relation between GNSS-IWV and rainfall as well as CAPE and rainfall varies with different rainfall percentiles. Based on our distribution fitting analysis, we observe an exponential relation of rainfall to GNSS-IWV. In contrast, we report a power-law relationship between the daily

[†]*submitted as Maryam RamezaniZiarani, Bodo Bookhagen, Torsten Schmidt , Jens Wickert, Alejandro de la Torre, Zhiguo Deng and Andrea Calori. "Using GNSS-derived integrated water vapour and CAPE to decipher rainfall in the eastern central Andes." Remote sensing.*

,

mean value of rainfall and CAPE at the GNSS-IWV station locations in the eastern central Andes that is close to the theoretical relationship based on parcel theory. Third, we generate a joint regression model through a multivariable regression analysis using both variables (CAPE and GNSS-IWV) to explain extreme rainfall occurrences. We find that rainfall can be characterised with a higher statistical significance for higher rainfall percentiles e.g., above the 90th percentile considering the joint effect of both variables. Fourth, we identify the temporal relation between extreme rainfall (90th, 95th, and 99th percentiles) and both GNSS-IWV and CAPE at 6 hourly time steps. We observe an increase before the rainfall event and at the time of peak rainfall - both for GNSS integrated water vapour and CAPE. We show higher values of CAPE and GNSS-IWV for higher rainfall percentiles (99th and 95th percentiles) compared to the 90th percentile at a 6-hour temporal scale. Based on our correlation analyses and the dynamics of the time series, rainfall-extreme events can be described by a combination of GNSS-IWV and CAPE in the eastern central Andes. This relation can be exploited in future studies to increase the prediction potential of extreme events.

Keywords: Global Navigation Satellite System (GNSS); GNSS Integrated Water vapour; convective available potential energy (CAPE); extreme rainfall; TRMM.

Introduction

The south–central Andes is an area that is affected by hydrometeorological extreme events (e.g., Castino et al., 2017; Boers et al., 2014a; De la Torre et al., 2015; Ramezani Ziarani et al., 2019). The combination of topography and climate forms the most important driver for generating deep convective storms along the eastern central Andes (e.g., Rasmussen and Houze, 2016; Pingel et al., 2016; Rohrmann et al., 2014; Bookhagen and Strecker, 2008). Atmospheric water vapour content is a crucial variable triggering the convection and rainfall extremes in the south–central Andes (Rasmussen and Houze, 2011). Water vapour also plays an important role in controlling atmospheric stability as it is the primary variable leading to the formation of convective storm systems (Priego and Porres, 2016) by enhancing the convective available potential energy (CAPE) (Adams et al., 2011).

However, the direct and three-dimensional measurements of water vapour in the atmosphere is difficult and requires atmospheric sounding (Berbery et al., 1998) or recent developments in radar processing such as Global Navigation Satellite System (GNSS) methods to monitor the atmospheric integrated water vapour (IWV) content (Bevis et al., 1992, 1994; Duan et al., 1996). GNSS-derived troposphere products derived from zenith total delay (ZTD) (Chen et al., 2018) are now used as a reliable meteorological data in climate studies (Guerova et al., 2016). The advantage of GNSS-IWV measurements is their high spatial and temporal resolutions.

Several previous research studies used GNSS atmospheric data to study extreme rainfall events (Brenot et al., 2013; Barindelli et al., 2018). Some studies have shown and documented that the variations in the GNSS-IWV are temporally correlated with rainfall. These studies have shown an increase in GNSS-IWV several hours before extreme rainfall, mostly followed by a decrease after the event (Benevides et al., 2015, 2019). Furthermore, Priego and Porres (2016) investigated the joint effect of GNSS-IWV and atmospheric pressure on extreme rainfall and they show a high spatiotemporal correlation between the variations of GNSS-IWV and severe rainfall in eastern Spain. Calori et al. (2016) indicated that GNSS-IWV can show moisture variability in connection with severe storms in the Cuyo region in Mendoza in the south–central Andes. Thus, GNSS-IWV has been identified as a reliable parameter for detecting atmospheric convection and extreme rainfall.

An additional parameter that triggers convection and rainfall extremes and describes the atmospheric stability is CAPE (Lepore et al., 2015). CAPE indicates the amount of energy available for convection (North and Erukhimova, 2009). Mesgana and Thian (2017) defined CAPE as a proxy for extreme rainfall over the United States and Southern Canada. Furthermore, Murugavel et al. (2012) have shown a high contribution of CAPE to heavy rainfall during the monsoon season over the Indian region. A different study suggested that the spatial pattern of rainfall-extreme events can be described by a combination of dew-point temperature and CAPE in the south–central Andes (Ramezani Ziarani et al., 2019).

These previous studies separately analyzed the spatiotemporal distribution of extreme rainfall related to IWV and CAPE (Calori et al., 2016; Mesgana and Thian, 2017), but they were not fully sufficient in explaining extreme rainfall based only on one variable. Our study aims to identify the relationship between rainfall, GNSS-IWV, and CAPE and to analyze the joint effect of GNSS-IWV and CAPE on extreme rainfall generation. We specifically focus on the south–central Andes where convection plays an important role in extreme rainfall generation.

Data and Methods

Data

We used the ERA-Interim reanalysis data (1979-present), version 2.0 of the ECMWF (European Centre for Medium-Range Weather Forecasts) (Dee et al., 2011), https://apps.ecmwf.int/datasets/data/interim-full-daily/levtype=sfc/ to analyse CAPE. ERA-Interim reanalysis data used in this study have a spatial resolution of $0.75° \times 0.75°$ and a temporal resolution of 6 hours. ERA-Interim reanalysis data are interpolated to the station points using a nearest-neighbour interpolation method. Because of the steep topographic gradient in that region, we have explored other interpolation methods such as bilinear interpolation, but this does not affect the results.

We used GNSS integrated water vapour data from the Argentine Continuous Satellite Monitoring Network (RAMSAC) for two stations: San Miguel de Tucumán (TUCU, 1999-2013) located at 65° 13' W and 26° 50' S and San Fernando del Valle de Catamarca (CATA, 2008-2013) located at 65° 46' W and 28° 28' S (Figure 3.1A). These two stations are selected as they have the longest data availability for this region. The RAMSAC network was created in 1998 and has grown to include around 100 continuously operating GNSS stations in north and central Argentina (Pinon et al., 2018). The GNSS-IWV data used in this study have a temporal resolution of 30 minutes. There were several missing data in the GNSS-IWV data set that were removed from the associated CAPE and rainfall data for these days or hours.

TRMM (Tropical Rainfall Measuring Mission) data (Kummerow et al., 1998), product 3B42 (Huffman et al., 2007) https://disc.gsfc.nasa.gov/datasets/TRMM_3B42_Daily_7/summary (Version 7) with a spatial resolution of $0.25° \times 0.25°$ and hourly temporal resolution have been used to analyse rainfall. TRMM rainfall data are interpolated at the station location using nearest neighbour interpolation method. TRMM data have been indicated to be a reliable dataset for investigating rainfall in South America (Ramezani Ziarani et al., 2019; Carvalho et al., 2012; Boers et al., 2015).

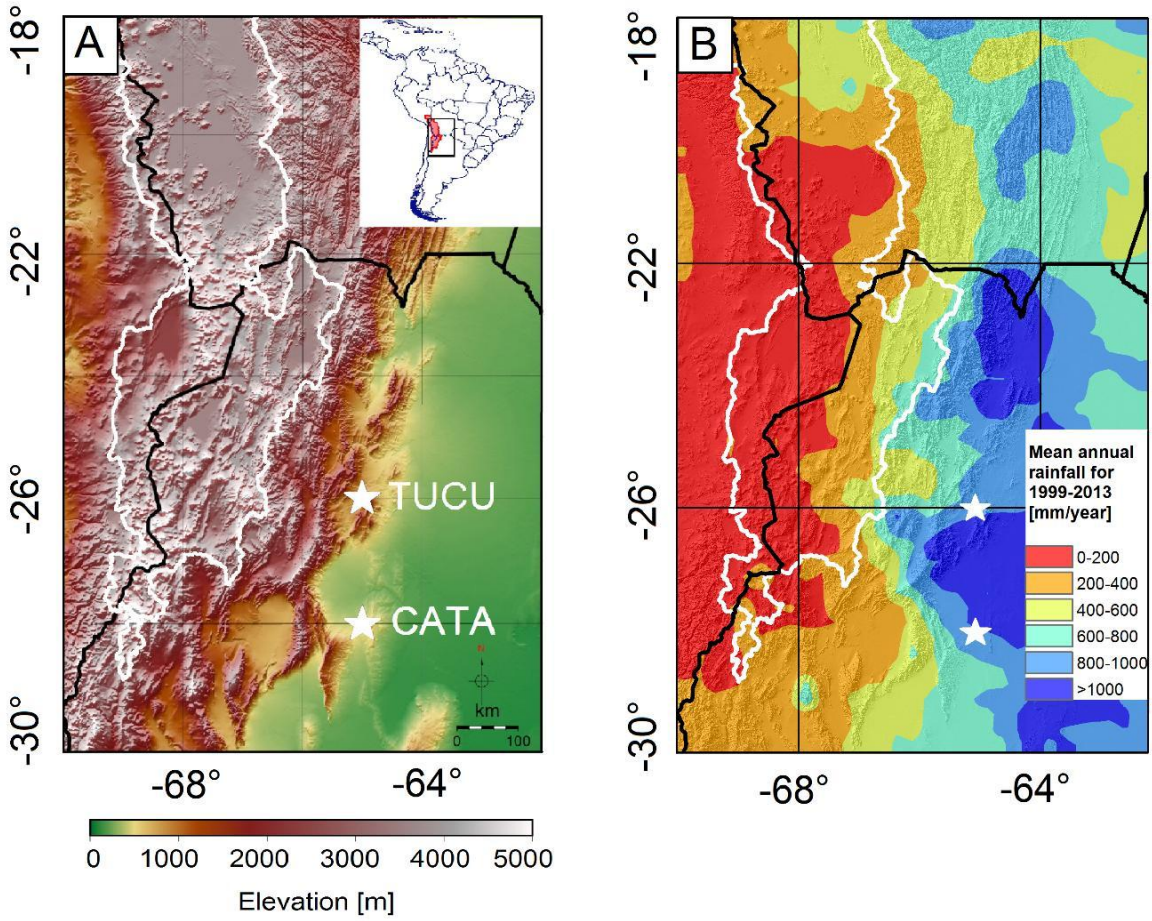

Figure 3.1 – (A) Topographic overview of the study region in the central Andes in northwestern Argentina with the outline of the internally-drained central Andes in white (see inset for location in South America with the internally-drained central Andes shown in red). Black lines are international borders. White stars show the GNSS stations used in this study: San Miguel de Tucumán (TUCU, n=15 years) and San Fernando del Valle de Catamarca (CATA, n=6 years). (B) annual mean rainfall derived from TRMM 3B42 (1999-2013) shows rainfall distribution on the station locations. White stars show the GNSS stations.

GNSS Integrated Water Vapour (IWV) Processing

The Global Navigation Satellite System (GNSS) data are organized in units of 24 hours periods and were processed using the earth parameter and orbit system software (EPOS) at the German research centre for geosciences (GFZ) (Gendt et al., 2013). The data processing was done based on the following steps: First, the two stations were processed in a Precise Point Positioning (PPP) model using the GFZ's own second reprocessed Global Positioning System (GPS) satellite clock and orbit products (Deng et al., 2015). In the PPP processing, the low quality observations and outliers were removed. In a second step, the remaining data were used for network processing. Several well distributed IGS (International GNSS Service) core stations are included in this network. In the next step, the estimated troposphere products of zenith path delay (ZPD) were converted to integrated water vapour (IWV). The

humidity-induced part of ZPD provides a valuable source of vertically integrated water vapour, e.g., (Bevis et al., 1992, 1994). To estimate IWV, meteorological information (ground pressure and mean temperature above the station) is needed. In this study, the ECMWF ground pressure and mean temperature data were used to convert the ZPD to IWV (Heise et al., 2009).

Identifying the Effect of GNSS-IWV and CAPE on Extreme Rainfall Formation

Understanding the conditions leading to extreme rainfall events is difficult, because of complex, interfering atmospheric processes in the eastern central Andes. Previous research indicates that extreme rainfall in the south-central Andes is often caused by deep convective storms (Rohrmann et al., 2014; Romatschke and Houze, 2010). An analysis requires the investigation of the dominant climatic variables leading to extreme rainfall events with reliable data. In this study, we analyze the joint effect of GNSS-IWV and CAPE on extreme rainfall generation.

First, we analyse the rainfall distribution for each GNSS-IWV station (TUCU and CATA, (Figure 3.1A)) in the south-central Andes using complementary cumulative distribution function (CCDF) and by comparing the best-fit parameters.

Second, we investigate the seasonal behaviour and the fluctuations in the GNSS-IWV and CAPE in conjunction with rainfall for both stations (TUCU and CATA) on the daily scale. We use the wavelet coherence analysis to confirm the seasonal agreement between rainfall, GNSS-IWV, and CAPE.

Third, we analyze the relation between the daily mean of GNSS-IWV and rainfall considering the rainfall percentiles for both station locations (TUCU and CATA). We perform a curve fitting process to model the rainfall as a function of the GNSS-IWV. After fitting several different models to the data, we find that data are best fitted by an exponential model (Equation (3.1)) based on model fitting statistics (root mean squared error, R-squared value, statistic test for the F-test on the regression model, and p-value).

$$rainfall = \exp(\alpha * \textit{GNSS-IWV}) \tag{3.1}$$

where α is the regression coefficient for GNSS-IWV.

We take natural log of both sides of the equation to linearize the equation:

$$\ln rainfall = \alpha * \textit{GNSS-IWV} \tag{3.2}$$

Fourth, we analyze the correlation between the daily mean of rainfall and CAPE at both station locations (TUCU and CATA) using a power-law relationship as described in previous research based on parcel theory (North and Erukhimova, 2009; Lepore et al., 2015; Ramezani Ziarani et al., 2019). Based on parcel theory, we expect the rainfall

intensity to be commensurate to $\sqrt{CAPE}$ (β= 0.5), if CAPE is efficiently transferred to parcel kinetic energy (North and Erukhimova, 2009; Lepore et al., 2015).

$$rainfall = CAPE^{\beta} \tag{3.3}$$

where β is the regression coefficients for CAPE

After data linearization, the following equation is substituted to describe the parcel theory:

$$\ln rainfall = \beta * \ln CAPE \tag{3.4}$$

Fifth, we generate the regression model equation (3.5), which shows a log-linear relationship between rainfall and both variables at both station locations. We show the joint effect of both variables on rainfall extreme events (events above the 90th percentile) by joint regression of both variables. We test the goodness of our model based on the statistics of the model.

$$\ln rainfall = c + \alpha * \textit{GNSS-IWV} + \beta * \ln CAPE \tag{3.5}$$

where α and β are the regression coefficients for GNSS-IWV and CAPE, respectively. Our approach and the formulations are based on previous studies for extreme rainfall (North and Erukhimova, 2009; Lepore et al., 2015; Ramezani Ziarani et al., 2019).

Sixth, we analyse the temporal relation between extreme rainfall and both GNSS-IWV and CAPE on the 6-hour scale. We select all data with rainfall above the 90th, 95th, and 99th percentiles, respectively, and their corresponding CAPE and GNSS-IWV amounts. We then averaged 6 hourly GNSS-IWV and CAPE data within the 72 hours (event day plus day before and day after) for each percentile in both stations, and we show the correlation between both variables and extreme rainfall.

Results

Observed Correlation of Rainfall, GNSS-IWV, and CAPE at the GNSS Station Locations

3.1.1 Rainfall and GNSS-IWV Characteristic at the GNSS-IWV Stations

In this study, we aim to decipher the influence of both GNSS-IWV and CAPE on rainfall-extreme events. We first show that each station (TUCU and CATA) in the eastern central Andes has a different rainfall distributions. We rely on a two-sample Kolmogorov-Smirnov (KS) test to compare the distribution of rainfall at both stations during (2008-2013) due to data availability for CATA station. Based on the test result the hypothesis that rainfall in both

station are from the same continuous distribution is rejected. Therefore, we accept the alternative hypothesis that each station has a different rainfall distributions. Also the p-value (p = 4%) confirms the difference between both distributions at the 5% level. Similarly, the KS test for the comparison of IWV data shows that they are drawn from different distribution.

Similar to a previous work (Foster et al., 2006), our analysis suggests that the rainfall and GNSS-IWV distributions are best fitted by a lognormal distributions. The estimated parameters μ and σ reveal different values for each station that underline their different climatic environments. We note that the tail of the rainfall distribution can be described by a power law starting at x_{min}= 12.9 and with the estimated exponent α=2.5 for TUCU station and x_{min}= 28 and the estimated exponent α=2.9 for CATA station.

In order to compare both stations, we show the exceedance probabilities of binned rainfall and GNSS-IWV data (Figure 3.2).

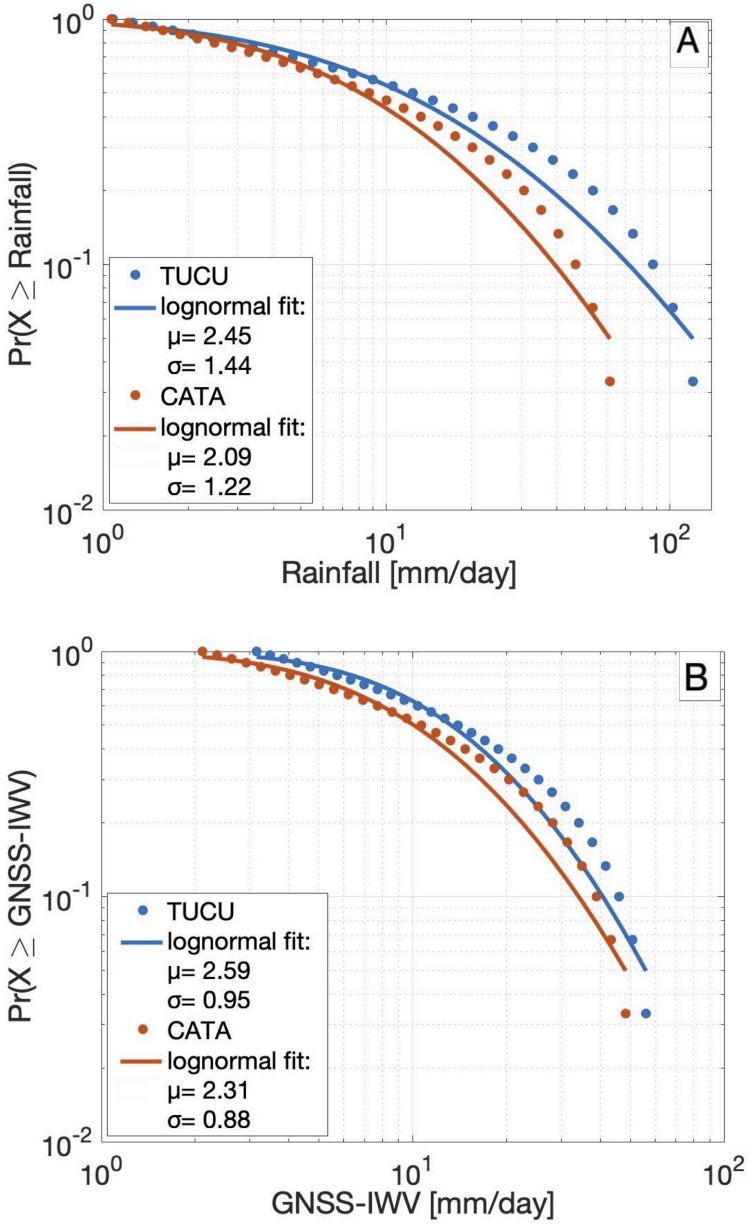

Figure 3.2 – Logarithmically binned rainfall data (A) and GNSS-IWV (B) for TUCU station (blue dots) and for CATA station (red dots). The fitting parameters of the lognormal distribution show the differences between two stations (2008-2013). We note that the tail of the distribution exhibits power-law behaviour starting at x_{min}= 12.9 and with the estimated exponent α=2.5 for TUCU station and x_{min}= 28 and the estimated exponent α=2.9 for CATA station.

Next, we show the seasonal pattern of both variables with respect to rainfall. Our results show that the daily values of GNSS-IWV and CAPE increase during the austral summer months and coincide with an increase in rainfall at both station locations (TUCU and CATA) (Figure 3.3). In contrast to the GNSS-IWV, which represents higher

absolute values during austral summer at the TUCU station location (Figure 3.3A,C), CAPE shows larger absolute values for the CATA station (Figure 3.3B,D) during austral summer months.

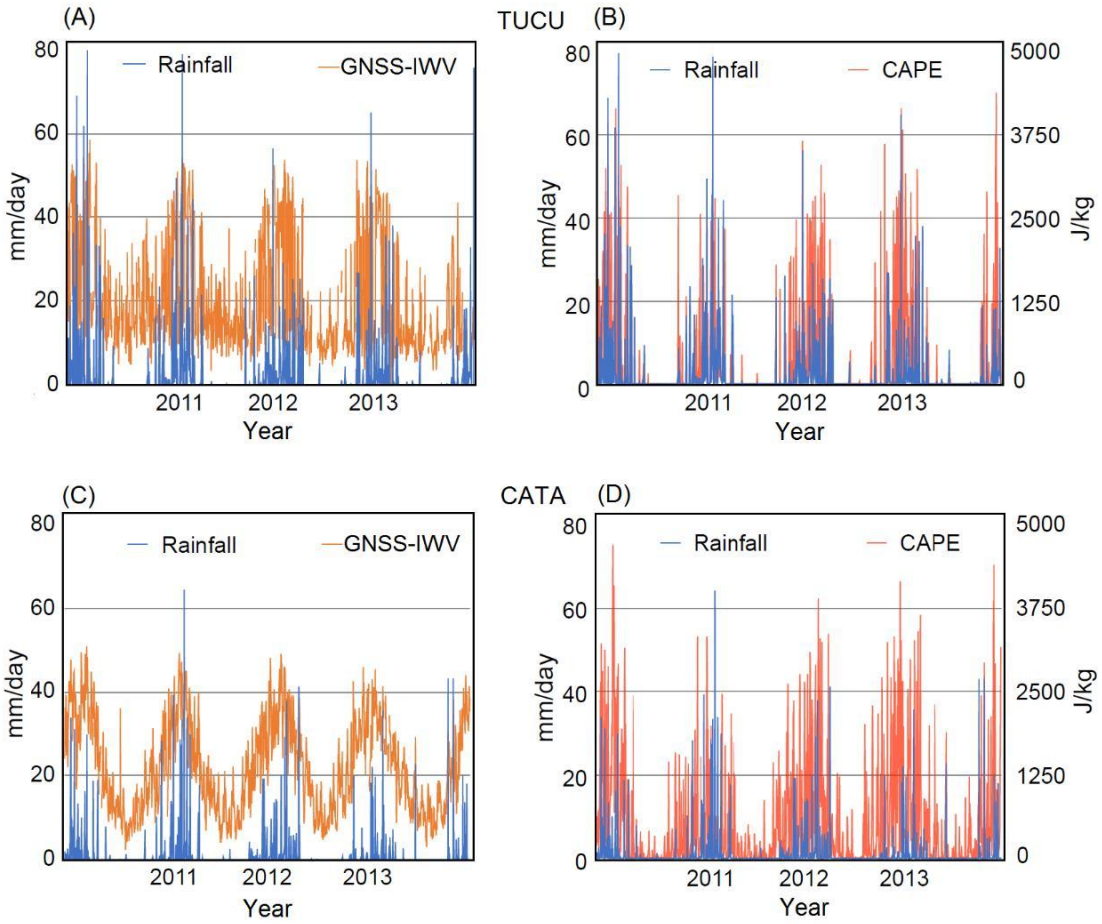

Figure 3.3 – Daily mean GNSS integrated water vapour (orange line) vs. daily mean rainfall from TRMM data (blue line) (A) for TUCU and (C) for CATA stations and daily mean CAPE (red line) from ERA-interim vs. daily mean rainfall from TRMM data (blue line) (B) for TUCU and (D) for CATA stations for (2010-2013). Both data represent a high seasonal agreement with rainfall in both stations.

We then show the cyclic behaviour of rainfall and CAPE as well as rainfall and GNSS-IWV using the wavelet coherency analysis. As it can be seen in Figure 3.4 the significant coherence area between CAPE and rainfall as well as GNSS-IWV and rainfall time series is observed from the cycle scale of 8 months to 16 months and more significantly around 12 months from 2008 to 2013. The arrows (phase) which are turning to the right at the period band 8-16 show in-phase coherence and argue that the CAPE and GNSS-IWV contribute to the rainfall.

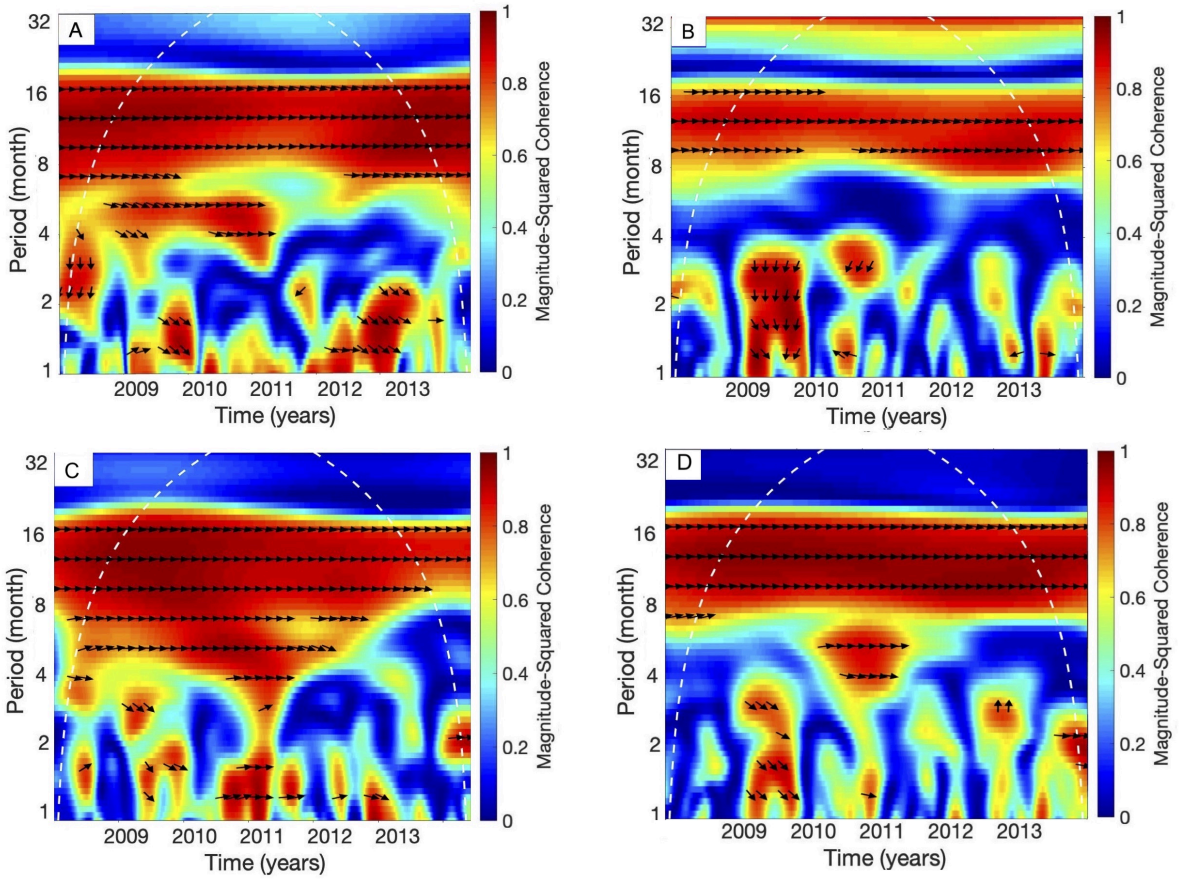

Figure 3.4 – Squared wavelet coherence between the CAPE and rainfall (2008-2013) for TUCU (A) and CATA (B) stations and between the GNSS-IWV and rainfall (2008-2013) for TUCU (C) and CATA (D) stations. The arrows indicates the lag phase relation between rainfall and CAPE and rainfall and GNSS-IWV.

3.1.2 Relation Between Rainfall and GNSS-IWV

In the next step, we analyze the relation of rainfall with GNSS-IWV. We determine the functional relationship for each station and investigate if the relation between GNSS-IWV and rainfall changes for higher rainfall percentiles. We show that for wet days with rainfall above 0.1 mm/day exist an exponential relationship between TRMM rainfall data and GNSS-IWV. The Q-Q (Quantile-Quantile) plot also shows an identical distribution within the assumed log-linear relation (after linearization) between rainfall and GNSS-IWV for wet days and above the 10th percentile (Figure 3.5 A,B). We observe that below the 10th percentile rainfall and GNSS-IWV do not follow an identical distribution (Figure 3.5 A,B).

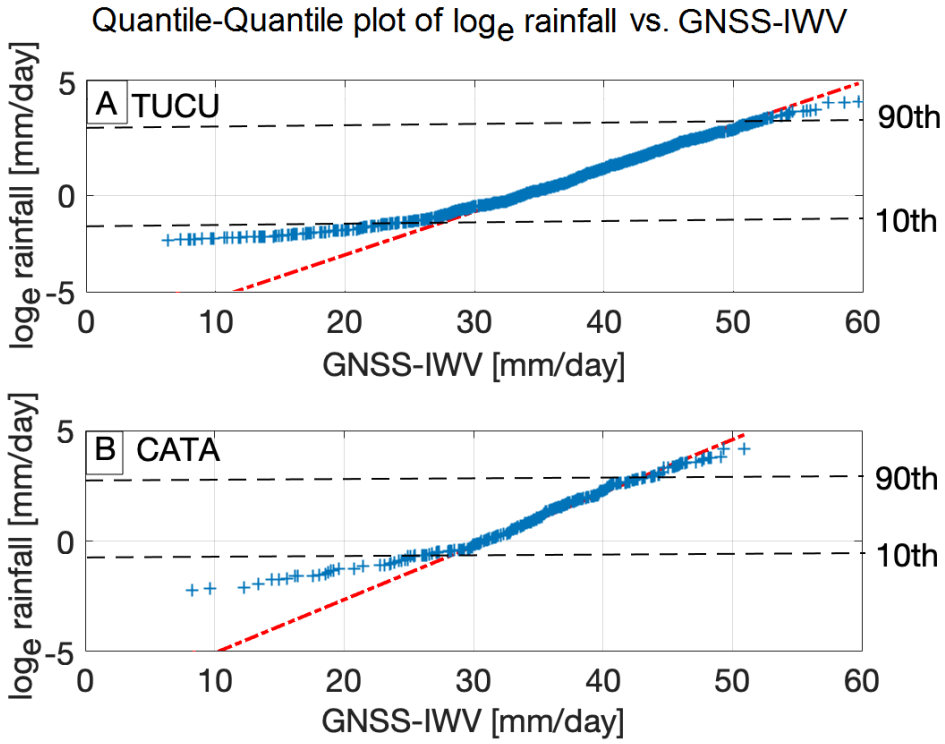

Figure 3.5 – Quantile-Quantile plot on log_e scale of rainfall vs. GNSS integrated water vapour shows that most of the data are well correlated when the log_e(TRMM rainfall) vs. GNSS-IWV is considered in both stations (A) for TUCU and (B) for CATA. Below the 10th percentile rainfall and GNSS-IWV do not follow an identical distribution at both stations. Black dashed lines indicate rainfall percentiles (10th and 90th percentiles).

We test our model for each percentile based on the statistics of the model. Our results show a significant relationship between rainfall and GNSS-IWV based on p-value $<<$ 0.001. Also, our F-value (F-statistic) argues that our model is more compatible with data than the intercept-only model with no independent variable.

We test our data for other possible model fits such as power, Gaussian, and polynomial, but we find that the exponential model fits the data better compared to other models based on the statistics of the fit (Table 3.1).

Table 3.1 – Comparing the quality of the fits for rainfall vs. GNSS-IWV based on RMSE and R-squared values for TUCU (top) and CATA (bottom) for different fitting models. Best-fit results are marked in italic font.

Model (TUCU)	RMSE	R-squared
exponential	*1.3*	*0.17*
power	10	0.13
gaussian	9	0.07
polynomial	11	0.09
Model (CATA)	**RMSE**	**R-squared**
exponential	*1.56*	*0.15*
power	11	0.10
gaussian	10	0.08
polynomial	11	0.09

By comparing the regression for different rainfall percentiles, we find that there is a better fit or more significant relationship between rainfall and GNSS-IWV for higher rainfall percentiles based on higher R-squared value and lower RMSE for both stations (Table 3.2). Our regression coefficients for different rainfall percentiles represent a higher dependence of rainfall to GNSS-IWV for higher rainfall percentiles (Table 3.2).

Table 3.2 – Comparing the quality of the fits for rainfall vs. GNSS-IWV (Equation (3.2)) based on RMSE and R-squared values for TUCU (top) and CATA (bottom) for different rainfall percentiles as well as the regression coefficient for the independent variable GNSS-IWV (Equation (3.2)) for TUCU (top) and CATA (bottom).

Rainfall percentiles (TUCU)	RMSE	R-squared	Regression coefficient (α)
10-100th	1.2	0.17	0.06
10-95th	1.3	0.15	0.03
10-90th	1.3	0.13	0.026
10-80th	1.2	0.11	0.02
Rainfall percentiles (CATA)	**RMSE**	**R-squared**	**Regression coefficient (α)**
10-100th	1.1	0.16	0.04
10-95th	1.2	0.14	0.035
10-90th	1.1	0.13	0.024
10-80th	1.2	0.1	0.02

3.1.3 Relation Between Rainfall and CAPE

Next, we analyzed the relation between rainfall and CAPE. Previous research based on the idealized parcel theory suggested a power-law relationship between rainfall and CAPE with an exponent $\beta = 0.5$ (Equation (3.3)) (Lepore et al., 2015; Ramezani Ziarani et al., 2019). The Q-Q plot indicates that below the 10th percentile rainfall and CAPE do not follow a same distribution within the assumed log-linear relation at both stations (Figure 3.6 A,B). Similar to rainfall vs. GNSS-IWV, we observe a more significant relationship between rainfall and CAPE for the higher rainfall percentiles based on higher R-squared values and lower RMSE for both stations (Table 3.3).

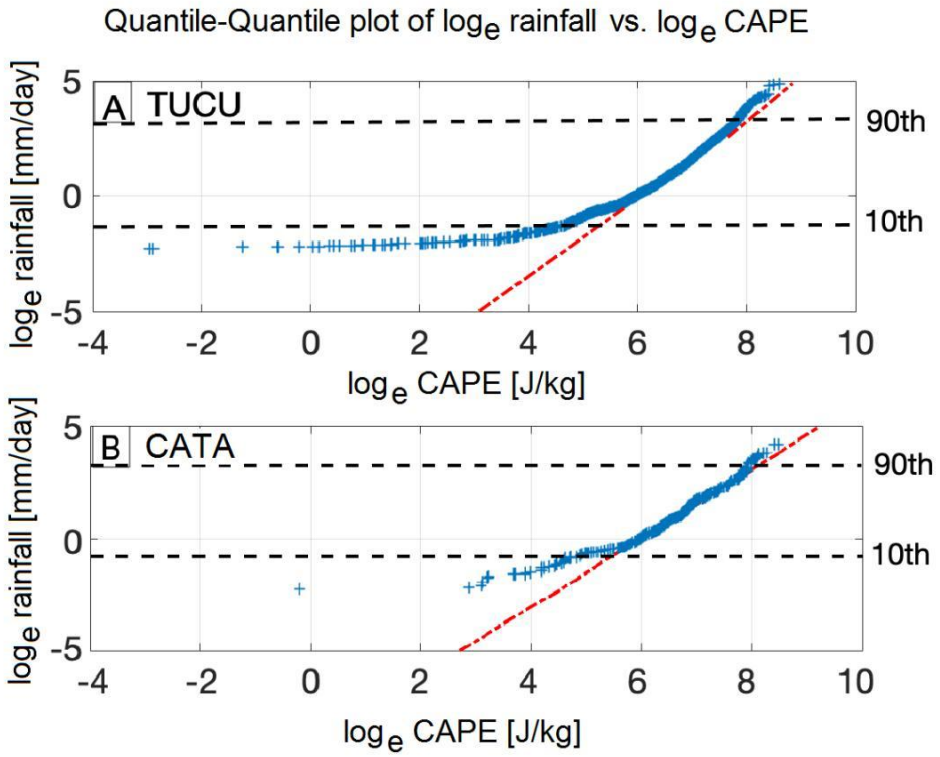

Figure 3.6 – Quantile-Quantile plot on log_e scale of rainfall vs. log_e scale of CAPE essentially shows that most of the data are well behaved within the assumed relation for both stations (A) for TUCU and (B) for CATA. Below the 10th percentile rainfall and CAPE do not follow an identical distribution at both stations. Black dashed lines indicate rainfall percentiles (10th and 90th percentiles).

Table 3.3– Comparing the goodness of the fits for rainfall vs. CAPE (Equation (3.4)) based on RMSE and R-squared values for TUCU (top) and CATA (bottom) for different rainfall percentiles as well as the regression coefficient for the independent variable CAPE (Equation (3.4)) for TUCU (top) and CATA (bottom).

Rainfall percentiles (TUCU)	RMSE	R-squared	Regression coefficient (β)
10-100th	1.2	0.06	0.19
10-95th	1.2	0.05	0.13
10-90th	1.2	0.04	0.08
10-80th	1.4	0.03	0.05
Rainfall percentiles (CATA)	RMSE	R-squared	Regression coefficient (β)
10-100th	1.1	0.11	0.26
10-95th	1.1	0.09	0.2
10-90th	1.7	0.08	0.17
10-80th	1.2	0.06	0.12

The regression coefficients for different rainfall percentiles show a higher dependence between rainfall and CAPE for higher rainfall percentiles. Also, the regression coefficient for all rainfall percentiles and for both stations shows values similar to the predicted value from the parcel theory (0.5) but generally lower (0.1 to 0.3, Table 3.3).

As an additional analysis and based on the approach described by Aaron Clauset (Clauset et al., 2009) we fit the power law distribution to CAPE data using maximum likelihood estimator discussed in their paper. Relying on the goodness-of-fit we observe that power law is a plausible hypothesis for the CAPE data. (Figure 3.7 A,B). In order to homogenize the number of observations of CAPE because there are many more observations at lower magnitudes as it is represented in (Figure 3.7 A,B) we use the logarithmically binned CAPE. We then indicate that there is a power-law relationship between logarithmically binned CAPE and median rainfall of each bin (Figure 3.8 A,B).

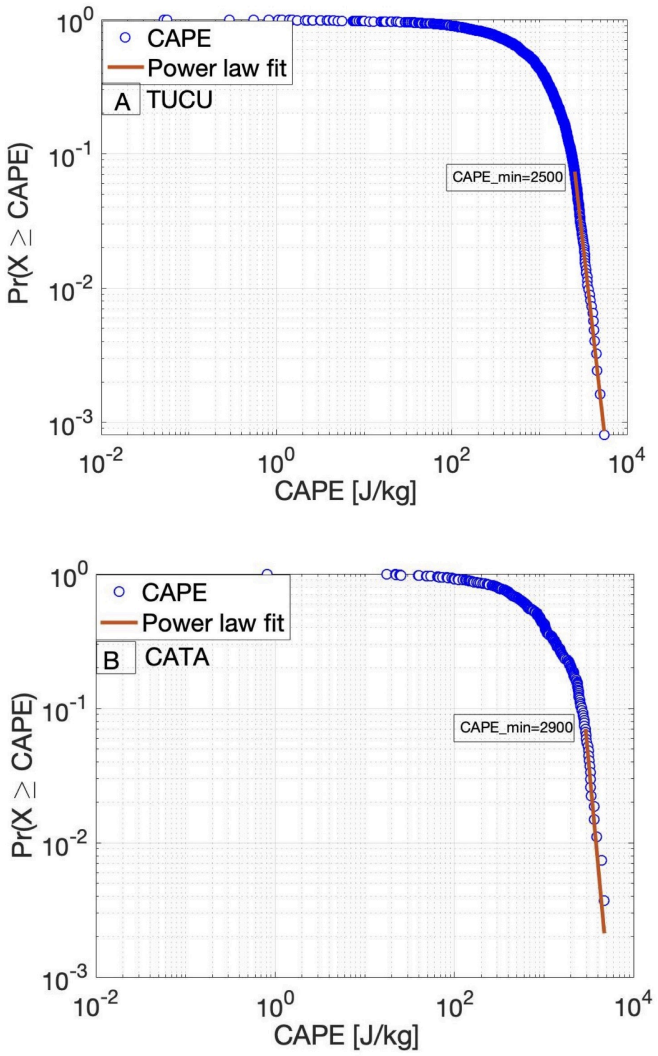

Figure 3.7 – The power-law behaviour using a maximum likelihood approach of log-binned data for the independent variable CAPE (A) for TUCU and (B) for CATA (Clauset et al., 2009). We identify a power-law like behaviour for CAPE values above 2500 J/kg (for TUCU) and 2900 J/kg for (CATA). The p-value greater than 0.1 (TUCU=0.9, CATA=0.4) confirms that power law is a plausible hypothesis for the data.

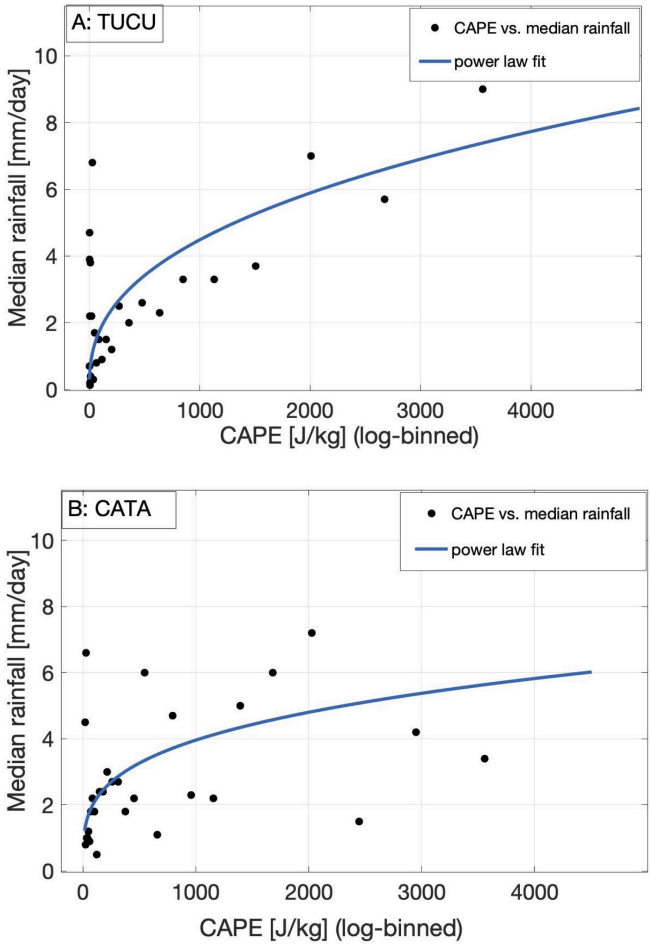

Figure 3.8 – The logarithmically binned CAPE vs. median rainfall (A) for TUCU and (B) for CATA. The exponent β in (Equation (3.3)) is 0.38 for TUCU and 0.3 for CATA.

3.1.4 Relation Between Rainfall, CAPE, and GNSS-IWV

As mentioned above, our regression analysis reveals an exponential relationship between rainfall and GNSS-IWV with a higher statistical significance for higher rainfall percentiles and a power-law relationship between rainfall and CAPE, which is supported by (Lepore et al., 2015; Ramezani Ziarani et al., 2019) (Figure 3.9). We used a linear multivariable regression model (Equation (3.5)) to show the joint effect of both climatic variables on extreme rainfall at both station locations. The regression analysis reveals a statistically significant relationship (p-value $<<$ 0.001) between the GNSS-IWV and CAPE and the 90th percentile rainfall at both stations. We show an improvement by jointly regressing CAPE and GNSS-IWV onto rainfall extremes as compared to individually regressing each variable onto rainfall (Table 3.4, 3.5). The regression coefficient β in Equation (3.5) has been described by parcel-theory to be 0.5 (North and Erukhimova, 2009; Lepore et al., 2015). Based on our results, the regression coefficient (β) reveals a value close to the parcel theory, but generally lower (0.1 to 0.3, Table 3.4, 3.5) at both stations.

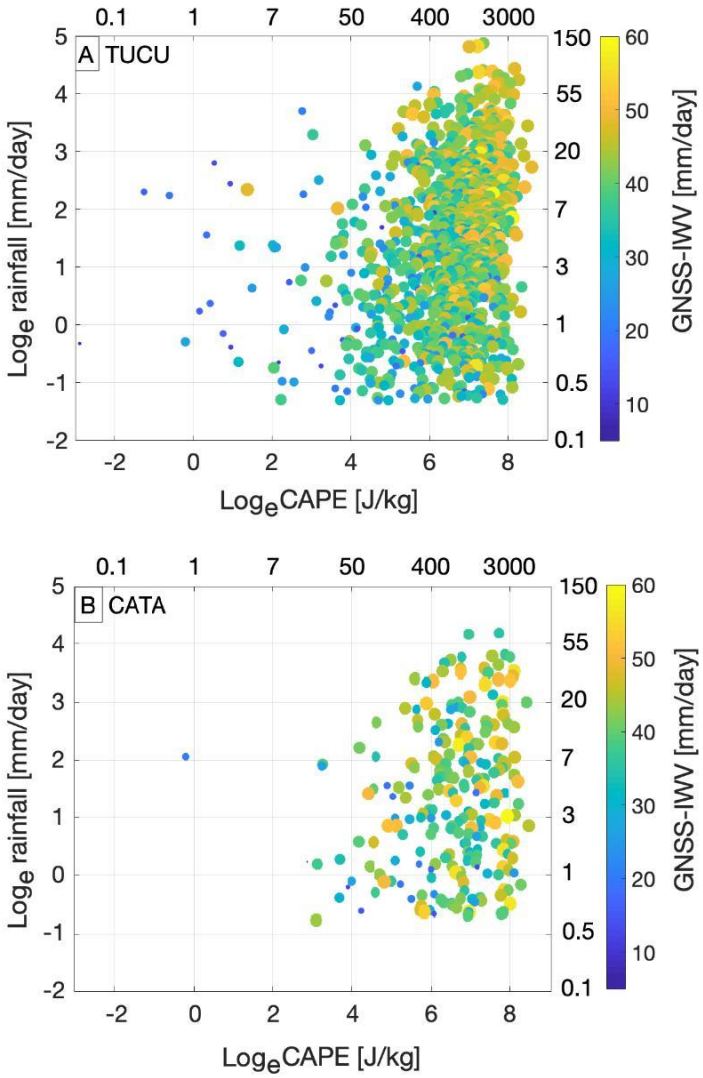

Figure 3.9 – Scatterplot showing log_e rainfall vs. log_e CAPE colored by GNSS-IWV for rainfall events above 0.1 mm/day for TUCU (A) and CATA (B). Point size is also scaled by GNSS-IWV amount.

Table 3.4 – Comparing the quality of the fit for the individual and joint regression (top) and the regression coefficients for data above the 90th percentile rainfall (bottom) for TUCU station.

Regression	RMSE	R-squared
Individual regression of rainfall vs. GNSS-IWV	0.4	0.15
Individual regression of rainfall vs. CAPE	0.3	0.30
Joint regression of rainfall vs. GNSS-IWV and CAPE	0.3	0.34
Regression	Regression coefficient (α)	Regression coefficient (β)
Individual regression of rainfall vs. GNSS-IWV	0.02	-
Individual regression of rainfall vs. CAPE	-	0.25
Joint regression of rainfall vs. GNSS-IWV and CAPE	0.07	0.26

Table 3.5 – Comparing the quality of the fit for single and joint regression (top) and the regression coefficients for 90th percentile rainfall for CATA station.

Regression	RMSE	R-squared
Individual regression of rainfall vs. GNSS-IWV	0.3	0.13
Individual regression of rainfall vs. CAPE	0.2	0.38
Joint regression of rainfall vs. GNSS-IWV and CAPE	0.2	0.40
Regression	Regression coefficient (α)	Regression coefficient (β)
Individual regression of rainfall vs. GNSS-IWV	0.02	-
Individual regression of rainfall vs. CAPE	-	0.25
Joint regression of rainfall vs. GNSS-IWV and CAPE	0.06	0.26

Temporal Relation Between Extreme Rainfall and Both GNSS-IWV and CAPE on the 6-hour scale

We show the correlation between GNSS-IWV and CAPE and extreme rainfall events averaged for the events above the 90th, 95th, and 99th rainfall percentiles. We average the correlation for 72 hours: 24 hours before the event, 24 hours on the event day, and 24 hours afterward. We averaged the 6 hourly mean values of CAPE and GNSS-IWV for all events above the 90th, 95th, and 99th rainfall percentiles separately. We show that for all three rainfall percentiles, the GNSS-IWV and CAPE generally increase during the day before the event and that peak values - both for GNSS-IWV and CAPE - are observed on the day of the 90th, 95th, and 99th percentiles rainfall events. We also

indicate that this increase is mostly followed by a decrease afterwards. Our results show the higher values of CAPE for the CATA station on the event day. In contrast, higher GNSS-IWV values for the TUCU station are observed at days of 90th, 95th, and 99th percentiles rainfall events. We show the higher values of CAPE and GNSS-IWV for the averaged 99th percentiles rainfall events as compared to the averaged 90th and 95th percentiles at both stations (Figure 3.10).

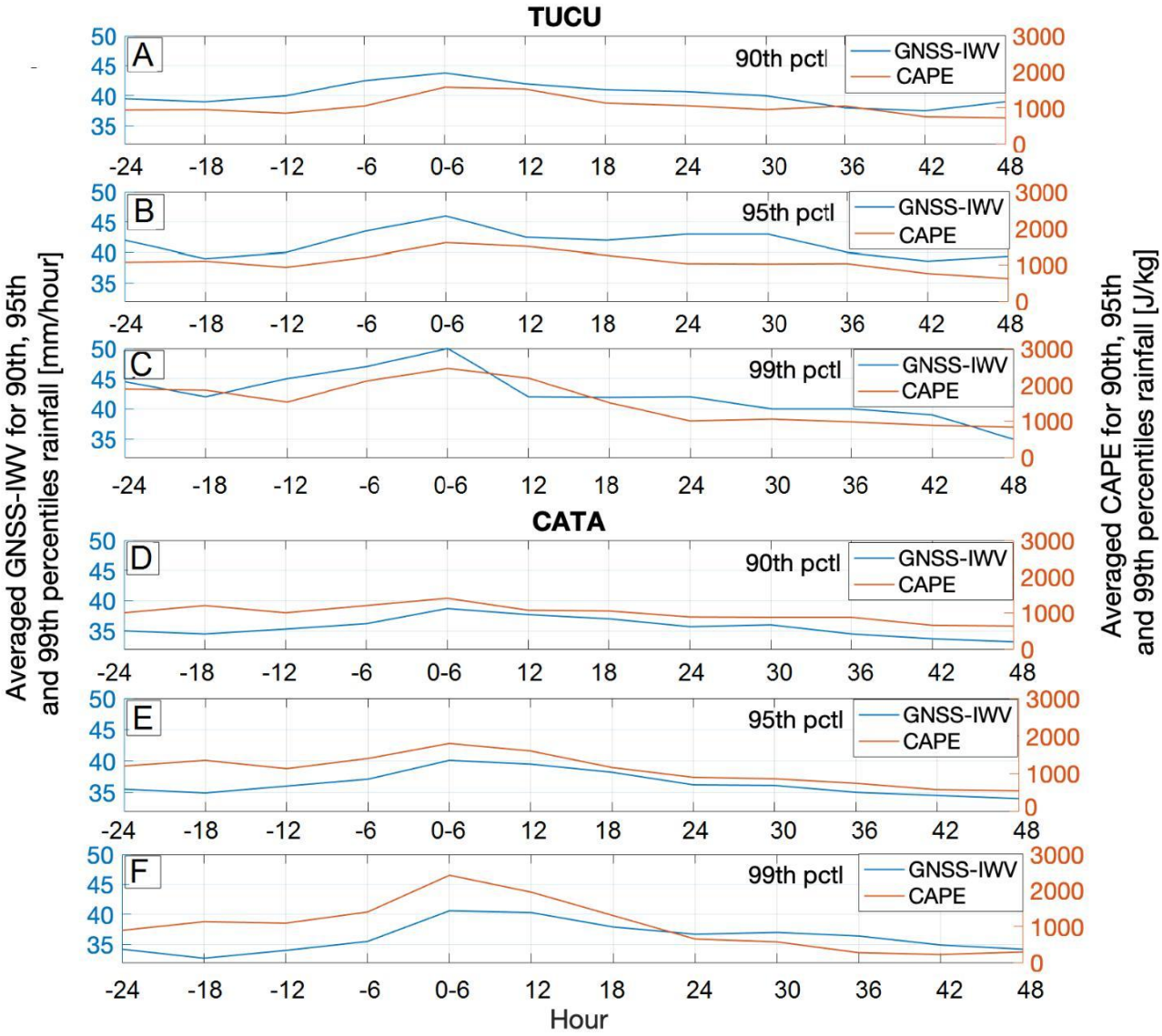

Figure 3.10 – The line plot shows the averaged GNSS integrated water vapour (blue line) and CAPE (red line) for the TUCU and CATA stations for the 90th percentile rainfall (A,D), for the 95th percentile rainfall (B,E), and for the 99th percentile rainfall (C,F). We selected all times with rainfall above the 90th, 95th, and 99th percentiles, respectively and their corresponding GNSS integrated water vapour and CAPE amounts. We then show the correlation for 72 h (event day plus day before and day after). Note that the GNSS integrated water vapour and CAPE generally increase during the day before the event and that peak values - both for GNSS integrated water vapour and CAPE - are observed at the day of the 90th, 95th, and 99th event rainfall.

Discussion

Our observations show that the two stations TUCU and CATA in the eastern central Andes, have different rainfall distributions. This can be attributed to the fact that each station is located at different topographic and climatic

regions. Past studies, (Ramezani Ziarani et al., 2019; Bookhagen and Strecker, 2008) investigated the different characteristics of rainfall along the climatic and topographic gradient over the south-central Andes. We show that the GNSS-IWV time series coincide with rainfall minima during austral winter and maxima during austral summer. Past studies also indicate a nearly homogeneous annual cyclical signal for GNSS-IWV data and a relation with heavy rainfall in Spain (Priego and Porres, 2016). Our wavelet coherence analyses support a seasonal agreement between GNSS-IWV and rainfall as well as CAPE and rainfall. Based on our results from the correlation between rainfall and GNSS-IWV, we show that the relation between both variables at the daily scale can be explained with an exponential relationship for rainfall percentiles above the 10th percentile. We show increased fitting statistics of GNSS-IWV for extreme rainfall at the TUCU station compared to CATA station. This may be related to the fact that extreme convection has occurred more often in the northern (tropical) part of the Andes, where wide convective cores as part of a large mesoscale convective system are more frequently observed than deep convective cores (Romatschke and Houze, 2010).

The correlation between rainfall and CAPE indicates that there is a higher correlation between both variables at the CATA station compared to the TUCU station for rainfall events above the 90th percentile. This can be explained by the fact that higher values of CAPE at the CATA station contributed to the higher correlation between CAPE and extreme rainfall. Previous research, (Ramezani Ziarani et al., 2019) also indicated higher importance of CAPE for extreme rainfall in the transition zone between the tropical and subtropical regions compared to tropical regions. These regions have been identified by intense rising of warm and moist air that triggers the formation of deep convective storms (Romatschke and Houze, 2010; Rohrmann et al., 2014; Ramezani Ziarani et al., 2019; Castino et al., 2017).

We show an improvement in jointly regressing CAPE and GNSS-IWV onto rainfall extremes as compared to a single regression of each variable separately. In order to explain the extreme rainfall over the eastern central Andes, where convection plays an important role in extreme rainfall generation, it is important to consider multi-proxy approaches, including both dominant climatic variables (GNSS-IWV and CAPE). Previous research by (North and Erukhimova, 2009; Lepore et al., 2015; Ramezani Ziarani et al., 2019) suggested a model that displays an exponential relationship between rainfall and dew-point temperature and describes a power-law relationship between rainfall and CAPE. Based on fitting function analysis in this study, we show that GNSS-IWV can be substituted as a reliable humidity data together with CAPE to analyse extreme rainfall. They are both responsible for convection and extreme rainfall.

A previous study (Santhi et al., 2014) investigated the stability indices to predict the occurrences of deep convective storms in India, with a focus on the convective available potential energy (CAPE). A different study suggested a mean increase of GNSS-IWV just before the extreme precipitation on the Mediterranean coast of Spain (Priego et al., 2017). Some other studies, (Benevides et al., 2019; Sharifi et al., 2015) emphasized that the investigation of IWV, together with other meteorological variables, can be used as a proxy of extreme rainfall. They found that high integrated water vapour peaks that lead to intense rainfall coincide with strong peaks of vapour pressure, relative humidity, and K-index (an indicator of the instability of the atmosphere) (Sharifi et al., 2015).

The correlation between the GNSS-IWV and CAPE during extreme rainfall events suggests that GNSS-IWV, in conjunction with CAPE, may be used to predict extreme rainfall events. In our analysis, we used 6 hourly CAPE data for the day before, during, and after the events (a total of 72 hours) and observe a strong correlation. Near real-time GNSS-IWV can improve the predictability of strong rainfall events. Our finding is supported by other studies that indicated an increase in GNSS-IWV just before the start of the extreme rainfall (Van Baelen et al., 2011; Li and Deng, 2013; Sapucci et al., 2018; Priego et al., 2017).

Conclusion

We investigated the contribution of GNSS-IWV and CAPE on rainfall-extreme events at two GNSS station locations in the eastern central Andes. We used a regression analysis to describe the single and joint effects of both atmospheric variables on extreme rainfall. We obtained the following key results:

First, we observe that the two GNSS-IWV stations in the eastern central Andes (CATA and TUCU) belong to different climatic conditions with varying lognormal parameters in the exceedance probability domain (Figure 3.2).

Second, based on the correlation analysis, we find that there is a statistically significant exponential relationship between GNSS-IWV and extreme rainfall at both station locations (Table 3.1).

Third, we support a statistically significant power-law relationship between rainfall and CAPE at the GNSS-IWV station locations in the eastern central Andes. The regression coefficient reveals a value around parcel theory (0.5) at both station locations (Table 3.3).

Fourth, we show the effect of both variables (GNSS-IWV and CAPE) on rainfall generation by multivariable regression analysis. We find that rainfall can be investigated with higher accuracy by considering both dominant climatic variables (Table 3.4, 3.5).

Fifth, we observe that the temporal variations of GNSS-IWV and CAPE are well correlated with extreme rainfall just before and after the extreme rainfall (Figure 3.10 A,B).

In this study, we show the effect of two important climatic variables (GNSS-IWV and CAPE) that trigger deep convection and lead to extreme rainfall in the eastern central Andes. We show that high-temporal resolution GNSS-IWV can be used as a reliable data source for extreme rainfall investigation. We indicate that the combination of GNSS-IWV with other dominant climate variables such as CAPE can be used as a proxy of extreme rainfall in the eastern central Andes.

Funding

This research was funded by the Deutsche Forschungsgemeinschaft (DFG) and the Brandenburg Ministry of Sciences, Research and Cultural Affairs, Germany, within the framework of the international research training group IGK2018 SuRfAce processes, TEctonics and Georesources: The Andean foreland basin of Argentina (StRATEGy).

Acknowledgments

We thank the Deutsche Forschungsgemeinschaft (DFG) and the Brandenburg Ministry of Sciences, Research and Cultural Affairs, Germany, within the framework of the international research training group IGK2018 SuRfAce processes, TEctonics and Georesources: The Andean foreland basin of Argentina (StRATEGy) for the financial support. We acknowledge the support of the Open Access Publishing Fund of University of Potsdam. Also, we thank the Instituto Geográfico Nacional (IGN) , Argentina, https://www.ign.gob.ar for the RAMSAC data.

The authors declare no conflict of interest.

Chapter 4

On the behavior of rainfall maxima at the eastern Andes †

Rodrigo Hierro[1], Yuditsabet Burgos Fonseca[4], Maryam Ramezani Ziarani[2,3], Pablo Llamedo [1], Torsten Schmidt[3], Alejandro de la Torre[1], Peter Alexander[4]

[1] *CONICET / Facultad de Ingeniería, Universidad Austral, LIDTUA (CIC), Argentina*

[2] *University of Potsdam, Institute of Geosciences, Potsdam, Germany*

[3] *Helmholtz Centre Potsdam, GFZ German Research Centre for Geosciences, Potsdam, Germany*

[4] *CONICET / Instituto de Física de Buenos Aires (IFIBA), Buenos Aires, Argentina*

Abstract

In this study, we detect high percentile rainfall events in the eastern central Andes, based on Tropical Rainfall Measuring Mission (TRMM) with a spatial resolution of $0.25^\circ \times 0.25^\circ$, a temporal resolution of 3 hours, and for the duration from 2001-2018. We identify three areas with high mean accumulated rainfall and analyze their atmospheric behaviour and rainfall characteristics with specific focus on extreme events. Extreme events are defined by events above the 95th percentile of their daily mean accumulated rainfall. Austral summer (DJF) is the period of the year presenting the most frequent extreme events over these three regions. Daily statistics show that the spatial maxima, as well as their associated extreme events, are produced during the night. For the considered period, ERA-Interim reanalysis data, provided by the European Centre for Medium-Range Weather Forecasts (ECMWF) with $0.75^\circ \times 0.75^\circ$ spatial and 6-hourly temporal resolutions, were used for the analysis of the meso- and synoptic-scale atmospheric patterns. Night- and day-time differences indicate a nocturnal overload of northerly and northeasterly low-level humidity flows arriving from tropical South America. Under these conditions, cooling descending air from the mountains may find unstable air at the surface, giving place to the development of strong local convection. Another possible mechanism is presented here: a forced ascent of the low-level flow due to the mountains, disrupting the atmospheric stratification and generating vertical displacement of air trajectories. A Principal Component Analysis (PCA) in T-mode is applied to day- and night-time data during the maximum and extreme events.

† *published as Hierro, R., Burgos Fonseca, Y., Ramezani Ziarani, M., Llamedo, P., Schmidt, T., de la Torre, A., Alexander, P. "On the behavior of rainfall maxima at the eastern Andes." Atmospheric Research, 2020, 234, 104792.* https://doi.org/10.1016/j.atmosres.2019.104792.

The results show strong correlation areas over each subregion under study during night-time, whereas during daytime no defined patterns are found. This confirms the observed nocturnal behavior of rainfall within these three hotspots.

Introduction

Rainfall distribution and occurrence over South America (SA) are strongly determined by their low-level circulation and by the presence of the Andes range. Moist air coming from the Atlantic Ocean enters the continent at northern Brazil and continues its journey westward over the Amazon basin (e.g., Fernández et al., 2006; Gulizia et al., 2013). It finally reaches the eastern Andes and heads towards the south (Seluchi and Marengo, 2000). It is the South Atlantic subtropical high which transports moist air from the ocean to the Amazon basin and toward extratropical South America (Vera et al., 2006a). The south-north flow at the western side of the Andes suggests that polar air masses are introduced by the Pacific subtropical high, giving place to a high contrast in the meridional component of the wind along the eastern side of the range, from higher to lower latitudes. This behaviour is also observable in humidity, yielding a good correspondence between moist air and meridional wind. A regional reinforcement of this southerward flow at the east of the Andes gives place to the principal low-level transport mechanism of the continent, the South American Low-Level Jet (e.g., Virji, 1981; Paegle et al., 1987). Regarding rainfall itself, Hoffman (1975) showed the north-south aligned precipitation band at the east of the Andes, reaching 30°S latitude with maximum at approximately 23°S over the mountains. As shown by Vera et al. (2006b), by September the convection migrates from Central America into SA, starting the wet season over the equatorial Amazon and spreading fast to the southeastern side of the region. Abundant rainfall follows the onset over the Amazon basin, which lasts for about one month (e.g., Kousky, 1988; Horel et al., 1989; Marengo et al., 2001; Liebmann and Marengo, 2001). This, in turn, is followed by a more frequent northerly cross-equatorial flow (Marengo et al., 2001; Wang and Fu, 2002). Seasonal changes of convection in tropical SA may be explained by the changing moisture content of the planetary boundary layer as well as by temperature changes at its top (Vera et al., 2006b) and references therein. Romatschke and Houze (2013) stated that solar heating triggers convection of small horizontal dimension over the slopes of the Andes. Moist flow coming from the Atlantic is capped by dry westerlies at the lee side of the range, making the diurnal lifting over the mountains one of the main factors for convection development (De la Torre et al., 2004; Rasmussen and Houze, 2011). Saavedra et al. (2020) have tested the output of precipitation in several high spatiotemporal simulations over the Peruvian area using different topography and land use data sources. A clear influence of moisture flux and its convergence in the Andes-Amazon transition was found, with differences of up to 25% in precipitation due to orography or land use changes. (Kumar et al., 2019) identified precipitating cloud systems in order to investigate the influence of surface wind flow and topography on precipitation over South America. They found that its features are modulated by different directional flows, giving place to higher rain rates at the eastern slope as compared to the western side and to brighter band characteristics in the northern vs. the southern Andes. Montero-López et al. (2014) pointed out that the understanding of how tectonic forcing influences climate and surface processes is closely linked to the knowledge of the distribution of the orographic development of mountain belts. In addition, they argued that the south-central Andes region presents an asymmetric

distribution of rainfall because high mountain range altitudes, and meteorological precipitation mechanisms affect erosion and deposition. Extreme rainfall is one of the major factors that control the hydrological cycle of SA, triggering landslides and flash floods along the eastern side of the Andes (e.g., Boers et al., 2015) and references therein). Marengo et al. (2012a) showed that floods in the Amazon river are related to positive precipitation anomalies as well as to the time when extreme rainfall occurs. The direction of the low-level flow drives the occurrence of extreme events along the Amazon basin as well as to the south, after it turns to the Peruvian and Bolivian Andes (Boers et al., 2014b). Bookhagen and Strecker (2008) explained this effect as a result of moist air lifting over the mountains along the eastern slope of the central Andes and determined that extreme events in the tropics are driven by the low-level flow. As stated by these authors, rainfall has a direct impact in shaping hillslope morphology and determining fluvial characteristics in mountain belts. In turn, the relief of mountain ranges and its relationship with orographic rainfall may re sult in different landscapes, where the mean precipitation in geological timescale is one of the key factors in the development of the Andes range (e.g., Lowman and Barros, 2014) and references therein). Moreover, this precipitation may give place to spatial correlations between fast tectonic uplift and strong rainfall, even in the absence of any erosional influence on tectonics (Whipple 2009). In the case of the Andes range, the extremely asymmetrical distribution of rainfall owing to the high topography strongly affects erosion and deposition. A key concept regarding the interactions between orography and climate interactions is based on the idea that over a region with similar geologic conditions, wet climate produces slower erosion than under dry conditions (Bookhagen and Strecker, 2012). Severe socio-economic effects are present along the Andes as a result of downstream floodings and landslides produced by strong precipitation events (e.g., Moreiras, 2005; Harden, 2006). The aim of the present work is to locate and characterize extreme rainfall events at the east of the subtropical Andes. The evolution of their occurrence time is described and some statistical results that may be used to allow better forecasting of their presence over this region are included. In section 2, we present the data used and describe the methodology employed. In section 3, we characterize the maximum and extreme events found, and in section 4 their dynamical conditions in different scales are considered. In section 5, a principal component analysis is performed, and in section 6 we outline some concluding remarks.

Methodology and database

We focus this study on the east of the Andes, in the region enclosed by [15S –27S, 70W– 60E], where strong signals of mean accumulated rainfall have been systematically observed (e.g., Hierro et al., 2015) (Figure 4.1). As mentioned by Rivera et al. (2018) (and references therein), South America presents limitations in its rainfall network as regards the density and frequency of observations. Moreover, over complex orography areas, large uncertainties appear due to difficulties in accessing the rain gauges.

Considering the high quality of TRMM verified data, the chosen period under analysis runs from summer 1998 to winter 2018. 3-hourly (0.25x0.25 km) accumulated rainfall data (R) are obtained from the Daily TRMM and Others Rainfall Estimate product (TRMM 3B42 V7 derived Data). The use of these data over any topographic region in South America offers a significant advantage, as far as this technique is not obstructed by orographic features. Technical details can be found in Kummerow et al. (2000), among others. TRMM data have been validated

over different regions and seasons around the world. Huffman et al. (2007), found that these data successfully reproduce the observed precipitation at small scales and is able to detect large daily events. Hobouchian et al. (2017) validated daily TRMM data over the subtropical Andes and found some limitations in these measurements associated with the type and location of the event in relation with the orography. Over the central Andes region, Mantas et al. (2015) found these products to be in good agreement with rain gauges during one-week periods, as well as a strong dependence on the analysed region, described by clearly diverse orography and climate features. Extreme precipitation events in the range of 50–200 mm/day and areas affected by high rainfall amounts have been well determined by TRMM data over the Philippines (Jamandre and Narisma, 2013). Fonseca and Cavalcanti (2012) detected, from TRMM measurements, a correlation between extreme precipitation, flooding and landslide events along the eastern South America coast. this was found to result from the passage of synoptic systems causing excess of daily rainfall. (Figure 4.1a) shows the daily accumulated field of R (R_d) during the 1998-2018 period, averaged over the region involved in the study. After a convenient rescaling of a portion of this figure, three relative strong mean R_d signals are observable over the base of the mountains, at the lee side of the Andes (Figure 4.1b).

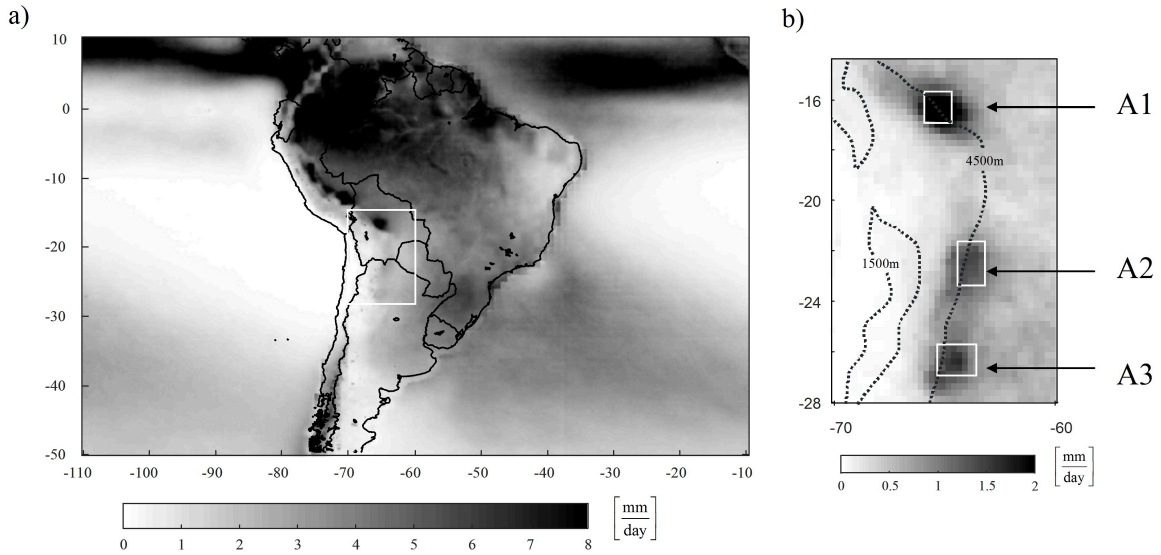

Figure 4.1 – (a) Mean daily R (R_d) during the period 1998-2018 over South America and (b) the same variable over the selected region, showing the subregions under study, A1, A2 and A3, respectively. The white rectangle in (a) is expanded in (b), with the scale conveniently rescaled. Note that in (b) R_d values saturate above 2 mm/day.

Each one of these preeminent R_d signals was arbitrarily enclosed into subregions A1 (16–17S, 64.5–65.5W), A2 (22–23.5S, 63.5–64.5W) and A3 (26–27S, 63–65W), respectively (Figure 4.1b). This allows to quantify 3 sets of spatial maximum precipitation events, respectively over A1, A2 and A3 (hereinafter, called M1, M2 and M3). In doing so, the methodology applied to detect M1, M2 and M3 is based on a comparison of rainfall at each Ai and that observed in an extended region around it (see Appendix for details). Following the establishment of M1, M2 and M3, the days detected within each subregion, now under the constraint imposed by the 95th percentile over M1, M2 and M3 (45mm/day, 28mm/day and 22mm/day), are called extreme event days. These are grouped in sets E1, E2 and E3, respectively.

Maximum and extreme values of precipitation

The dynamical condition characterizing these extreme cases is explored, from Era-interim reanalysis with a spatial resolution of 0.75°. After identifying the hotspots and considering that previous studies extensively discussed different initiation mechanisms for convection and moist instability regimes depending on local time, day- and night-time data are separately considered below. Day-time is defined as the interval 21Z–00Z before the event day, and night-time to the interval 00Z–09Z during the event day. Below, M(i)day / M(i)night and E(i)day / E(i)night) represent, respectively, Mi and Ei associated to day-time / night-time, where i = 1, 2, 3. The monthly distribution of maximum rainfall reveals that December to March (austral summer) are the months with highest occurrence (Figure 4.2a). $\overline{\mathrm{R}}_{48h}$ is defined by averaging all Mi events every 3 hours during the day of the event and the day before. It is computed over 3-hour intervals during M1, M2 and M3, and is shown in Figure 4.2b, including the median, to test a possible influence of outliers in the data. Shaded areas in this figure indicate the event day. For M1, 06Z (3 a.m. or 2 a.m. local time (LT)) indicates the mean maximum rainfall. Remarkably, the rainfall increase begins during the previous hours, whereas its intensity decreases after the 06Z peak of the event day. In the cases contained in M2, the time of maximum precipitation occurs earlier, at 03Z. The total evolution resembles a one-wavelength structure, with maximum and minimum values respectively at 03Z and 12 hours later, at 15Z. M1, M2 and M3 indicate low values of $\overline{\mathrm{R}}_{48h}$ during the first 24 hours (the previous day to the maximum event), with a slight increase during the last hours and a steep increase at the beginning of the event day. This behaviour clearly evidences the occurrence of a systematic nocturnal maximum of precipitation within each subregion.

Following the definition given above, we select extreme events for each subregion. (Figure 4.3a) shows the monthly distribution of E1, E2 and 3.

In all cases, summertime includes the totality of extreme events classified in this study with the 95th percentile. E1 shows January as the month with more frequent extreme events and in general, austral summer appears as the period with the highest activity. In E2 this is clearer, with almost all the events taking place between December and March. A similar behaviour is observed in E3, where January-March is the period with more frequent extreme events. Mean and median of $\overline{\mathrm{R}}_{48h}$ (Figure 4.3b) clearly show low values during the previous day, with a steep increase starting before 18Z. As observed in M1, M2 and M3, these extreme rainfalls originate during the previous day, mostly in the interval 18–21Z. Only E1 presents a steep slope beginning on 00Z of the extreme event day. This (shaded area) shows a behaviour similar to that of M1, M2 and M3, with increasing values of rainfall during the local night, reaching a maximum at 06Z in E1 events and 03Z in the two others. In previous works, persisting mesoscale convective systems clouds at the region considered have been already documented (e.g., Rozante and Cavalcanti, 2008). From numerical simulations and satellite imagery, this night rainfall behaviour has been already found close to this region (e.g., Trachte et al., 2010). A possible mechanism explaining this phenomenon can be found, for example, in Chavez and Takahashi (2017) -and references therein-, who stated that, when cooling downslope air converges at the surface with low-level unstable layers, a maximum of precipitation at the base of the mountain may occur. Banta (1990) and references therein, provided that three ingredients are present: 1) a conditionally unstable temperature lapse rate, mostly important in the warm season, 2) an initiation or triggering mechanism provided daily by mountain

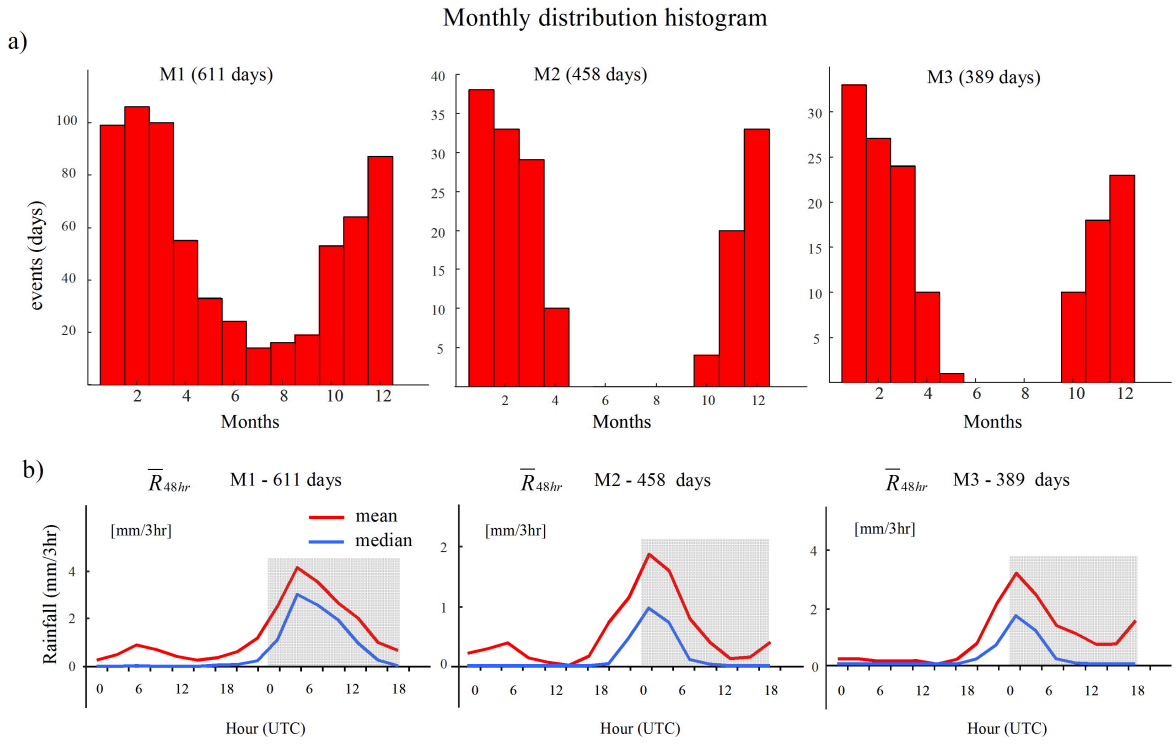

Figure 4.2 – (a) Monthly distribution of M1, M2 and M3. (b) Mean and median of R over each region during each event day and the previous day. Shaded areas indicate the event day. Local time (LT) corresponds to UTC-3 or UTC-4 depending on the region. Peaks occur at 2 a.m. or 3 a.m. (LT) in M1 cases and 11 p.m. or 12 a.m. (LT) in M2 and M3 cases.

circulations, and 3) adequate moisture, which is generally advected in by the larger-scale flow. We know that adiabatic lifting represents the most important process in the atmosphere, since air can be brought to saturation by evaporation, by cooling, or by expansion from adiabatic lifting,. In effect, mountains produce rising motion and adiabatic ascent in two ways: forced ascent and convergence caused by the heating of elevated topography. Under this first mechanism, mountains disrupt the atmospheric stratification and force vertical displacement of air trajectories. In these regions, moist air ascents and clouds can form. Then, in addition to the stability properties of the atmosphere, the characteristics of the flow disturbance given by the lifting created by the mountain appear to be essential. A major difference between potential and latent instability (Iribarne and Godson, 1973) is that mountain lifting does not affect the potential stability or instability of a layer with respect to its vertical displacement. However, it can destabilize a column of the atmosphere with respect to vertical parcel displacements in such a way that a stable column becomes unstable. Following this concept, the question is whether the flow pattern is able to lift air to its lifting condensation level and form clouds. Moreover, if the flow pattern is able to lift air at any level to its level of free convection, unstable cumuliform clouds can form; if not, the clouds will be stable or stratiform (Banta, 1990). An alternative point of view to explain the occurrence of nocturnal mountain rainfall may be proposed by Barros and Lang (2003), who analyzed a case of nocturnal storm close to the Himalaya range detected using TRMM data. They found that a constant night and day flow is blocked by the mountains giving place to

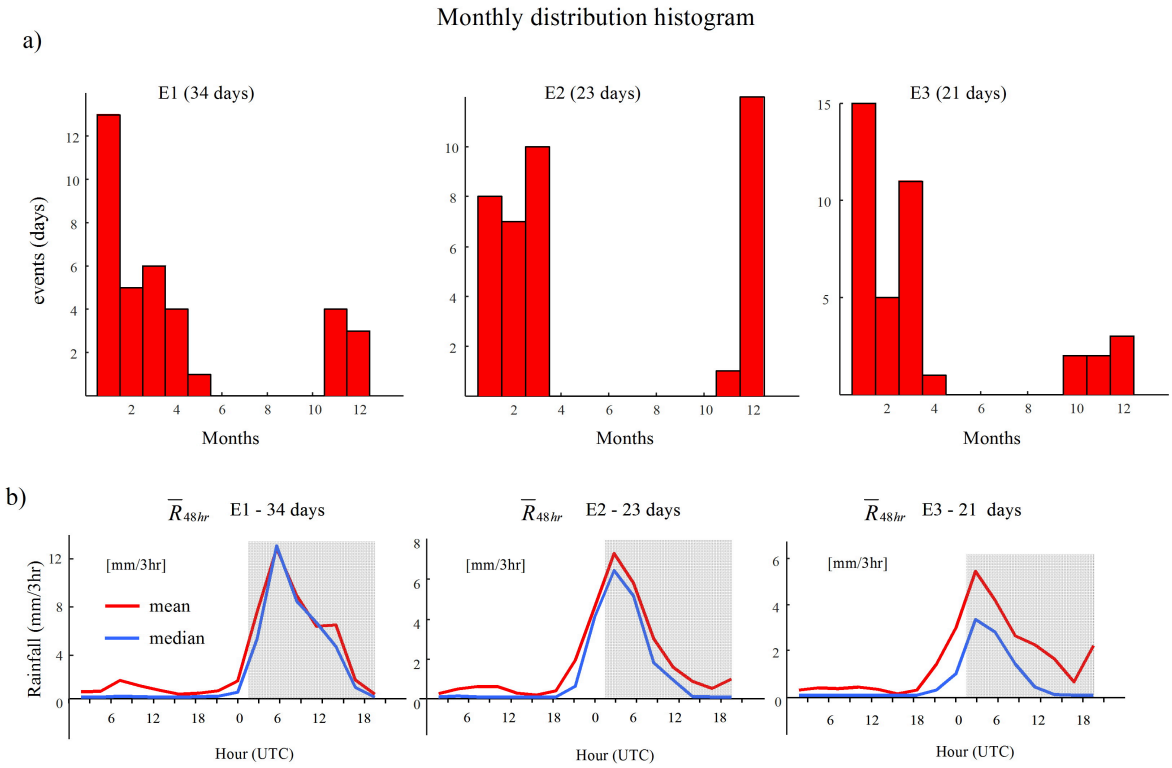

Figure 4.3 – Same as Figure 4.2, now for E1, E2 and E3. Peaks occur at 2 a.m. or 3 a.m. (LT) in E1 cases and 11 p.m. or 12 a.m. (LT) in E2 and E3 cases.

convergence at low levels. This convergence is weakened during the day by upslope flow which reduces in turn, the spatial gradients in wind. At night, however, the convergence close to the surface increases given the decreasing in wind intensity at lower levels, which yields upward motion and convection. This convection is promoted by the increasing of advected moisture and the nocturnal increasing instability by the interaction between the diurnal atmospheric cooling and heating and the steady enhance of moisture close to the surface. The nocturnal peak is thus produced by the surface forcing, the instability coinciding with available humidity.

Large and small-scale dynamical conditions

Following the arguments in section 3, the dynamical differences affecting the extreme events between day and night are distinguished from Era-interim reanalysis, under a spatial resolution of 0.75°. According to Figure 4.2 and Figure 4.3, the increasing values of rainfall during the night begin at approximately 18Z of the day before the event.

We test the specific humidity (q) and lower levels wind ($\overrightarrow{V}$) patterns during extreme days (Figure 4.4) using Erainterim reanalysis each 3 hours. We define day-time as 18Z–21Z (subindex d) of the day before the event and night-time (subindex n), as 00Z–12Z of the event day. Figure 4.4a-c shows the mean humidity transport at 850 hPa, calculated as:

$$\overrightarrow{q}_T = q\overrightarrow{V}$$

In all cases, a strong humidity transport from the North following the climatological low-level circulation mainly during summer is observed, when moist air from the Atlantic goes through the Amazon region. Then, it is channelled towards the south, giving place to the South American Low Level Jet (SALLJ) events. This transport undergoes a rotation close to latitudes defining each extreme events subregion, yielding to an accumulation of humidity at the base of the mountains. Figure 4.4e-f present the differences between the average, for E1, E2 and E3, of $\overrightarrow{V}_{(d)}$ and $\overrightarrow{V}_{(n)}$, $\Delta\overrightarrow{V} = \overrightarrow{V}_{(n)}$ - $\overrightarrow{V}_{(d)}$ (differential wind) at 850 hPa and the mean specific humidity at the same level ($\overline{q}$) (shaded). As mentioned before, this variable seems to reach higher values close to the base of the mountains at the lee side of the range over the studied area of each extreme, following the transport pattern shown in Figure 4.4a-c. The differential wind shows a zonal westwards component during the night in each case. This gives place to a convergence over the mountains where a core of humidity prevails over the region. This behaviour is emphasized in Figure 4.5, which shows the mean differential zonal wind averaged over each latitude band corresponding to E1, E2 and E3. As can be seen, the maximum negative values at the subregions immediately to the west of the mountains are more evident for E1 and E3 than for E2.

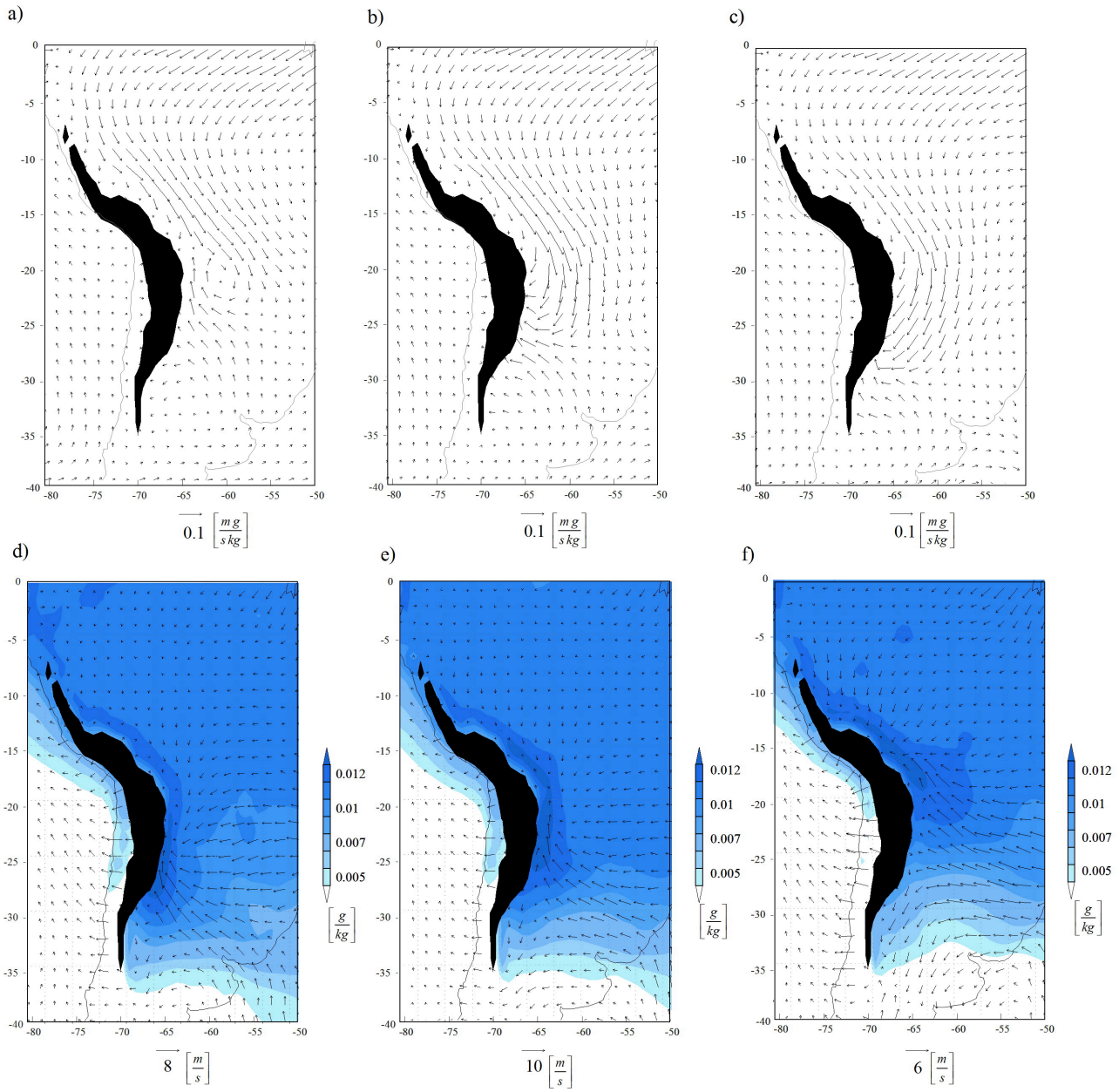

Figure 4.4 – a-c) Mean humidity transport (in m g / s kg) at 850 hPa for E1, E2 and E3, respectively. d-f) Differential wind (in m/s) (night-day) at 850 hPa averaged for E1, E2 and E3, respectively, and the mean specific humidity at the same level (shaded).

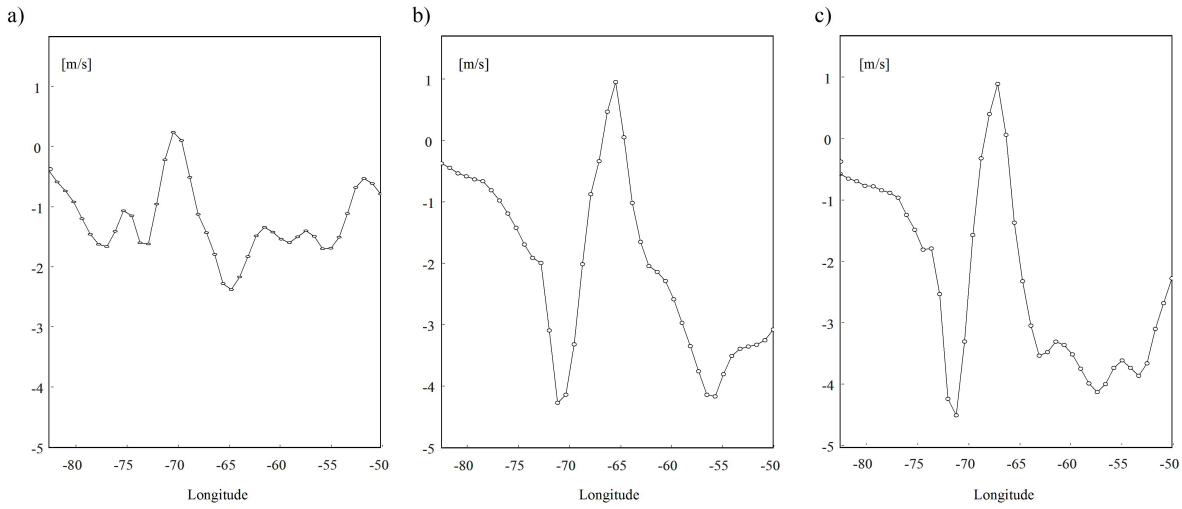

Figure 4.5 – Mean difference night - day of zonal wind averaged over each latitude band corresponding to E1, E2 and E3.

Principal Component Analysis

In previous meteorology and climatology studies, some elementary features of events characterized by large data sets have been detected by applying Principal Component Analysis (PCA). In particular, some tropospheric and stratospheric mechanisms over South America were successfully analysed through this technique (e.g., Compagnucci et al., 2001). There are six different recognized ways to interpret PCA: Q, R, P, O, S and T modes (Cattell, 1952). In this case, given the expectedly relevance of the spatial variability, the most useful mode to be applied is the T-mode (e.g., Compagnucci and Richman, 2008). In T-mode, the statistical variables are defined by the spatial fields of the studied variable at a given time. The grid points are the statistical observations and the domain is given by the time of occurrence. The obtained time series are called PC loading. They show the moment of occurrence of a given pattern, called PC scores, and also indicate the significance with respect to the actual field at that time. In T-mode, the PC loadings represent the correlation between the represented pattern by the PC scores and the real field of the variable. The PC scores, in turn, provide the patterns which correspond to the leading spatial field. As stated by Compagnucci et al. (2001), T-mode determines the main spatial pattern field types in a parameter. In this work, a PCA analysis in T-mode is separately applied to M(i) and E(i) night and day respectively, over the study region. This allows to determine the correlation areas of rainfall for each M(i) and E(i) during night and day with a certain percentage of explained variance. It is not referred to the PC loadings, since we are not dealing with time but with selected cases, so we cannot consider the temporal behavior of the PC scores.

Figure 4.6 presents PC1 in T-mode applied to M1, M2 and M3 during night-time and day-time, following the definitions given in section 2. It is important to mention that we do not show the PCs loadings. This is due to the fact that we are dealing with case studies, which are not equally spaced in time, so we cannot consider time series. However, we point out that in all cases, they are positive, which means that the patterns shown in each PC1 are always the same. Figure 4.6a, corresponding to M1, shows a strong positive correlation among grid points over A1

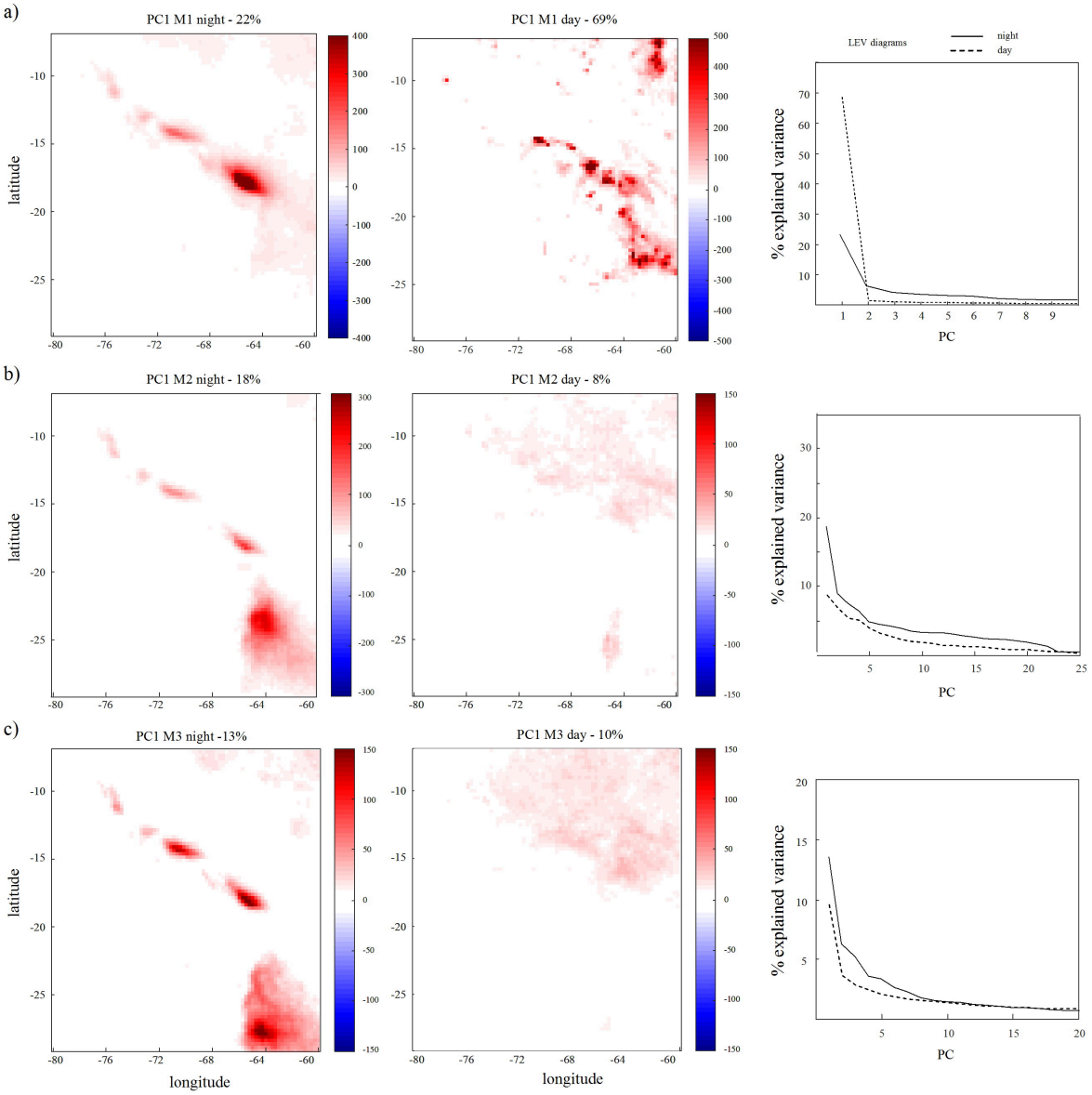

Figure 4.6 – a-c) T-Mode applied to M1, M2 and M3 events. On the left side, PC1 at night-time is shown; on the center, PC1 at day-time; on the right side we present the explained variance for PC1 at night-time (solid line) and day-time (dashed line)

during the night, with an explained variance of 22%. During the day-time (Figure 4.6a, center) there are no clear correlated regions. Although it seems that close to A1 there are some positively correlated areas, this PC explains around 70% of the total variance, with a small contribution of the other PCs (Figure 4.6a, right). In the case of night-time, PC1 and PC2 contribute with 22% and 5% respectively, while the rest present smaller values. (Figure 4.6b, left), shows M2 PC1 during night-time. As in the previous case, we can distinguish the A2 grid points with a strong positive correlation, explaining around 18% of the total variance. On the right side, we can see that the second PC explains around 5% of the total variance, decreasing with increasing PCs. During day-time (Figure 4.6b, center) it

is clear that no correlation among points is found in PC1 scores. Although 8% seems to be a small value, it is the largest one compared with the other PCs. The following pattern (PC2) -not shown-, presents a similar behaviour without correlation in A2 and the others. Similar results are found for PC3 during the night (Figure 4.6c, left) and during day-time when there is no correlation over A3. Both cases present low values of explained variance; however, PC2 explains around 5% in each one, decreasing with the following PCs. This procedure was also followed for E1, E2 and E3. Figure 4.7a, (left) shows positive correlation over A1 during night for PC1. Around 44% of the variance is explained by this PC. PC1 during day-time does not show any correlation in the region. Although not shown, the following PCs do not show significative values. As in the case of M2, Figure 4.7b, (right) presents PC1 scores with high positive values over A2 during night-time. In this case, this PC explains 46% of the total variance, whereas the second only explains around 10% (Figure 4.7b, center). During day-time again, no correlation is found in PC1 and the following E3 cases, shown in (Figure 4.7c, right), exhibit high correlation over A3, explaining 40% of the total variance during night-time. As with the remaining events, E3 during day-time does not show a clear pattern in PC1 scores. From the PCA applied both to maximum and extreme events, we can see that the latter contain less dispersion than the former, since the total explained variances are always higher.

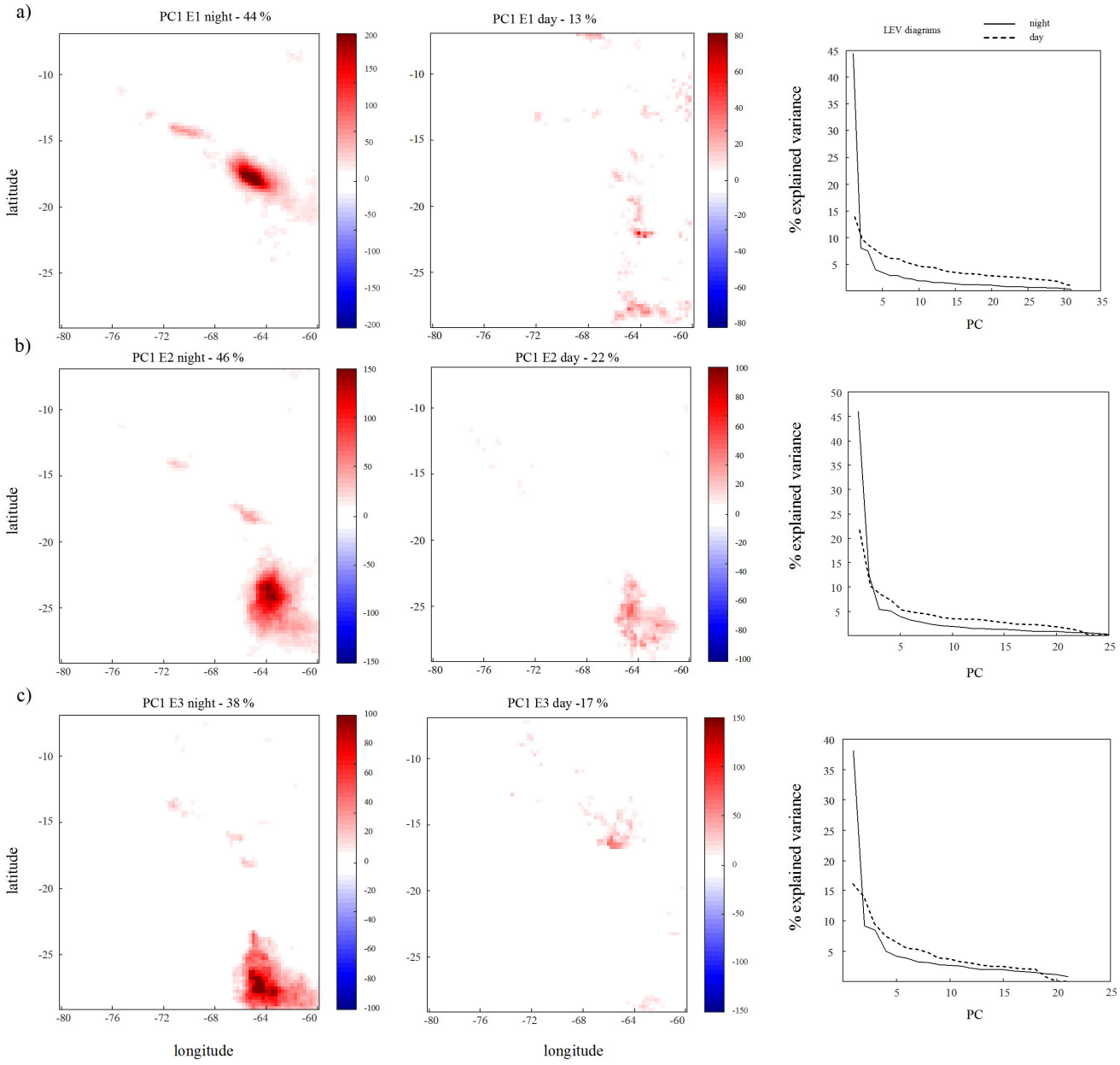

Figure 4.7 – Idem Figure 4.6 for E1, E2 and E3.

Summary and Conclusions

Looking at the mean field of daily accumulated precipitation over the study region, three regions with relative maximum values were identified. 611, 458 and 389 cases (days) respectively, were found. Austral summers are the periods with higher frequencies of occurrence. Night peaks were found in all cases. The 95th percentile of each one was considered as a cutoff for extreme events. The cutoff values were 45 mm/day, 28 mm/day and 22 mm/day for each region respectively. 34 days, 23 days and 21 days with extreme values were found in each region respectively. The monthly distribution of days with extreme values shows austral summer as the period of higher activity for each one. January, and December-March and January-March are the periods where the occurrence of these extreme values is most frequent. Their daily average also shows peaks at night. The average daily evolution shows a similar behaviour in the three cases, with increasing values of rainfall during the local night, reaching a maximum at 06Z. The idea of night convection given by cooling descending air that reaches unstable air at the base of the mountains was tested using Erainterim data. It shows that during the night, there is an increase of differential humidity over the regions studied. In all of them, we found stronger low-level winds and a differential northern transport of humidity with a strong meridional component during the night. Through PCA, it was determined that for maximum events, there is a strong correlation among grid points over each area studied during the night time, defined as 00Z–09Z of the event day. The day-time events (18Z–21Z of the day after of the event), in turn, show that there is no correlation found at any PC. The same occurs for extreme events, which present less dispersion considering their enhanced explained variance by PC1 with respect to maximum events. We can conclude that in the presence of humidity and warm air, mostly during the last hours of summer days, extreme precipitation may occur in the region under study during local night hours. Two mechanisms are proposed as possible sources responsible for this rainfall distribution: i) cooling downslope air converging at the surface with low-level unstable layers and ii) a forced lifting created by the mountains.

Acknowledgments

The study has been supported by the CONICET under grants CONICET PIP 11220120100034 and ANPCYT PICT 2013-1097 and by the German Federal Ministry of Education and Research (BMBF) under grant 01DN14001 The TMPA data were provided by the NASA/Goddard Space Flight Center's Mesoscale Atmospheric Processes Laboratory and Precipitation Processing system.

Appendix

The methodology applied to detect the relative spatial maximum is as follows. First, the total mean of R_d for the complete time interval (2001-2018) is computed. This is performed within each Ai subregion (to illustrate this, see the example in Figure 4.8 for A1), with i = 1, 2, 3), namely Ri_{mean}. Then, the total mean of R_d is now computed over the Ai_{lat} and Ai_{lon} rectangles (see Figure 4.8) associated to each Ai, namely Ri_{lat} and Ri_{lon}. Ri_{lat} and Ri_{lon} are, expectedly, less than Ri_{mean}. The selected limits of Ai_{lat} and Ai_{lon} contain Ai and are arbitrarily specified, on the basis of the observed R distribution. To perform this, we took into account the systematically

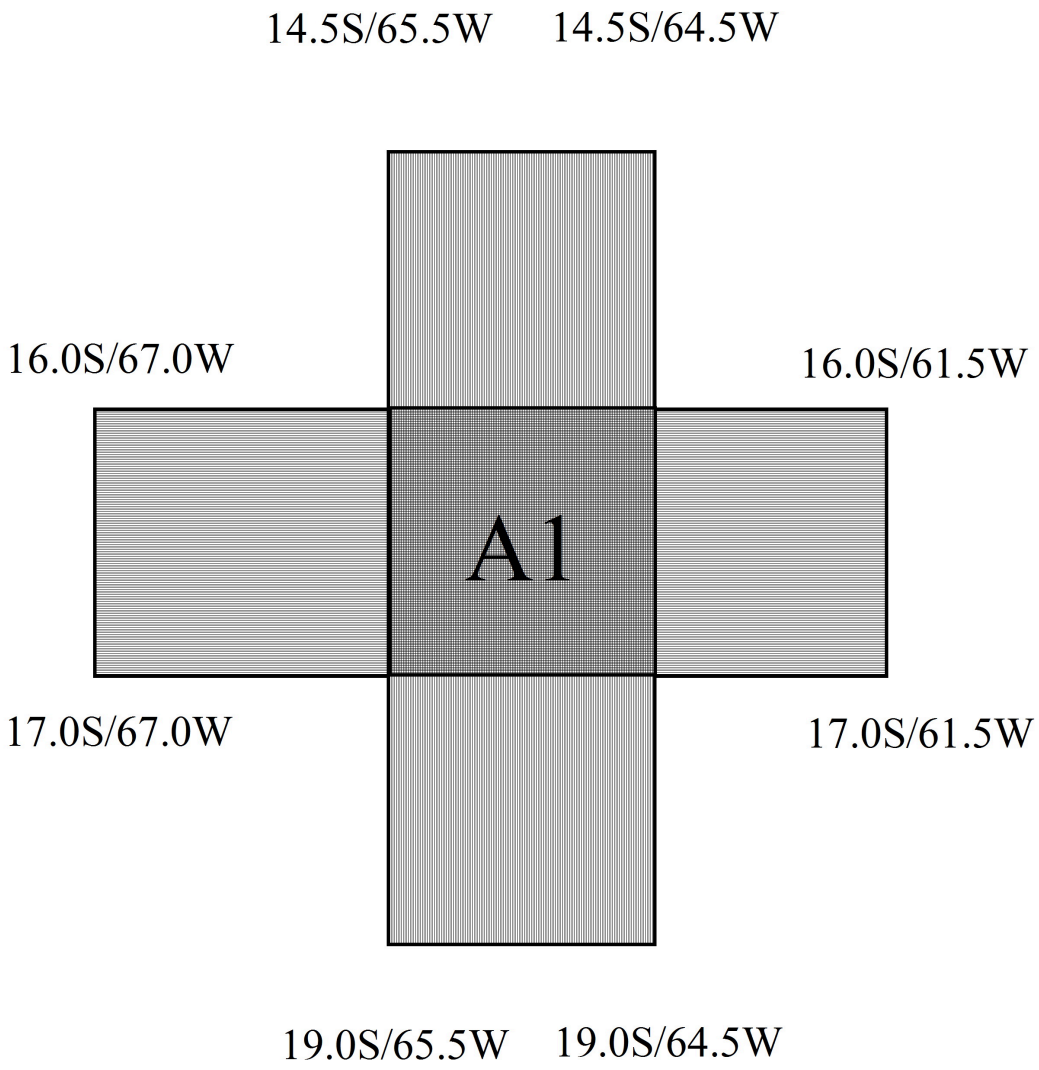

Figure 4.8 –
$A1_{lat}$ (horizontally shaded) and $A1_{lon}$ (vertically shaded), both including subregion A1 (see text), which corresponds to the northern hotspot of precipitation found.

observed deep decrease and steep increase of precipitation over the W-E and N-S boundaries, in Ai_{lat} and Ai_{lon} respectively, due to the SALLJ effect and the income of humidity.

With the definition of $Ri_{mean} - Ri_{lat} = diff_{lat}$ and $Ri_{mean} - Ri_{lon} = diff_{lon}$(Ri) (both of them positive values), the events belonging to Mi are selected only for those k days that verify Ri_{mean}(k) – Ri_{lat}(k) > $diff_{lat}$(Ri) and Ri_{mean}(k) – Ri_{lon}(k) > diff$_{lon}$(Ri). Ri_{mean}(k), Ri_{lat}(k) and Ri_{lon}(k) specify that the R averages are computed over a single k day.

Chapter 5

Conclusion

Conclusion

The main goal of this study is to analyze the atmospheric conditions leading to rainfall-extreme events in the south-central Andes of NW Argentina. Particular emphasis is placed on characterizing the dominant climatic variables and atmospheric conditions that trigger the extreme rainfall in this region along the strong E-W topographic and N-S climatic gradients. Both topographic and climatic gradients impose strong rainfall asymmetry (Bookhagen and Strecker, 2008, 2012; Castino et al., 2017; Ramezani Ziarani et al., 2019) in the south-central Andes. The better understanding of hydro-meteorological extreme events will provide a higher possibility of predicting these events, and hence, better mitigation for their environmental and socio-economic impacts.

While several studies which have analyzed deep convective storms and rainfall over South America and along the eastern Andes exist (e.g., Castino et al., 2017; Boers et al., 2015, 2016; Bookhagen and Strecker, 2008; De la Torre et al., 2015; Pingel et al., 2016; Carvalho et al., 2002; Lenters and Cook, 1999; Espinoza et al., 2015; Thibeault et al., 2010; Minvielle and Garreaud, 2011; Hierro et al., 2015; Moya-Álvarez et al., 2018), the atmospheric boundary conditions leading to deep convection and extreme rainfall have not yet been well understood.

In this study, I analyzed the contribution of dominant climatic variables on deep convective storms and extreme rainfall. I used a multivariable regression analysis to explain the correlation between rainfall extremes and the dominant climatic variables. The analysis relied on both the theoretical relationship and fitting function analysis. Contribution of climatic variables on rainfall extremes underwent a comparison with lower rainfall percentiles along both the topographic and climatic gradients.

I summarize the main key findings of all three studies of chapters 2 through 4 in the following subsections.

The Effect of Temperature on Extreme Rainfall Generation Along the Climatic and Topographic Gradients in the NW Argentine Andes

In this study, the crucial effect of temperature on atmospheric humidity (Td) and on convection (CAPE) for deep convective storms in three topographic as well as three climatic areas was investigated. The ECMWF (European Centre for Medium-Range Weather Forecasts)-Reanalysis (ERA-interim) data (Dee et al., 2011),

https://apps.ecmwf.int/datasets/data/interim-full-daily/levtype=sfc/ were used to analyze temperature, dew-point temperature, and CAPE and TRMM (Tropical Rainfall Measuring Mission) data (Kummerow et al., 1998), product 3B42 (Huffman et al., 2007),

https://disc.gsfc.nasa.gov/datasets/TRMM_3B42_Daily_7/summary (Version 7) were used to analyze the rainfall. I used a multivariable regression model to show the correlation between rainfall and both variables. The regression model relied on the theoretical relationship, which explains a power-law relation between rainfall and CAPE and exponential sensitivity of rainfall to dew-point temperature (North and Erukhimova, 2009; Lepore et al., 2015). The temporal correlation between both variables and surface temperature in conjunction with extreme rainfall argued that both climatic variables and surface temperature are correlated eastward of the south-central Andes along all topographic and climatic sub-regions. By relying on a functional relationship, the relative impacts of both variables on extreme rainfall along the topographic and climatic gradients were analyzed. It was concluded that dew-point temperature is the most important climatic variable for the extreme (90th percentile) rainfall in the tropical regions, and over lower elevation areas compared to the high-elevation Puna Plateau. Comparing this with the lower rainfall percentiles, a more efficient transformation of dew-point temperature to rainfall was observed when the rain intensity is higher. Regarding the CAPE, it was concluded that CAPE is the most important climatic variable in the transition zone between the tropical and subtropical regions and over the intermediate area. Similarly, CAPE revealed a more realistic explanation of rainfall for higher rainfall percentiles based on the statistics of the model.

In summary, this analysis clearly showed that both dew-point temperature and CAPE play an important role in generating extreme rainfall over the south-central Andes, and both are important for understanding the spatial pattern and dynamics of extreme rainfall in the eastern Andes.

Using the GNSS-IWV Data to Understand Convective Processes Leading to Extreme Rainfall in the Eastern Andes

To test if GNSS-IWV data, https://www.ign.gob.ar can be used as reliable data to explain the extreme rainfall in the eastern central Andes, I selected two GNSS stations with the longest data availability. Two GNSS stations are located at two different regions in the eastern central Andes and represent different rainfall patterns (San Miguel de Tucumán (TUCU, 1999-2013) located at 65° 13' W and 26° 50' S and San Fernando del Valle de Catamarca (CATA, 2008-2013) located at 65° 46' W and 28° 28' S). I used a multivariable regression model based on both theoretical

relationships and fitting function analysis in order to explore the effect of both GNSS-IWV and CAPE on extreme rainfall. GNSS-IWV data as humidity data induced convection and rainfall and CAPE as an indicator of available energy for deep convective storms to form were used. The correlation analysis represented exponential sensitivity of rainfall to GNSS-IWV at both station locations and supported the theoretical power-law relationship between rainfall and CAPE (North and Erukhimova, 2009; Lepore et al., 2015). It was concluded that both variables play a crucial role in rainfall extreme formation. The multiple regression of both variables explained the extreme rainfall with higher statistical significance compared to a single regressing of each variable into rainfall. Based on my analysis at 6 hourly time steps a high agreement between temporal variations of GNSS-IWV and CAPE and extreme rainfall was observed.

In summary, this study suggested that (near real-time) GNSS-IWV measurements provide reliable data representing the humidity, which triggers the convection. In combination with CAPE, GNSS-IWV are crucial parameters describing atmospheric stability that can be used as a proxy of extreme rainfall in the eastern central Andes.

The Effect of Local Convection and Associated Formation Time on Extreme Rainfall in the Eastern Andes

In this study, three regions with strong mean accumulated rainfall in the eastern Andes were selected. The associated atmospheric behavior with a focus on extreme events was analyzed. The study relied on a Principal Component Analysis (PCA) which was applied to day- and night-time data during the extreme events. It was observed that in the presence of moist and warm air, there is a higher chance of extreme rainfall occurrence during local night hours in all three study regions. It is proposed that two possible mechanisms are involved in triggering the convection and extreme rainfall; 1) Wind shear between upper-level winds and the low-level flow leading to formation of mesoscale convective systems (Romatschke and Houze, 2010; Rasmussen and Houze, 2016; Pingel et al., 2016; Rohrmann et al., 2014) ; 2) a forced lifting associated with the mountains (Barros and Lang, 2003).

In summary, this study suggested that local convection plays an essential role in generating extreme rainfall specially during the night hours in the Eastern Andes.

Summary

This study revealed that there is a strong rainfall asymmetry in the eastern south-central Andes due to strong topographic and climatic gradients. The study characterized the atmospheric conditions and climatic parameters associated with extreme rainfall generation along the above-mentioned gradients over this region.

The observed relationship between dew-point temperature and CAPE and extreme rainfall was consistent with the theoretical value (North and Erukhimova, 2009; Lepore et al., 2015) that confirm the contribution of both climatic variables on rainfall generation.

The work suggested that the GNSS-IWV data, https://www.ign.gob.ar are reliable data that temporally well correlated with extreme rainfall, which is supported by Benevides et al. (2015, 2019). It was observed that in the

presence of high CAPE, the GNSS-IWV is associated with extreme rainfall formation in the eastern south-central Andes.

The local convection induced by mountains (Barros and Lang, 2003) or mesoscale convective systems (Romatschke and Houze, 2010; Rasmussen and Houze, 2016; Pingel et al., 2016; Rohrmann et al., 2014) triggering the extreme rainfall formation mostly during the night hours in the Eastern Andes.

References

Adams, D. K., Fernandes, R. M., Kursinski, E. R., Maia, J. M., Sapucci, L. F., Machado, L. A., Vitorello, I. ; Monico, J. F., Holub, K. L., Gutman, S. I., Filizola, N., and Bennett, R. A.: A dense GNSS meteorological network for observing deep convection in the Amazon, Atmosph. Sci. Lett., 12, 207–212, doi: 10.1002/asl.312, 2011.

Allmendinger, R., Jordan, T., Kay, S., and Isacks, B.: The Evolution of the Altiplano-Puna Plateau of the Central Andes, Annu. Rev. Earth Planet. Sci., 25, doi: 10.1146/annurev.earth.25.1.139, 1997.

Banta, R.: The role of mountain flows in making clouds. In: Atmospheric processes over Complex Terrain, Meteorol. Monographs, 23, 229–283, 1990.

Barindelli, S., Realini, E., Venuti, G., Fermi, A., and Gatti, A.: Detection of water vapour time variations associated with heavy rain in northern Italy by geodetic and low-cost GNSS receivers, Earth Planets Space., 70, doi: 10.1186/s40623-018-0795-7, 2018.

Barreiro, M., Chang, P., and Saravanan, R.: Variability of the South Atlantic convergence zone simulated by an atmospheric general circulation model, J. Clim., 15, 745–763, doi: 10.1175/1520-0442(2002)015<0745:VOTSAC>2.0.CO;2, 2002.

Barros, A. and Lang, T.: Monitoring the Monsoon in the Himalayas: observations 424 in Central Nepal, June 2001, Mon. Wea. Rev., 131, 1408–1427, doi: 10.1175/1520-0493(2003)131, 2003.

Barstad, I. and Schüller, F.: An Extension of Smith's Linear Theory of Orographic Precipitation: Introduction of Vertical Layers, J. Atmospheric Sci., 68, 2695–2709, 2011.

Benevides, P., Catalao, J., and Miranda, P.: On the inclusion of GPS precipitable water vapour in the nowcasting of rainfall, Nat. Hazards Earth Syst. Sci., 15, 2605–2616, doi: 10.5194/nhess-15-2605-2015, 2015.

Benevides, P., Catalao, J., and Nico, G.: Neural Network Approach to Forecast Hourly Intense Rainfall Using GNSS Precipitable Water vapour and Meteorological Sensors, Remote Sens., 11, doi: 10.3390/rs11080966, 2019.

Berbery, E. H., Douglas, M., Enfield, D., Garreaud, R., Grimm, A., Jones, C., Kousky, V. E., Lawford, R., Liebmann, B., Mechoso, R., Miranda, G., Mo, K., Nicolini, M., N-Paegle, J., Patterson, M., Podesta, G., Silva-Dias, P., and C, V.: Report of the VAMOS Working Group on the South American Monsoon System (SAMS), Miami, Florida, 1998.

Berg, P. and Haerter, J.: Unexpected increase in precipitation intensity with temperature as A result of mixing of precipitation types?, Atmospheric Res., 119, 56–61, doi: 10.1016/j.atmosres.2011.05.012, 2013.

Berg, P., Haerter, J., Thejll, P., Piani, C., Hagemann, S., and Christensen, J. H.: Seasonal characteristics of the relationship between daily precipitation intensity and surface temperature, J. Geophys. Res., 114, doi: 10.1029/2009JD012008, 2009.

Berg, P., Moseley, C., and Haerter, J.: Strong increase in convective precipitation in response to higher temperatures, Nat. Geosci., 6, 181–185, doi: 10.1038/ngeo1731, 2013.

Bevis, M., Businger, S., Herring, T. A., Rocken, C., Anthes, R. A., and Ware, R. H.: GPS meteorology: Remote sensing of atmospheric water vapour using the global positioning system, J. Geophys. Res., 97(D14), 15 787–15 801, doi: 10.1029/92JD01517, 1992.

Bevis, M., Businger, S., Chiswell, S., Herring, T. A., Anthes, R. A., Rocken, C., and Ware, R. H.: GPS Meteorology: Mapping Zenith Wet Delays onto Precipitable Water, J. Appl. Meteor., 33, 379–386, doi: 10.1175/1520-0450(1994)033<0379:GMMZWD>2.0.CO;2, 1994.

Blanchard, D.: Assessing the Vertical Distribution of Convective Available Potential Energy, Weather Forecast., 13, 870–877, doi: 10.1175/1520-0434(1998)013<0870:ATVDOC>2.0.CO;2, 1998.

Bluestein, H. B.: Synoptic-Dynamic Meteorology in Midlatitudes. Volume II. Observations and Theory of Weather Systems, New York, NY, USA; Oxford University Press: Oxford, UK, 1993.

Boers, N., Bookhagen, B., Barbosa, H. M. J., Marwan, N., Kurths, J., and Marengo, J.: Prediction of extreme floods in the eastern Central Andes based on a complex networks approach, Nat. Commun., 5, doi: 5199.10.1038/ncomms6199, 2014a.

Boers, N., Rheinwalt, A., Bookhagen, B., Barbosa, H., Marwan, N., Marengo, J., and Kurths, J.: The South American Rainfall Dipole: A Complex Network Analysis of Extreme Events, J. Geophys. Res., 41, 7397–7405, doi: 10.1002/2014GL061829, 2014b.

Boers, N., Bookhagen, B., Marengo, J., Marwan, N., von Storch, J., and Kurths, J.: Extreme Rainfall of the South American Monsoon System: A Dataset Comparison Using Complex Networks, J. Clim., 28, 1031–1056, doi: 10.1175/JCLI-D-14-00340.1, 2015.

Boers, N., Bookhagen, B., Marwan, N., and Kurths, J.: Spatiotemporal characteristics and synchronization of extreme rainfall in South America with focus on the Andes Mountain range, Clim. Dyn., 46, 601–617, doi: 10.1007/s00382-015-2601-6, 2016.

Bonner, W. D.: Climatology of the low level jet, Mon. Weather Rev., 96, 833–850, doi: 10.1175/1520-0493(1968)096<0833:COTLLJ>2.0.CO;2, 1968.

Bookhagen, B. and Burbank, D.: Topography, relief and TRMM—Derived rainfall variations along the Himalaya, J. Geophys. Res., 33, doi: 10.1029/2006GL026037, 2006.

Bookhagen, B. and Burbank, D.: Toward a complete Himalayan hydrological budget: Spatiotemporal distribution of snowmelt and rainfall and their impact on river discharge, J. Geophys. Res-Earth., 115, doi: 10.1029/2009JF001426, 2010.

Bookhagen, B. and Strecker, M.: Orographic barriers, high-resolution TRMM rainfall, and relief variations along the eastern Andes, Geophys. Res. Lett., 35, doi: 10.1029/2007GL032011, 2008.

Bookhagen, B. and Strecker, M.: Spatiotemporal trends in erosion rates across a pronounced rainfall gradient: Examples from the southern Central Andes, Earth Planet. Sci. Lett., 327–328, 97–110, doi: 10.1016/j.epsl.2012.02.005, 2012.

Bookhagen, B., Strecker, M., edited by Hoorn, C., Wesselingh, and F.P: Modern Andean Rainfall Variation during ENSO Cycles and its Impact on the Amazon Drainage Basin, in Amazonia: Landscape and Species Evolution: A look into the past, Blackwell Publishing: Oxford, UK, 2011.

Brenot, H., Neméghaire, J., Delobbe, L., Clerbaux, N., De Meutter, P., Deckmyn, A., Delcloo, A., Frappez, L., and Van Roozendael, M.: Preliminary signs of the initiation of deep convection by GNSS., Atmos. Chem. Phys., 13, 5425–5449, doi: 10.5194/acp-13-5425-2013, 2013.

Calori, A., Santos, J., Blanco, B., Pessano, H., Llamedo, P., Alexander, P., and de la Torre, A.: Ground-based GNSS network and integrated water vapour mapping during the development of severe storms at the Cuyo region (Argentina), Atmos. Res., 176, 267–275, doi: 10.1016/j.atmosres.2016.03.002, 2016.

Carvalho, L., Jones, C., and Liebmann, B.: Extreme precipitation events in southeastern South America and large-scale convective patterns in the South Atlantic convergence zone, J. Clim., 15, 2377–2394, doi: 10.1175/1520-0442(2002)015<2377:EPEISS>2.0.CO;2, 2002.

Carvalho, L., Jones, C., and Liebmann, B.: The South Atlantic Convergence Zone: Intensity, Form, Persistence, and Relationships with Intraseasonal to Interannual Activity and Extreme Rainfall, J. Clim., 17, 88–108, doi: 10.1175/1520-0442(2004)017<0088:TSACZI>2.0.CO;2, 2004.

Carvalho, L., Jones, C., Adolfo, P., Roberto, Q., Bookhagen, B., and Liebmann, B.: Precipitation Characteristics of the South American Monsoon System Derived from Multiple Datasets, J. Clim., 25, 4600–4620, doi: 10.1175/JCLI-D-11-00335.1, 2012.

Castino, F., Bookhagen, B., and Strecker, M.: River Discharge Dynamics in the Southern Central Andes and the 1976-77 Global Climate Shift: Discharge dynamics in the Central Andes, Geophys. Res. Lett., 43, doi: 10.1002/2016GL070868, 2016.

Castino, F., Bookhagen, B., and Strecker, M.: Rainfall variability and trends of the past six decades (1950–2014) in the subtropical NW Argentine Andes, Climate Dyn., 48, 1049–1067, doi: 10.1007/s00382-016-3127-2, 2017.

Cattell, R. B.: Factor analysis : an introduction and manual for the psychologist and social scientist, Harper and Row, New York, 1952.

Chavez, S. P. and Takahashi, K.: Orographic rainfall hot spots in the Andes-Amazon transition according to the TRMM precipitation radar and in situ data, J. Geophys. Res. Atmos., 122, 5870–5882, doi: 10.1002/2016JD026282, 2017.

Chen, B., Dai, W., Z, L., Wu, L., Kuang, C., and Ao, M.: Constructing a precipitable water vapour map from regional GNSS network observations without collocated meteorological data for weather forecasting, Atmos. Meas. Tech., 11, 5153–5166, doi: 10.5194/amt-11-5153-2018, 2018.

Chen, T., Weng, S., and Schubert, S.: Maintenance of Austral Summertime Upper-Tropospheric Circulation over Tropical South America: The Bolivian High-Nordeste Low System, J. Atmos. Sci., 56, 2081–2100, doi: 10.1175/1520-0469(1999)056<2081:MOASUT>2.0.CO;2, 1999.

Clauset, A., Shalizi, C., and Newman, M.: Power-Law Distributions in Empirical Data, SIAM Rev., 51, 661–703, doi: 10.1137/070710111, 2009.

Colby, F.: Convective Inhibition as a Predictor of Convection during AVE-SESAME II, Mon. Weather Rev., 112, 2239–2252, doi: 10.1175/1520-0493(1984)112<2239:CIAAPO>2.0.CO;2, 1984.

Compagnucci, R. H. and Richman, M. B.: Can principal component analysis provide atmospheric circulation or teleconnection patterns?, Int. J. Climatol., 28, 703–726, doi: 10.1002/joc.1574, 2008.

Compagnucci, R. H., Salles, M. A., and Canziani, P. O.: The spatial and temporal behaviour of the lower stratospheric temperature over the Southern Hemisphere: the MSU view. Part I: data, methodology and temporal behaviour, Int. J. Climatol., 21, 419–437, doi: 10.1002/joc.606, 2001.

De la Torre, A., Daniel, V., Tailleaux, R., and Teitelbaum, H.: A deep convection event above the Tunuyán Valley near to the Andes Mountains, Mon. Weather Rev, 132, 2259–2268, 2004.

De la Torre, A., Hierro, R., Santos, J., Llamedo, P., and Alexander, P.: The influence of topography on vertical velocity of air in relation to severe storms near the Southern Andes Mountains, Atmos. Res., 156, doi: 10.1016/j.atmosres.2014.12.020, 2015.

Dee, D., Uppala, S., Simmons, A., Berrisford, P., Poli, P., Kobayashi, S., Andrae, U., Balmaseda, M., Balsamo, G., Bauer, P., and et al.: The ERA-Interim reanalysis: configuration and performance of the data assimilation system, Q. J. R. Meteorol. Soc., 137, 553–597, doi: 10.1002/qj.828, 2011.

Deng, Z., Gendt, G., and Schöne, T.: : Proceedings of the IAG Scientific Assembly in Postdam, Germany, 2013, (International Association of Geodesy Symposia ; 143), International Association of Geodesy Symposia, Springer, Cham., pp. 33–40, doi: 10.1007/1345_2015_156, 2015.

Duan, J., Bevis, M., Fang, P., Bock, Y., Chiswell, S., Businger, S., Rocken, C., Solheim, F., van Hove, T., Ware, R., McClusky, S., Herring, T. A., and King, R. W.: GPS Meteorology: Direct Estimation of the Absolute Value of Precipitable Water, J. Appl. Meteor., 35, 830–838, doi: 10.1175/1520-0450(1996)035<0830:GMDEOT>2.0.CO;2, 1996.

Durkee, J. and Mote, T.: A climatology of warm-season mesoscale convective complexes in subtropical South America, Int. J. Climatol., 30, 418–431, doi: 10.1002/joc.1893, 2010.

Durkee, J., Mote, T., and Shepherd, J.: The Contribution of Mesoscale Convective Complexes to Rainfall across Subtropical South America, J. Climate., 22, 4590–4605, doi: 10.1175/2009JCLI2858.1, 2009.

Espinoza, J. C., Chavez, S., Ronchail, J., Junquas, C., Takahashi, K., , and Lavado, W.: Rainfall hotspots over the southern tropical Andes: Spatial distribution, rainfall intensity, and relations with large-scale atmospheric circulation, Water Resour. Res., 51, 3459– 3475, doi: 10.1002/2014WR016273, 2015.

Fernández, J. P. R., Franchito, S., and Rao, B.: Simulation of the summer circulation over South America by two regional climate models. Part I: Mean climatology, Theor. Appl. Climatol, 86, 247–260, 2006.

Fonseca, I. and Cavalcanti, A.: Large scale and synoptic features associated with extreme precipitation over South America: A review and case studies for the first decade of the 21st century, Atmos. Res., 118, 27–40, doi: 10.1016/j.atmosres.2012.06.012, 2012.

Foster, J., Bevis, M., and Raymond, W.: Precipitable water and the lognormal distribution, Geophys. Res., 111, 2851–2859, doi: 10.1029/2005JD006731, 2006.

Gandu, A. and Silva Dias, P.: Impact of tropical heat sources on the South American tropospheric upper circulation and subsidence, Meteorol. Atmos. Dyn. Gener. Miscell., 103, 6001–6015, doi: 10.1029/97JD03114, 1998.

Garreaud, R.: The Andes Climate and Weather, Adv. Geosci., 22, 3–11, doi: 10.5194/adgeo-22-3-2009, 2009.

Garreaud, R. and Aceituno, P.: Interannual rainfall variability over the South American Altiplano, J. Clim., 14, 2779–2789, 2001.

Gendt, G., Deng, Z. ; Ge, M., Nischan, T., Uhlemann, M., Beeskow, G., Brandt, A., and Bradke, M.: GFZ analysis center of IGS - Annual Report for 2013, pp. 1–10, 2013.

Gettelman, A., Seidel, D., Wheeler, M., and Ross, R.: Multidecadal trends in tropical convective available potential energy, J. Geophys. Res., 107, doi: 10.1029/2001JD001082, 2002.

Grodsky, S. and Carton, J.: The Intertropical Convergence Zone in the South Atlantic and the Equatorial Cold Tongue, J. Clim., 16, 723–733, doi: 10.1175/1520-0442(2003)016<0723:TICZIT>2.0.CO;2, 2003.

Guerova, G., Jones, J., Douša, J., Dick, G., Haan, S., Pottiaux, E., Bock, O., Pacione, R., Elgered, G., Vedel, H., and et al.: Review of the state of the art and future prospects of the ground-based GNSS meteorology in Europe, Atmos. Meas. Tech., 9, 5385–5406, doi: 10.5194/amt-9-5385-2016, 2016.

Gulizia, C., Camilloni, I., and Doyle, M.: Identification of the principal patterns of summer moisture transport in South America and their representation by WCRP/CMIP3 global climate models, Theor. Appl. Climatol., 112, 227–241, doi: 10.1007/s00704-012-0729-4, 2013.

Gutman, G. and Schwerdtfeger, W.: The role of latent and sensible heat for the development of a high pressure system over the subtropical Andes, in the summer, Meteorl. Rundsch., 18, 69–75, 1965.

Haider, A., Hayley, F. J., and Vimal, M.: Global Observational Evidence of Strong Linkage Between Dew Point Temperature and Precipitation Extremes, J. Geophys. Res., 45, 12 320–12 330, doi: 10.1029/2018GL080557, 2018.

Harden, C. P.: Human Impacts on Headwater Flu- vial Systems in the Northern and Central Andes, Geo- morphology, 79, 249–263, 2006.

Heise, S., Dick, G., Gendt, G., Schmidt, T., and Wickert, J.: Integrated water vapour from IGS ground-based GPS observations: initial results from a global 5-min data set, Ann. Geophys., 27, 2851–2859, doi: 10.5194/angeo-27-2851-2009, 2009.

Hierro, R., Pessano, H., Llamedo, P., de la Torre, A., Alexander, P., and Odiard, A.: Orographic effects related to deep convection events over the Andes region, Atmos. Res., 120–121, 216–225, doi: 10.1016/j.atmosres.2012.08.020, 2013.

Hierro, R., Llamedo, P., Torre, A., and Alexander, P.: Spatiotemporal structures of rainfall over the Amazon basin derived from TRMM data., Int. J. Climatol., doi: 10.1002/joc.4429, 2015.

Hobouchian, M., Salio, P., García Skabar, Y., Vila, D., and Garreaud, R.: Assessment of satellite precipitation estimates over the slopes of the subtropical Andes, Atmos. Res., 190, 43 – 54, doi: 10.1016/j.atmosres.2017.02.006, 2017.

Hoffman, J.: Maps of mean temperature and precipitation, in Climatic Atlas of South America, vol. 1, World Meteorol. Org., Geneva, Switzerland, 1975.

Horel, J. D., Hahmann, A., and Geisler, J. E.: An investigation of the annual cycle of convective activity over the tropical Americas, J. Climate, 2, 1388–1403, 1989.

Huffman, G., Bolvin, D., Nelkin, E., Wolff, D., Adler, R., Gu, G., Hong, Y., Bowman, K., and Stocker, E.: The TRMM Multisatellite Precipitation Analysis (TMPA): Quasi-Global, Multiyear, Combined-Sensor Precipitation Estimates at Fine Scales, J. Hydrometeorol., 8, 38–55, doi: 10.1175/JHM560.1, 2007.

Iribarne, J. V. and Godson, W. L.: Atmospheric Thermodynamics, Springer Netherlands, 1973.

Jamandre, C. A. and Narisma, G. T.: Spatio-temporal validation of satellite-based rainfall estimates in the Philippines, Atmos. Res, 122, 599–608, doi: https://doi.org/10.1016/j.atmosres2012.06.024, 2013.

Khan, S., Kuhn, G., Ganguly, A., Erickson, D., and Ostrouchov, G.: Spatio-temporal variability of daily and weekly precipitation extremes in South America, Water Resourc Res., 43, 1–25, doi: 10.1029/2006WR005384, 2007.

Kodama, Y.: Large-Scale Common Features of Subtropical Precipitation Zones (the Baiu Frontal Zone, the SPCZ, and the SACZ) Part I: Characteristics of Subtropical Frontal Zones, J. Meteorol. Soc. Jpn. Ser. II, 70, 813–836, doi: 10.2151/jmsj1965.70.4_813, 1992.

Kousky, V. and Alonso Gan, M.: Upper tropospheric cyclonic vortices in the tropical South Atlantic, Tellus, 33, 538–551, doi: 10.1111/j.2153-3490.1981.tb01780.x, 1981.

Kousky, V. and Kayano, M.: Principal Modes of Outgoing Longwave Radiation and 250-mb Circulation for the South American Sector, J. Clim., 7, 1131–1143, doi: 10.1175/1520-0442(1994)007<1131:PMOOLR>2.0.CO;2, 1994.

Kousky, V. E.: Pentad outgoing longwave radiation climatology for the South American sector, Rev. Bras. Meteorol, 3, 217–231, 1988.

Kumar, S., Vidal, Y., Moya-Álvarez, A., and Martínez-Castro, D.: Effect of the surface wind flow and topography on precipitating cloud systems over the Andes and associated Amazon basin: GPM observations, Atmos. Res., 225, 193 – 208, doi: 10.1016/j.atmosres.2019.03.027, 2019.

Kummerow, C., Barnes, W., Kozu, T., Shiue, J., and Simpson, J.: The Tropical Rainfall Measuring Mission (TRMM) Sensor Package, J. Atmos. Ocean. Technol., 15, 809–817, doi: 10.1175/1520-0426(1998)015<0809:TTRMMT>2.0.CO;2, 1998.

Kummerow, C., Simpson, J., Thiele, O., Barnes, W., Chang, A. T. C., Stocker, E., Adler, R. F., Hou, A., Kakar, R., Wentz, F., Ashcroft, P., Kozu, T., Hong, Y., Okamoto, K., Iguchi, T., Kuroiwa, H., Im, E., Haddad, Z., Huffman, G., Ferrier, B., Olson, W. S., Zipser, E., Smith, E. A., Wilheit, T. T., North, G., Krishnamurti, T., and Nakamura, K.: The Status of the Tropical Rainfall Measuring Mission (TRMM) after Two Years in Orbit, J. Appl. Meteor, 39, 1965–1982, doi: 10.1175/1520-0450(2001)040<1965:TSOTTR>2.0.CO;2, 2000.

Lenderink, G., Barbero, R., Loriaux, J., and Fowler, H.: Super-Clausius–Clapeyron Scaling of Extreme Hourly Convective Precipitation and Its Relation to Large-Scale Atmospheric Conditions, J. Clim., 30, 6037–6052, doi: 10.1175/JCLI-D-16-0808.1, 2017.

Lenters, J. and Cook, K.: On the Origin of the Bolivian High and Related Circulation Features of the South American Climate, J. Atmos. Sci., 54, 656–678, doi: 10.1175/1520-0469(1997)054<0656:OTOOTB>2.0.CO;2, 1997.

Lenters, J. and Cook, K.: Summertime Precipitation Variability over South America: Role of the Large-Scale Circulation, Mon. Weather Rev., 127, 409–431, doi: 10.1175/1520-0469(1997)054<0656:OTOOTB>2.0.CO;2, 1999.

Lepore, C., Veneziano, D., and Molini, A.: Temperature and CAPE dependence of rainfall extremes in the eastern United States, J. Geophys. Res., 42, 74–83, doi: 10.1002/2014GL062247, 2015.

Li, G. and Deng, J.: Atmospheric water monitoring by using ground-based GPS during heavy rains produced by TPV and SWV, Adv. Meteorol., 793957, 1–12, doi: 10.1155/2013/793957, 2013.

Liebmann, B. and Marengo, J. A.: Interannual variability of the rainy season and rainfall in the Brazilian Amazon Basin, J. Climate, 14, 4308–4318, 2001.

Lowman, L. E. and Barros, A. P.: Investigating links between climate and orography in the central Andes: Coupling erosion and precipitation using a physical-statistical model, J. Geophys. Res. Earth Surf, 119, 1322–1353, doi: 10.1002/2013JF002940, 2014.

Mantas, V., Liu, Z., Caro, C., and Pereira, A.: Validation of TRMM multi-satellite precipitation analysis (TMPA) products in the Peruvian Andes, Atmos. Res, 163, 132–145, doi: https://doi.org/10.1016/j.atmosres.2014.11.012, 2015.

Marengo, J., Liebmann, B., Grimm, A., Misra, V., Silva Dias, P., Cavalcanti, I., Carvalho, L., Berbery, E., Ambrizzi, T., Vera, C., and et al: Recent developments on the South American monsoon system, Int. J. Climatol., 32, 1–21, doi: 10.1002/joc.2254, 2012.

Marengo, J. A., Liebmann, B., Kousky, V. E., Filizola, N. P., and Wainer, I. C.: Onset and end of the rainy season in the Brazilian Amazon Basin, J. Climate, 14, 833–852, 2001.

Marengo, J. A., Soares, W. R., Saulo, C., and Nicolini, M.: Climatology of the Low-Level Jet East of the Andes as Derived from the NCEP-NCAR Reanalyses: Characteristics and Temporal Variability, J. Clim., 17, 2261–2280, doi: 10.1175/1520-0442(2004)017<2261:COTLJE>2.0.CO;2, 2004.

Marengo, J. A., Tomasella, J., Soares, W., Alves, L., and Nobre, C.: Extreme climatic events in the Amazon basin: Climatological and hydrological context of recent floods, Theor. Appl. Climatol, 107, 73–85, doi: doi:10.1007/s00704-011-0465-1, 2012a.

Mesgana, S. and Thian, Y.: Trends in Convective Available Potential Energy (CAPE) and Extreme Precipitation Indices over the United States and Southern Canada for summer of 1979–2013, Civ. Eng. Res. J., pp. 1979–2013, doi: 10.19080/CERJ.2017.01.555556, 2017.

Minder, J. R., Roe, G. H., V.P, S., Singh, P., and (eds): Haritashya, U.: Orographic Precipitation, Encyclopedia of Snow, Ice and Glaciers. Encyclopedia of Earth Sciences Series, Springer: Dordrecht, 2011.

Minvielle, M. and Garreaud, R.: Projecting Rainfall Changes over the South American Altiplano, J. Climate., 24, 4577–4583, doi: 10.1175/JCLI-D-11-00051.1, 2011.

Monkam, D.: Convective available potential energy (CAPE) in Northern Africa and tropical Atlantic and study of its connections with rainfall in Central and West Africa during Summer 1985, Atmos. Res., 62, 125–147, doi: 10.1016/S0169-8095(02)00006-6, 2002.

Montero-López, C., Strecker, M., Schildgen, T., Hongn, F., Guzmán, S., Bookhagen, B., and Sudo, M.: Local high relief at the southern margin of the Andean plateau by 9 Ma: evidence from ignimbritic valley fills and river incision, Terra Nova, 26, 454–460, doi: 10.1111/ter.12120, 2014.

Montini, T. L., Jones, C., and Carvalho, L. M. V.: The South American low-level jet: A new climatology, variability, and changes, Geophys Res Atmos., 124, 1200–1218, doi: 10.1029/2018JD029634, 2019.

Moreiras, S. M.: Climatic effect of ENSO associated with landslide occurrence in the central Andes, Mendoza Province, Argentina, Landslides, 2, 53–59, doi: https://doi.org/10.1007/s10346-005-0046-4, 2005.

Moya-Álvarez, A., Gálvez, J., Holguín, A., Estevan, R., Kumar, S., Villalobos, E., Martínez-Castro, D., and Silva, Y.: Extreme Rainfall Forecast with the WRF-ARW Model in the Central Andes of Peru, Atmosphere., 9, doi: 10.3390/atmos9090362, 2018.

Murugavel, P., Pawar, S. D., and Gopalakrishnan, V.: Trends of Convective Available Potential Energy over the Indian region and its effect on rainfall, Int. J. Climatol., 32, 1362–1372, doi: 10.1002/joc.2359, 2012.

Norris, J., Carvalho, L., Jones, C., Cannon, F., Bookhagen, B., Palazzi, E., and Tahir, A.: The spatiotemporal variability of precipitation over the Himalaya: evaluation of one-year WRF model simulation, Clim. Dyn., 49, 2017.

North, G. and Erukhimova, T.: Cambridge Univ. Press: New York, NY, USA, 2009.

Olen, S. and Bookhagen, B.: Mapping Damage-Affected Areas after Natural Hazard Events Using Sentinel-1 Coherence Time Series, Remote Sens., 10, doi: 10.3390/rs10081272, 2018.

Paegle, J., Zhang, C. D., and Baumhefner, D. B.: Atmospheric response to tropical thermal forcing in real data integrations, Mon. Weather Rev, 115, 2975–2995, 1987.

Panthou, G., Vischel, T., and Lebel, T.: Recent trends in the regime of extreme rainfall in the Central Sahel, Int. J. Climatol., 34, 3998–4006, doi: 10.1002/joc.3984, 2014.

Pingel, P., Mulch, A., Alonso, R., Cottle, J., Hynek, S., Poletti, J., Rohrmann, A., Schmitt, A., Stockli, D., and Strecker, M.: Surface uplift and convective rainfall along the southern Central Andes (Angastaco Basin, NW Argentina), Earth Planet. Sci. Lett., 440, 33–42, doi: 10.1016/j.epsl.2016.02.009, 2016.

Pinon, D., Gomez, D., Smalley, R., Cimbaro, S., Lauria, E., and Bevis, M.: The History, State, and Future of the Argentine Continuous Satellite Monitoring Network and Its Contributions to Geodesy in Latin America, Seismol Res Lett., 89, doi: 10.1785/0220170162, 2018.

Priego, E. ; Seco, A. . J. J. and Porres, M. J.: Heavy rain analysis based on GNSS water vapour content in the Spanish Mediterranean area, Met. Apps., 23, 640–649, doi: 10.1002/met.1586, 2016.

Priego, E., Jones, J., Porres, M., and Seco, A.: Monitoring water vapour with GNSS during a heavy rainfall event in the Spanish mediterranean area, GEOMAT NAT HAZ RISK, 8 (2), 282–294, doi: 10.1080/19475705.2016.1201150, 2017.

Ramezani Ziarani, M., Bookhagen, B., Schmidt, T., Wickert, J., de la Torre, A., and Hierro, R.: Using Convective Available Potential Energy (CAPE) and Dew-Point Temperature to Characterize Rainfall–Extreme Events in the South–Central Andes, Atmosphere., 10, doi: 10.3390/atmos10070379, 2019.

Rasmussen, K. and Houze, R.: Orogenic Convection in Subtropical South America as Seen by the TRMM Satellite, Mon. Weather Rev., 139, 2399–2420, doi: 10.1175/MWR-D-10-05006.1, 2011.

Rasmussen, K. and Houze, R.: Convective Initiation near the Andes in Subtropical South America, Mon. Weather Rev., 144, 2351–2374, doi: 10.1175/MWR-D-15-0058.1, 2016.

Rasmussen, K., Chaplin, M., Zuluaga, M., and Houze, R.: Contribution of Extreme Convective Storms to Rainfall in South America, J. Hydrometeorol., 17, doi: 10.1175/JHM-D-15-0067.1, 2016.

Rivera, J., Marianetti, G., and Hinrichs, S.: Validation of CHIRPS precipitation dataset along the Central Andes of Argentina, Atmos. Res., 213, 437 – 449, doi: 10.1016/j.atmosres.2018.06.023, 2018.

Rohrmann, A., Strecker, M., Bookhagen, B., Mulch, A., Sachse, D., Pingel, H., Alonso, R., Schildgen, T., and Montero, C.: Can stable isotopes ride out the storms? The role of convection for water isotopes in models, records, and paleoaltimetry studies in the central Andes, Earth Planet. Sci. Lett., 407, 187–195, doi: 10.1016/j.epsl.2014.09.021, 2014.

Romatschke, U. and Houze, R.: Extreme Summer Convection in South America, J. Clim., 23, 3761–3791, doi: 10.1175/2010JCLI3465.1, 2010.

Romatschke, U. and Houze, R. A. J.: Characteristics of precipitating convective systems accounting for the summer rainfall of tropical and subtropical South America, J. Hydrometeorol, 14, 25–46, 2013.

Rozante, J. R. and Cavalcanti, F. A.: Regional Eta model experiments: SALLJEX and MCS development, J. Geophys. Res, 113, doi: 10.1029/2007JD009566, 2008.

Saavedra, M., Junquas, C., Espinoza, J., and Silva, Y.: Impacts of topography and land use changes on the air surface temperature and precipitation over the central Peruvian Andes, Atmos. Res., 234, 104 711, doi: 10.1016/j.atmosres.2019.104711, 2020.

Salio, P., Nicolini, M., and Zipser, E.: Mesoscale Convective Systems over Southeastern South America and Their Relationship with the South American Low-Level Jet, Wea. Rev., 135, 1290–1309, doi: 10.1175/MWR3305.1, 2007.

Santhi, Y., Ratnam, M., Dhaka, S., and Rao, S.: Global morphology of convection indices observed using COSMIC GPS RO satellite measurements, Atmos. Res., 137, 205–215, doi: 10.1016/j.atmosres.2013.10.002, 2014.

Sapucci, L., Machado, L., de Souza, E., and Campos, T.: Global positioning system precipitable water vapour (GPS-PWV) jumps before intense rain events: a potential application to nowcasting, Met. Applicat., 26 (1), 49–63, doi: 10.1002/met.1735, 2018.

Seluchi, M. E. and Marengo, J. A.: Tropical-midlatitude exchange of air masses during DJF and JJA in South America: Climatic aspects and examples of intense events, Int. J. Climatol, 20, 1167–1190, 2000.

Sharifi, M., Khaniani, A., and Joghataei, M.: Comparison of GPS precipitable water vapour and meteorological parameters during rainfalls in Tehran, Meteorog. Atmos.Phys., 127, 701–710, doi: 10.1007/s00703-015-0383-3, 2015.

Smith, R. and Barstad, I.: A linear theory of orographic precipitation., J. Atmos. Sci., 61, 1377–1391, doi: 10.1175/1520-0469(2004)061<1377:ALTOOP>2.0.CO;2, 2004.

Smith, R. B.: The Influence of Mountains on the Atmosphere, Adv. Geophys., 21, 87–230, 1979.

Smith, R. B.: A linear time-delay model of orographic precipitation, J. Hydrol., 282, 2003.

Smith, R. B.: Progress on the theory of orographic precipitation, GSA Spec. Pap., 398, 1–16, 2006.

Smith, R. B. and Evans, J. P.: Orographic precipitation and water vapor fractionation over the southern Andes, J. Hydrometeorol., 8, 3–19, 2007.

Thibeault, J. M., Seth, A., and Garcia, M.: Changing climate in the Bolivian Altiplano: CMIP3 projections for temperature and precipitation extremes, J. Geophys. Res., 115,D08103, doi: 10.1029/2009JD012718, 2010.

Trachte, K., Rollenbeck, R., and Bendix, J.: Nocturnal convective cloud formation under clear-sky conditions at the eastern Andes of south Ecuador, J. Geophys. Res, 115, doi: 10.1029/2010JD014146, 2010.

Van Baelen, J., Reverdy, M., Tridon, F., Labbouz, L., Dick, G., Bender, M., and Hagen, M.: On the relationship between water vapour field evolution and the life cycle of precipitation systems, Q.J.R. Meteor.Soc., 137 (S1), 204–223, doi: 10.1002/qj.785., 2011.

Vera, C., Baez, J., Douglas, M., Emmanuel, C. B., Marengo, J., Meitin, J., Nicolini, M., Nogues-Paegle, J., Paegle, J., Penalba, O., Salio, P., Saulo, C., Silva Dias, M. A., Dias, P. S., and Zipser, E.: The South American Low-Level Jet Experiment, Bull. Amer. Meteor. Soc, 87, 63–77, doi: https://doi.org/10.1175/BAMS-87-1-63, 2006a.

Vera, C., Higgins, W., Amador, J., Ambrizzi, T., Garreaud, R., Gochis, D., Gutzler, D., Lettenmaier, D., Marengo, J., Mechoso, C. R., Nogues-Paegle, J., Dias, P. L. S., and Zhang, C.: Toward a Unified View of the American Monsoon Systems, J. Climate, 19, 4977–5000, doi: https://doi.org/10.1175/JCLI3896.1, 2006b.

Virji, H.: A preliminary study of summertime tropospheric circulation patterns over South America estimated from cloud winds, Mon. Weather Rev, 109, 599–610, doi: 10.1175/1520-0493(1981)109<0599:APSOST>2.0.CO;2, 1981.

Vuille, M.: Atmospheric circulation over the Bolivian Altiplano during dry and wet periods and extreme phases of the Southern Oscillation, Int. J. Climatol., 19, 1579–1600, doi: 10.1175/1520-0442(2004)017<3334:IVOSCC>2.0.CO;2, 1999.

Vuille, M. and Keimig, F.: Interannual Variability of Summertime Convective Cloudiness and Precipitation in the Central Andes Derived from ISCCP-B3 Data, J. Clim., 17, 3334–3348, doi: 10.1175/1520-0442(2004)017<3334:IVOSCC>2.0.CO;2, 2004.

Wallace, J. and Hobbs, P.: Atmospheric Science An Introductory Survey, New York Academic Press: New York, NY, USA„ 2006.

Wang, H. and Fu, R.: Cross-equatorial flow and seasonal cycle of precipitation over South America, J Clim, 15, 1591–1608, 2002.

Westra, S., Fowler, H., Evans, J., Alexander, L., Berg, P., Johnson, F., Kendon, E. J., Lenderink, G., and Roberts, N. M.: Future change to the intensity and frequency of short duration extreme rainfall, Rev. Geophys., 52, 522–555, doi: 10.1002/2014RG000464, 2014.

Ye, B., Del Genio, A., and Lo, K.: CAPE Variations in the Current Climate and in a Climate Change, J. Clim., 11, 1997–2015, doi: 10.1175/1520-0442-11.8.1997, 1998.

Zhou, J. and Lau, K.: Does a Monsoon Climate Exist over South America?, J. Clim., 11, 1020–1040, doi: 10.1175/1520-0442(1998)011<1020:DAMCEO>2.0.CO;2, 1998.

Declaration

This work has not been submitted to any other institution of higher education, and was prepared independently by Maryam Ramezani Ziarani.

Potsdam, October 28, 2019
Maryam Ramezani Ziarani